

**Functional analysis of the septate
junction protein complex in *Drosophila
melanogaster***

Dissertation

for the award of the degree
“Doctor rerum naturalium”
of the Georg-August-University Göttingen

within the doctoral program Genes and Development
of the Georg-August-University School of Science (GAUSS)

submitted by
Tatiana Königsmann
from Bogen, Germany
Göttingen, February 2019

Thesis Committee

Prof. Dr. Reinhard Schuh

Research Group Molecular Organogenesis
Max-Planck-Institute for Biophysical Chemistry Göttingen

Prof. Dr. Ernst A. Wimmer

Department of Developmental Biology
Georg-August-University Göttingen

Prof. Dr. Jörg Großhans

Institute of Developmental Biochemistry
University Medical Center Göttingen

Members of the Examination Board

1st Referee

Prof. Dr. Reinhard Schuh

Research Group Molecular Organogenesis
Max-Planck-Institute for Biophysical Chemistry Göttingen

2nd Referee

Prof. Dr. Ernst A. Wimmer

Department of Developmental Biology
Georg-August-University Göttingen

Prof. Dr. Jörg Großhans

Department of Developmental Biochemistry
University Medical Center Göttingen

Dr. Gerd Vorbrüggen

Research Group Molecular Cell Dynamics
Georg-August-University Göttingen

Prof. Dr. Ahmed Mansouri

Research Group Molecular Cell Differentiation
Max-Planck-Institute for Biophysical Chemistry Göttingen

Dr. Nico Posnien

Department of Developmental Biology
Georg-August-University Göttingen

Date of oral examination: 02.04.2019

Affidavit

Herewith I ensure that I prepared the Dissertation “Functional analysis of the septate junction protein complex in *Drosophila melanogaster*” on my own and with no other sources and aids than quoted. This thesis has not been published so far.

Abstract

Body cavities and external surfaces of metazoic organisms are covered with sheets of epithelial cells that act as physical and chemical barriers. Epithelial tissues divide the body into differentiated compartments with different chemical properties providing the barrier function in the trachea and lung, the blood brain barrier in the central nervous system and a powerful shield against pathogens and bacteria.

In invertebrates the so- called septate junctions (SJs) mediate the barrier forming structures of epithelial cells. SJs are localized apicolaterally and consist of a highly stable and immobile core complex as well as core complex associated SJ proteins.

The first part of this thesis investigates the protein domains of the claudin Megatrachea (Mega), an essential component of the SJ core complex in *Drosophila melanogaster*. The generation of various synthetic *mega* mutants under the endogenous promotor of *mega* gives new insights on essential Mega domains for *in vivo* function and stability. Amino acid deletions or exchanges lead to wild-type protein function, impaired protein trafficking, affected protein localization, defects in tracheal morphology, impaired barrier function and unusual exocytosis.

In the second part of this thesis the novel bicistronic gene *würmchen* (*wrm*) was identified and characterized. *wrm* is expressed in ectodermally derived tissues during embryogenesis, including epidermis, trachea and hindgut. *wrm* encodes the two transmembrane domain proteins Wrm1 and Wrm2, which both are essential for tracheal development. Wrm1 represents a SJ core component and is required for SJ morphology, epithelial barrier function and tracheal system morphogenesis. Wrm2 is essential for tracheal development during larval stages and represents a genuine or a transiently associated SJ component.

Contents

1	Introduction	1
1.1	Functions of epithelia	1
1.2	Cell junctions in vertebrates	2
1.2.1	Tight junctions	2
1.3	Cell junctions in invertebrates	4
1.3.1	Septate junctions	4
1.4	The tracheal epithelium of <i>Drosophila melanogaster</i>	8
2	Aim of this thesis	10
3	Results	11
3.1	Protein domain analysis of the claudin Megatrachea	11
3.1.1	Generation of synthetic <i>mega</i> mutant lines	11
3.1.2	Mega mutations in the 2nd extracellular loop reveal wild-type-like Mega localization in the hindgut epithelium	18
3.1.3	Dlg and Kune show wild-type-like localization in mutant embryos affecting the 2nd extracellular loop	19
3.1.4	Exocytosis of Serpentine is affected in mutant M18 embryos	22
3.2	Identification and characterization of <i>würmchen</i>	24
3.2.1	Identification of Mega interaction partners <i>via</i> co-immunoprecipitation and mass spectrometry	24
3.2.2	Expression and knockdown phenotypes of potential Megatrachea interaction partners	25
3.2.3	Genomic organization of <i>würmchen</i> and Würmchen protein structure	27
3.2.4	<i>würmchen</i> is expressed in ectodermal tissues during embryonic development	28
3.2.5	Generation of <i>würmchen</i> mutant alleles	29
3.2.6	Würmchen1 and Würmchen2 are two functionally independent proteins	33

3.2.7	Würmchen1 is expressed in SJs of ectodermal tissues during embryonic development	34
3.2.8	Lack of Würmchen1 affects tracheal morphology	35
3.2.9	<i>würmchen</i> mutant embryos affecting Würmchen1 show affected liquid clearance	36
3.2.10	Würmchen1 is essential for epithelial barrier function	37
3.2.11	The localization of SJ core components depends on Würmchen1	40
3.2.12	Würmchen1 does not affect cell polarity	42
3.2.13	Würmchen1 is necessary for exocytosis of Serpentine	43
3.2.14	SJ and taenidial folds morphology is compromised in <i>würmchen</i> mutant embryos affecting Würmchen1	44
3.2.15	Würmchen1 is essential for SJ core complex stability	46
3.2.16	Tracheal-specific overexpression of Würmchen1 leads to elongated tracheal tubes	48
3.2.17	Würmchen1 binds to <i>Drosophila</i> claudins	48
3.2.18	Würmchen2 binds to Mega	50
3.2.19	Würmchen1 binds to Würmchen2	51
3.2.20	Würmchen1 and Würmchen2 expressing S2R+ cells lack homophilic adhesion capability	53
4	Discussion	55
4.1	Functional domain analysis of the claudin Megatrachea	55
4.2	Functional analysis of the bicistronic gene <i>wrm</i>	60
4.2.1	Würmchen1 is an essential SJ core component	60
4.2.2	Würmchen1 is involved in tracheal morphology and function during embryogenesis	61
4.2.3	Würmchen2 is a putative transient binding partner of SJ core components	63
5	Materials and methods	64
5.1	Material	64
5.2	Fly protocol	80
5.3	Generation of $\Delta attP$ mutant lines	80
5.4	Histological methods for whole embryos	82
5.5	Protocols for <i>in situ</i> hybridization in whole embryos	84
5.6	Live imaging techniques	86

5.7 Cell culture protocol	86
5.8 Histological methods for cells	87
5.9 Molecular biological methods	88
5.10 Methods for co-immunoprecipitation	94
5.11 Mass spectrometry	96
5.12 Electron microscopy	97
5.13 Image documentation and microscopy	97
A Summary of exchanges, domain switches and deletions of Mega domains	106
B Mass spectrometry data	108
C FRAP intensities	135
D Synthesized double stranded DNA fragment	138
Abbreviations	140
List of figures	143
List of tables	145

1 Introduction

1.1 Functions of epithelia

The emergence of epithelia was an evolutionary novelty in metazoans. By forming epithelial sheets and thereby generating isolated and controlled internal compartments, the animal is able to undergo distinct chemical and physical processes simultaneously. Thus, the animal gains a selective advantage and complexity.

In general, epithelial tissues have multiple functions including the formation of an intact barrier function, defense from pathogens and bacteria as well as protection from chemical stress and radiation. Based on the exposure to different substances, organs develop a variety of epithelial tissues depending on their localization in the body. Additionally, epithelia are involved in endocytic and exocytic processes as well as the highly selective transport of molecules. The controlled secretion and absorbance of molecules is particularly important in the digestive tract and respiratory system (Bellmann et al., 2015; Joseph et al., 2013).

Epithelial tissues are defined by the following criteria: 1. Individual cells of an epithelium share an aligned polarity (apical and basal surfaces), 2. individual cells are joint by belt-forming junctions (tight or septate junctions) and 3. individual cells interact with the extracellular matrix only at their apical and basal side (Tyler, 2003). Sponges are the most basal phylum, where epithelial-like structures are found. They form minor sealed cavities which are only sealed transiently. However, the lack of belt-forming junctions indicates an incomplete isolation (Green and Bergquist, 1982). Therefore, epithelia in sponges are not considered true epithelia.

The earliest true epithelia are found in Cnidarians, fulfilling all the criteria for a true epithelium. Epithelia are considered as the primary structure providing complex differentiation. True epithelial tissues set Eumetazoans aside from sponges and give rise to mesenchymal structures in Bilaterians during the epithelial-mesenchymal-transition, causing epithelial cells to differentiate into mesenchyme (Tyler, 2003).

Comparative studies of the insect *Drosophila melanogaster* (*Drosophila*), rat, mouse, cnidarian *Hydra* and nematode *Caenorhabditis elegans* show that proteins involved in epithelial differentiation are uncommonly similar, indicating highly conserved biological

mechanisms (Knust and Bossinger, 2002; Krämer, 2000).

Organ development is highly dependent on epithelial morphogenesis in metazoans. During early developmental stages, invagination, migration, rearrangement and barrier forming events occur, which require control and communication of epithelial cells. However, these early events, in particular the barrier formation, are not fully understood yet.

1.2 Cell junctions in vertebrates

Most of the communication between two neighboring cells occurs *via* gap-junctions. Gap-junctions connect the plasma membranes of two cells generating a narrow uniform gap. This gap is spanned by connexins, which are essentially channel forming proteins. The channels allow small, water-soluble molecules and inorganic ions to pass directly from the cytoplasm of one cell to the other, leading to an electrical and metabolic coupling of connected cells (Hervé and Derangeon, 2013).

Connexins are four-transmembrane-domain proteins. Six connexins form one stable aqueous continuous gap channel (connexon; Hervé et al., 2012). 21 different members associated with the connexin family have been identified in humans and each has a specific tissue distribution (Laird, 2006).

A different type of junctions in vertebrates is represented by the adherens junctions (AJs). AJs provide the adhesive forces in order to prevent a multi cellular structure from dissociating into single cells. This is of special importance during cell rearrangement or movement of the organism. The strong cell adhesion is mediated by cadherin adhesion molecules that function as homophilic adhesion receptors to accelerate cell-cell recognition (Harris and Tepass, 2010). Cadherins were also shown to play essential roles in epithelial integrity and morphogenesis (Gumbiner, 2000; Halbleib and Nelson, 2006).

1.2.1 Tight junctions

A selective permeability barrier is one common feature of all epithelial tissues, separating body compartments with different physiological properties. In contrast to transcellular transport mechanisms, paracellular transport does not occur in an energy-dependent manner. In vertebrates, tight junctions (TJs) create a tight seal between two epithelial cells, limiting paracellular flow of molecules and solutes. However, in transporting epithelia TJs mediate a directed flow of distinct ions and solutes, requiring critical organization and interaction between epithelial cells. TJs are the apical-most connections at the lateral sides of neighboring cells and were detected as rows of membrane contacts (kissing points; Chalcroft and Bullivant, 1970), which vary in amount and morphology in different tissues

(Claude and Goodenough, 1973).

An essential core component of the TJs are proteins called claudins, belonging to the PMP22/EMP/MP20/claudin, or pfam00822 superfamily (Van Itallie and Anderson, 2006) and were first discovered in 1998 (Furuse et al., 1998). The barrier tightness does not only correlate with the number of adjacent cell contacts (Claude and Goodenough, 1973), but is also depending on the distinct expression profile of the claudins (Schneeberger and Lynch, 2004). So far, more than 25 claudins have been identified in mammals, all sharing a highly similar protein structure. Claudins consist of four transmembrane domains, a short N-terminus, two extracellular and one intracellular domain as well as an intracellular C-terminus (Furuse et al., 1998). Moreover, claudins are rather small proteins ranging from 20 - 27 kDa. A conserved sequence motif of amino acids W-GLW-C-C represents a common feature in the 1st extracellular loop of claudins. It is proposed that the two cysteins in this motif form a disulfide bond, enhancing stability for polymerized claudins. It was also shown that the first extracellular loop has an impact on paracellular charge selectivity (Colegio et al., 2002), whereas the second extracellular loop plays a role in bacterial toxin recognition (Fujita et al., 2000). Another important and highly conserved sequence is the PDZ-binding motif at the very end of the C-terminus, where the PDZ-domains of the cytoplasmic scaffolding proteins Zonula occludens (ZO) ZO-1, ZO-2 and ZO-3 from the membrane-associated guanylyl kinase (MAGUK) family bind (Itoh et al., 1999). Additionally, the membrane-associated guanylyl kinase inverted proteins MAGI-1, MAGI-2 and MAGI-3 and the multi-PDZ domain protein 1 (MUPP-1) also interact with claudins *via* their PDZ domains (Schneeberger and Lynch, 2004).

The interaction of claudins with PDZ-domain containing proteins seems to be required in establishing TJs strands, since no TJs strands are formed in the mouse breast epithelial cell line Eph4, which lacks the scaffolding proteins ZO-1 and ZO-2 (Umeda et al., 2006). However, evidence shows that claudins have the potential to self-organize into strand structures (Yamazaki et al., 2011) and will still oligomerize into TJ in epithelial cells without PDZ-domain interaction (Rüffer and Gerke, 2004). Cis (within the same membrane) and trans (with the opposing membrane) as well as homo and hetero interactions have been documented in claudins (Piontek et al., 2011; Furuse et al., 1999). These interactions could affect distinct TJ strand architectures with dominating claudin-claudin and claudin PDZ-scaffolding protein interactions. Distinct expression profiles of claudins in one tissue might lead to specific resistance and charge selectivity of the barrier. However, the underlying mechanisms and claudin properties of controlling the paracellular transport are unclear (Van Itallie and Anderson, 2006).

In conclusion, it seems highly likely that contributions of both, PDZ-domain scaffolding proteins and claudins, determine TJ strand architecture and finally the epithelial barrier.

1.3 Cell junctions in invertebrates

Multi-cellular invertebrates possess an intercellular communication apparatus, called gap junction. As described for vertebrates, gap junction oligomerize to direct pores between two adjacent epithelial cells, allowing a fast and direct exchange of metabolic material. However, gap junctions in invertebrates, despite being ultrastructurally alike in vertebrates and invertebrates, do not contain any connexin proteins, but instead are made up by a protein family called innexins (Phelan, 2005). No sequence homology and oligomerization *in vitro* was detected between connexins and innexins (Oshima et al., 2016).

In contrast to gap-junctions, AJs of vertebrates and invertebrates are highly similar, providing cell-cell adhesion and stability between epithelial cells. Essential homologs of AJ proteins, such as DE-cadherin and Δ catenin have been identified in *Drosophila* (Oda et al., 1994; Oda et al., 1993; Peifer, 1993).

1.3.1 Septate junctions

Similar to vertebrate TJs, septate junctions (SJs) form a paracellular barrier between epithelial cells. SJs form wide intercellular gaps, unlike the kissing points of two membranes in vertebrate TJs. Despite their morphological differences, both structures are functionally homologous. However, the position of TJs and SJs differs greatly between invertebrates and vertebrates.

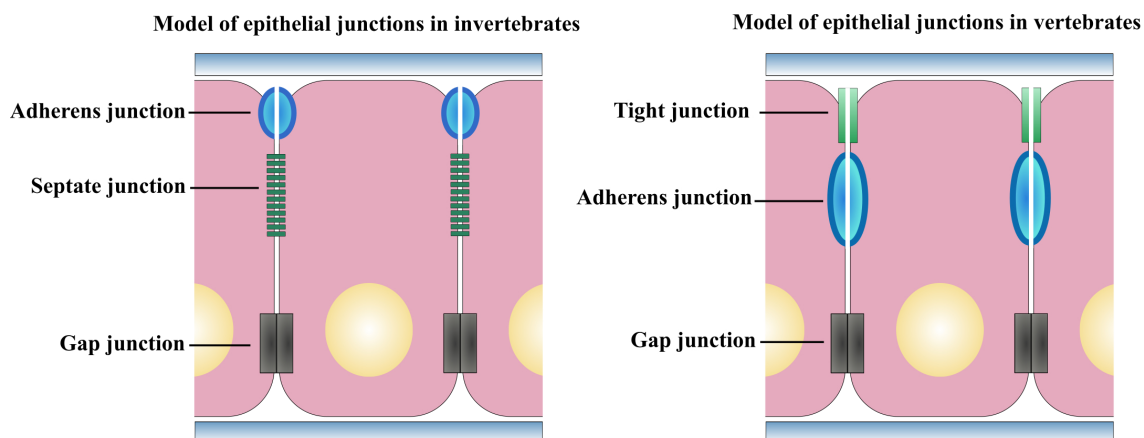


Figure 1.1 Schematic representation of cell-cell contacts of invertebrates and vertebrates. Comparison of an invertebrate (left) and vertebrate (right) epithelial cell. In invertebrates SJs are localized basal to the AJs. TJs are the apical-most junctional structure in vertebrates.

TJs are the apical-most type in an epithelial vertebrate cell. In contrast to vertebrates, SJ in invertebrates are basal to the AJs (Fig. 1.1). Gap-junctions are the most basal junctional complexes in both vertebrates and invertebrates.

The *Drosophila* embryo is particularly suited for the analysis of epithelial tissues. It undergoes major developmental changes within hours making faulty processes easily to be observed. Also, the toolkit for genetic manipulation of *Drosophila* has grown over the past decades, providing an almost ideal model organism to gain further insight into epithelial processes.

In *Drosophila* several proteins involved in the establishment or maintenance of SJs have been identified. Some of the SJ associated proteins are membrane proteins containing extracellular motifs, which indicate cell- adhesion (Izumi and Furuse, 2014).

SJ assembly starts at stage 12 (staging according to Campos-Ortega and Hartenstein, 1985) of embryonic development, where most SJ proteins are membrane bound and localize along the lateral membranes of epithelial cells (Fig. 1.2 stage 12).

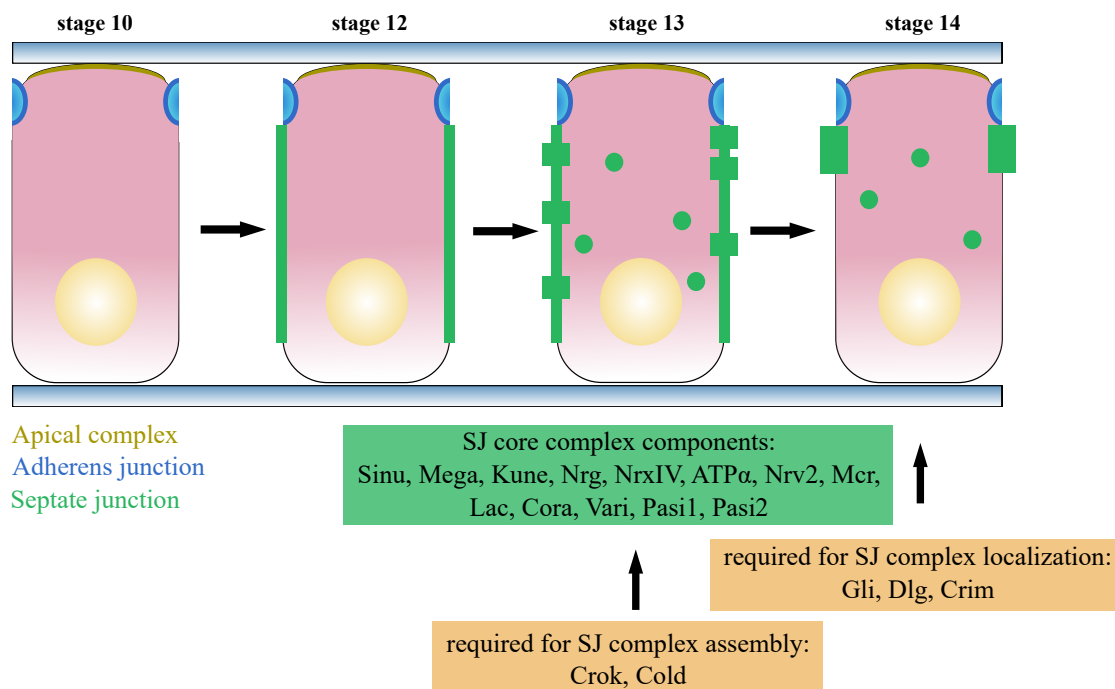


Figure 1.2 Timeline and key components of SJ maturation.

The SJ complex consists of a small group of core components (highlighted in green). Crok and Cold are required for assembly of complexes during stage 13, whereas exocytic trafficking and the SJ protein Gli and Dlg are essential for complex relocalization during stage 14. Modified from Oshima and Fehon, 2011.

Later, during stage 13 (Fig. 1.2 stage 13), some SJ proteins co-localize with early endosomal markers, indicating a trafficking and rearrangement at the lateral membrane

(Tiklová et al., 2010). A progressive enrichment of SJ proteins at the apical lateral side of the membrane is observed during embryonic stages 14 (Fig. 1.2 stage 14) and 15, whereas at stage 16, SJ proteins tightly localize at the very most apical region of the lateral membrane (Oshima and Fehon, 2011).

SJ are multiprotein complexes consisting of several known proteins in *Drosophila*. A highly stable subcomplex, referred to as SJ core complex, is found within the SJ protein complex. Disturbance of the core complex leads to disassociation of the remaining core components along the lateral cell membrane. The core complex includes the transmembrane proteins Sinuous (Sinu; Wu et al., 2004), Megatrachea (Mega; Behr et al., 2003), Kune-kune (Kune; Nelson et al., 2010), Neuroglian (Nrg; Genova and Fehon, 2003), NeurexinIV (NrxIV; Baumgartner et al., 1996), Na⁺/K⁺-ATPase alpha-subunit (ATP α ; Genova and Fehon, 2003; Paul et al., 2003), Nervana2 (Nrv2, Na⁺/K⁺-ATPase beta-subunit; Paul et al., 2003), Macroglobulin complement-related (Mcr; Batz et al., 2014), Pasiflora 1 and Pasiflora 2 (Pasi1 and Pasi2; Deligiannaki et al., 2015), the GPI-anchored protein Lachesin (Lac; Llimargas et al., 2004) and the cytoplasmatic proteins Coracle (Cora; Fehon et al., 1994) and Varicose (Vari; Moyer and Jacobs, 2008; Figure 1.2). These cytoplasmatic proteins are members of the 4.1 protein family, which is also known as the FERM-domain (Protein4.1, Ezrin, Radixin and Meosin) family that plays key roles in interconnection of the SJ to the cytoskeleton. Vari is essential for SJ formation and binds directly to the C-terminus of NrxIV *via* the PDZ-binding domain. During organogenesis, Cora forms complexes with ATP α and NrxIV, which is essential for epithelial cell polarity (Laprise et al., 2009).

SJ complex assembly depends upon core complex associated proteins including Coiled (Hijazi et al., 2011) and Crooked (Crok). It is suggested that Crok localizes in intracellular vesicles to assist the cell membrane localization of SJ components (Nilton et al., 2010).

The tumor suppressor Discs large (Dlg; Woods and Bryant, 1991), Gliotactin (Gli; Schulte et al., 2003) and Barkbeetle (Bark; Hildebrandt et al., 2015), also known as Anaconda (Byri et al., 2015), are required for SJ complex localization. Bark is a putative transmembrane scavenger receptor-like protein, which is essential for the maturation and correct localization of the SJ complex during stage 16 and 17 during *Drosophila* embryogenesis. During these stages and further development of the embryo, major recycling, trafficking and cell rearrangement events occur to position the SJ complex at novel cell membrane locations. It is proposed that Bark shuttles from sites of SJ breakdown to sites of SJ assembly *via* recycling endosomes. However, Bark is not required for the establishment of the SJ complex during embryonic stage 13 (Hildebrandt et al., 2015).

One major protein class important for SJ integrity are claudins (PMP22/ EMP/ MP20/ claudin family). In *Drosophila* three claudins, Mega, Sinu and Kune (Behr et al., 2003; Wu et al., 2004; Nelson et al., 2010) have been identified. All three claudins show expression in ectodermally derived tissues, such as the hindgut, trachea, epidermis and salivary gland and are essential for the establishment of the SJ complex and the formation of a functioning paracellular barrier. Similar to vertebrate claudins, invertebrate claudins consist of 2 extracellular loops (ECL1, ECL2), one intracellular loop (ICL), four transmembrane domains and cytoplasmic termini as is depicted in Figure 1.3. Additionally, invertebrate claudins include the highly conserved G-L-W-C-C motif and a PDZ-binding domain (Fig. 1.3) at the C-terminus. However, the function of the G-L-W-C-C motif and the PDZ-binding domain remains unclear in invertebrates. Moreover, no specific functional analysis was reported for ECL1, ECL2 and ICL in invertebrates.

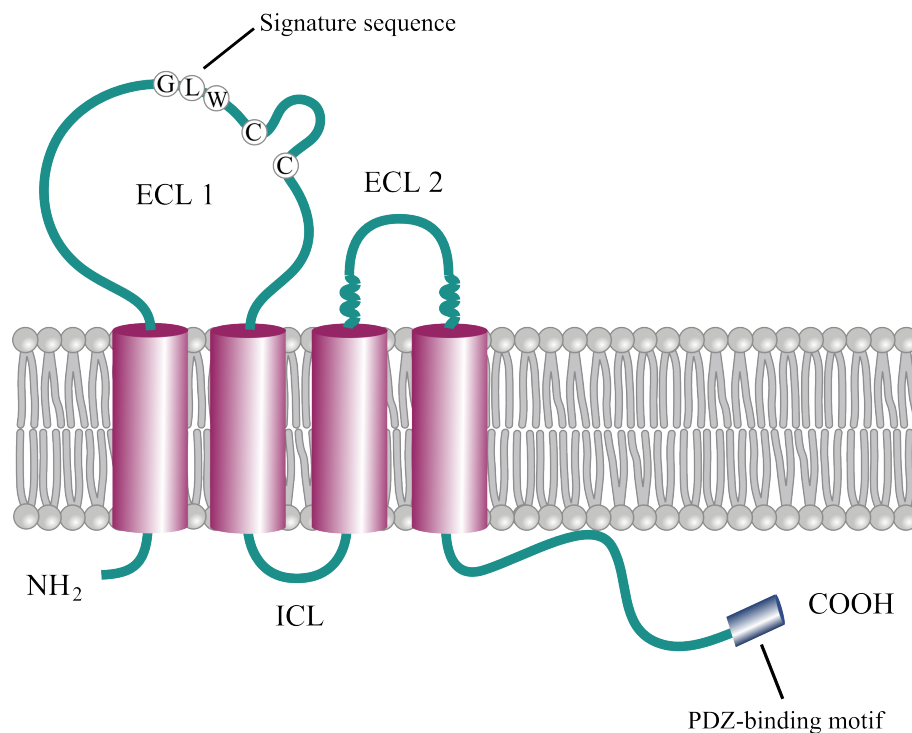


Figure 1.3 Claudin structure of vertebrates and invertebrates.

Claudins are transmembrane proteins consisting of four transmembrane domains (pink), two extracellular loops (ECL1 and ECL2), one intracellular loop (ICL) and cytoplasmic N- and C-termini (all in turquoise). The signature sequence GLW-C-C is found in the ECL1, whereas the PDZ-binding motif (blue) is established at the 3' end of the C-terminus. Modified from Günzel and Yu, 2013.

The exocytosis of the chitin modifying enzymes Serpentine and Vermiform (Luschnig et al., 2006) is another crucial process mediated by the SJs. Serpentine as well as Vermi-

form are required for a normal fibrillar chitin structure in the tracheal lumen. Also, SJ components are interdependent on SJ protein localization. Mutations in SJ components lead to mislocalization of the remaining SJ components alongside the lateral cell membrane and to an impaired barrier function (Behr et al., 2003; Nelson et al., 2010).

1.4 The tracheal epithelium of *Drosophila melanogaster*

The tracheal epithelium is a tubular network formed by a distinct number of cells, allowing oxygen to enter passively into the organism. Tracheal organogenesis has been investigated to some extent, however, some underlying mechanisms are still poorly understood.

Tracheal development starts during the second half of embryonic development, originating from 10 so-called tracheal placodes on each side of the embryo, that are formed by the invaginating epidermal cells. 80 cells are found in each placode during embryonic stage 11. No further cell division occurs during subsequent development of the tracheal system, implicating that further development is solely depending on the expansion and intercalation of tracheal cells (Kondo and Hayashi, 2013).

During the following tracheal organogenesis, major branching events occur including primary and secondary branching, branch fusion and terminal branch formation. The primary branching is initiated by *Drosophila* Branchless (FGF-) signaling, stimulating six primary branches to develop from each tracheal placode. The main multicellular tube of the trachea ("dorsal trunk") is formed by migration, rearrangement, elongation and intercalation of cells within the primary branch (Affolter and Shilo, 2000; Samakovlis et al., 1996). Further intercalation and rearrangement events at the ends of primary branches give rise to the secondary branches, that are formed by one single cell wrapped around the tracheal lumen. In addition, specialized tracheal cell, the so-called terminal cells, form several terminal branches. The terminal cells develop cytoplasmatic extensions with narrow lumina, supplying connected tissues with oxygen. The number of terminal branches is variable and determined by the oxygen demand of the target tissue (Samakovlis et al., 1996; Ribeiro et al., 2004).

Fusion and intercalation events are essential to provide a connection between the 20 tracheal placodes and the establishment a functional tracheal network spanning the embryo with one continuous tracheal lumen. The length and diameter of the lumen are determined by the structure and modification of the apical extracellular matrix. One crucial event for the control of tube diameter is the deposition of chitin into the lumen (Tønning et al., 2005). A complex taenidial matrix and a continuous chitin cable are formed by chitin itself as well as chitin associated proteins. The chitin cable is degraded in the tubes before larval

hatching.

The tracheal network length is controlled by two chitin modifying enzymes, Vermiform and Serpentine, whose exocytosis into the lumen is dependent on SJs (Luschnig et al., 2006). The lack of both chitin modifying enzymes leads to morphological defects of the tracheal network, represented by highly elongated and convoluted tubes, in contrast to straight branches in wild-type embryos (Behr et al., 2003; Nelson et al., 2010). Lack of mature SJs leads to impaired exocytosis, resulting in the accumulation of Vermiform and Serpentine in the tracheal cells. The tubes size is regulated by the SJ proteins Cora, Scribble and Yurt, which modulate the localization of the apical membrane protein Crumbs (Laprise et al., 2010).

At the end of embryogenesis, essential endocytosis and modification events occur clearing the tracheal lumen of solid contents and providing essential stabilizing structures (taenidial folds) that prevent luminal collapse (Tsarouhas et al., 2007). After the liquid clearance (LC) of the tubular network, the lumen is filled with an uncharacterized gas. When SJs are impaired, no functioning barrier is established between neighboring cells, leading to a disturbed gas-filling process and persistent liquid inside the tracheal lumen (Ile et al., 2012).

2 Aim of this thesis

The generation of various synthetic mutants of the *Drosophila* claudin Mega should lead to the investigation of functional protein domains critical for epithelial barrier function, protein trafficking and localization as well as tracheal morphogenesis. Furthermore, co-immunoprecipitation followed by mass spectrometry of the Mega protein complex will be used to identify and characterize novel SJ components.

3 Results

3.1 Protein domain analysis of the claudin Megatrachea

SJs represent cell junctions essential for establishing the transepithelial barrier. Providing a wide variability of tightness in different organs, the composition of SJ may vary from tissue to tissue and protein binding partners may exhibit a lower degree of binding tightness. In addition, SJ not only establish the epithelial barrier function, but also mediate other processes, such as the endocytosis of Serpentine and Vermiform into the tracheal lumen during organogenesis (Luschnig et al., 2006).

Claudins were shown to play key roles in the establishment and maintenance of SJs in vertebrates and invertebrates. In *Drosophila*, the claudin Megatrachea (Mega) was identified in 2003 (Behr et al., 2003). Mega shows all claudin-defining features described in section 1.3.1. To investigate, which protein domains may contribute to SJ complex formation and/or exocytosis, Mega was used as a model to sequentially mutate its protein domains and to analyze the mutated Mega *in vivo*.

3.1.1 Generation of synthetic *mega* mutant lines

In a first step the *Drosophila* allele *mega^{attP}* was generated, which carries an *attP* site at the deleted endogenous *mega* locus. The *attP* site allows fast and direct recombination with *attB* site containing DNA constructs after DNA injection into the corresponding embryos (Keravala and Calos, 2008). The generation of the *mega^{attP}* line is depicted in Figure 3.1. To establish the *mega^{attP}* allele, DNA regions flanking the *mega* gene were cloned into the *pGX-attP* vector, which contains the *white⁺* marker, *loxP* sites and the *attP* site. This construct was injected into *Drosophila* embryos. Flies with randomly integrated vector DNA were selected by appearance of the *white* marker. By crossing *white⁺* flies with *Flp* recombinase and its ubiquitous expression by Ubi-Gal4, the construct is mobilized and may integrate into the *mega* locus *via* the homologous regions (Fig. 3.1 A). Constructs that stay in the original integration site express Reaper (mediated by Ubi-Gal4), which causes lethality of the corresponding animals. Integration into the *mega* locus was confirmed by sequencing. Correct lines were balanced with the X-chromosomal balancer *FM7i*.

3.1 Protein domain analysis of the claudin Megatrachea

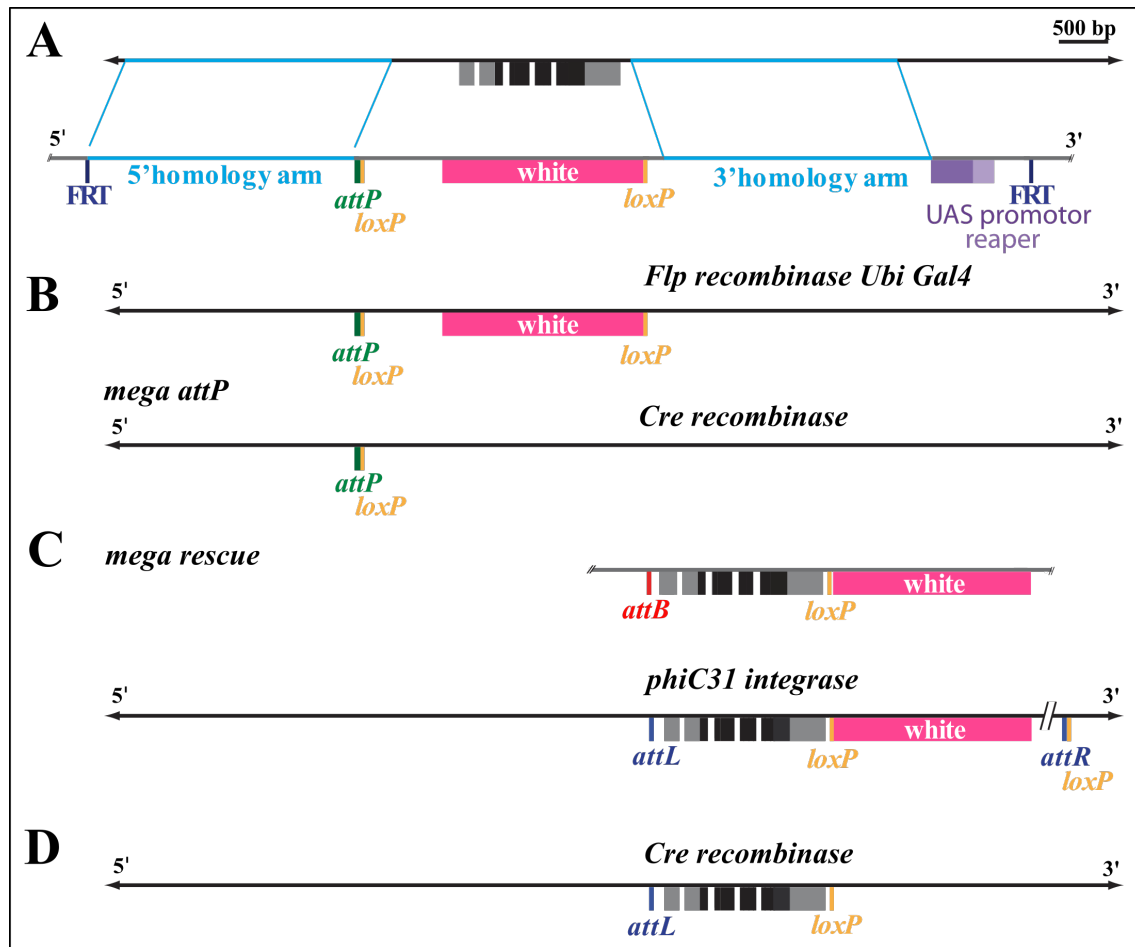


Figure 3.1 Generation of the *mega*^{attP} allele.

(A) Schematic representation of the *mega* genomic DNA region and the donor vector containing two homology arms (blue), the *white* gene, the *attP* site and two *loxP* sites. After random integration into the *Drosophila* genome the donor construct was mobilized with *Flp* recombinase. Additionally, *Ubi-Gal4* was expressed to eliminate immobilized constructs. (B) *mega* genomic region after homologous recombination (top) and Cre recombinase-mediated *white* gene excision (bottom). (C) Donor vector for *phiC31*-integrase mediated integration (top) and generation of *white*⁺, mega rescue allele (bottom). (D) *mega* rescue allele after Cre recombinase-mediated *white* gene excision.

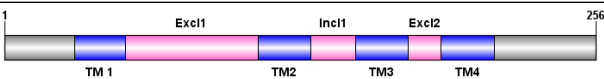
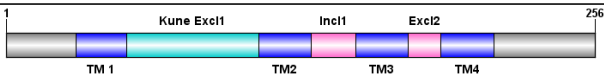
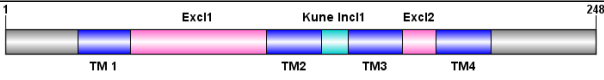
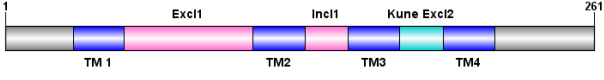
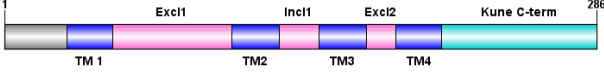
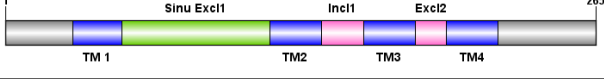
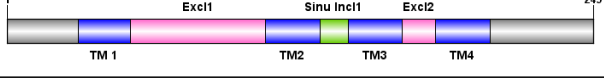
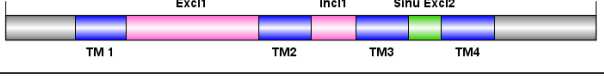
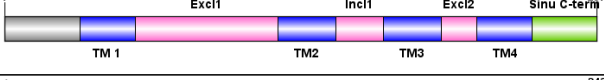
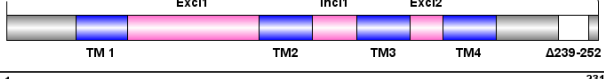
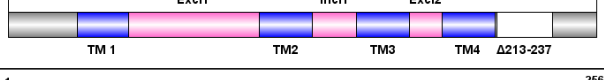
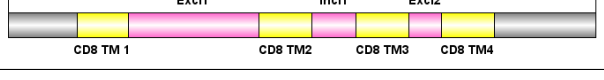
Crossing *white*⁺ flies to Cre recombinase expressing flies deletes the *white*⁺ marker, which is flanked by *loxP* sites, leaving the *attP* site and a *loxP* site (Fig. 3.1 B). *mega*^{attP} mutant embryos show the *mega* lack-of-function phenotype, i.e. elongated tracheal branches, lack of tracheal gas filling and embryonic lethality. The mutant *mega*^{attP} line was used for direct integration of rescue and synthetic *mega* constructs.

To rescue the *mega* phenotype, which includes the elongation of the main breathing tube (dorsal trunk), the wild-type *mega* locus was amplified *via* PCR from the *w*¹¹¹⁸ line. The locus was cloned into the *pGE-attB* vector, following injection of the rescue construct into the *mega*^{attP} line (Fig. 3.1 C). A vector coding for the *phiC31* integrase was co-injected

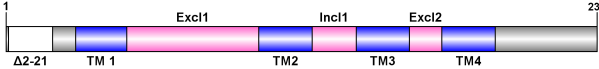
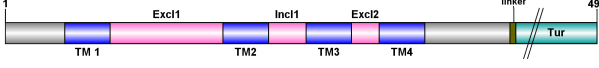
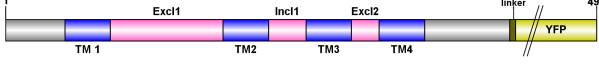
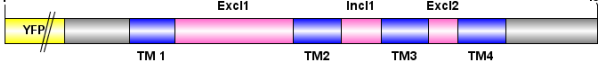
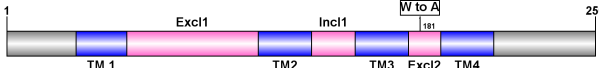
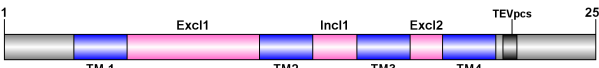

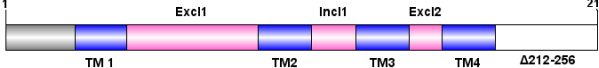
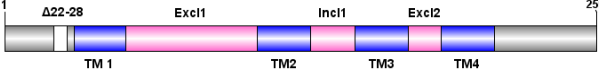
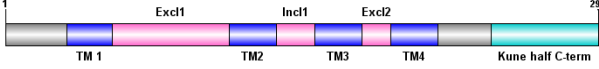
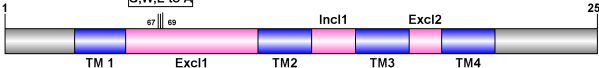
to mediate recombination between *attP* and *attB* sites. The integration marker *white*⁺ was crossed out using a *Cre* recombinase expressing line (Fig. 3.1 D). Homozygous *mega*^{attP}-*mega* rescue flies are viable and fertile, indicating no essential mutations outside the *mega* locus in the *mega*^{attP} line.

Similar injection/crossing approaches were used to alter different domains of the coding *mega* locus and the resulting mutant lines were analyzed *via* immunohistological staining (sec. 5.4.3) and the barrier function was investigated *via* Texas[®]-Red injections (sec. 5.6.1).

69 synthetic *mega* mutant constructs were generated, exhibiting mutations at distinct Mega domains. The generated synthetic mutant lines are categorized in three groups: 1. domain swaps with domains of claudin Sinuous or Kune-kune, 2. point mutations at evolutionary conserved positions and 3. deletions of differently sized protein fragments. Mutated protein schemes are summarized in Table 3.1.

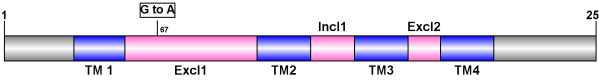
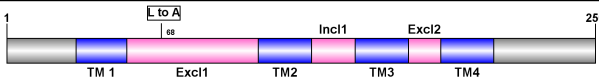
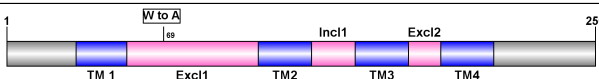
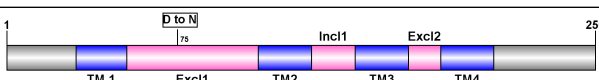
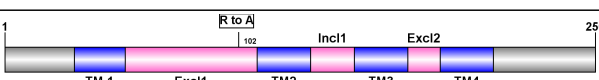
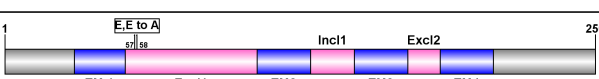
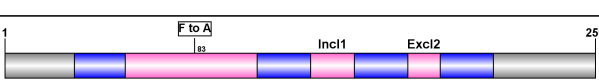
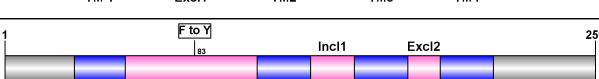
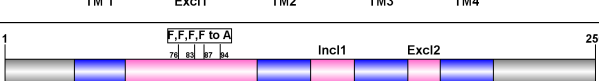

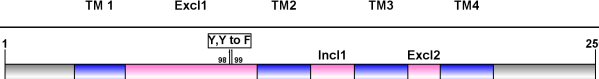
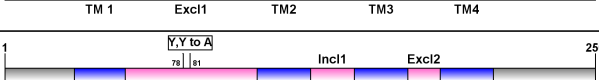



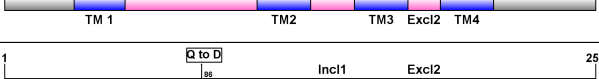
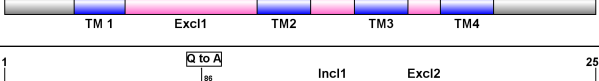

ID	Construct scheme	V	ML	DT	LC	BF
M0		yes	wt	wt	yes	yes
M1		no	mi	el	no	no
M2		no	mi	el	no	no
M3		no	mi	el	no	no
M4		no	mi	el	no	no
M5		no	mi	el	no	no
M6		no	mi	el	no	no
M7		no	mi	el	no	no
M8		yes	wt	wt	yes	yes
M9		yes	wt	wt	yes	yes
M10		yes	wt	wt	yes	yes
M11		no	mi	el	no	no

3.1 Protein domain analysis of the claudin Megatrachea

ID	Construct scheme	V	ML	DT	LC	BF
M12		yes	wt	wt	yes	yes
M13		yes	wt	wt	yes	yes
M14		yes	wt	wt	yes	yes
M15		yes	wt	wt	yes	yes
M16		no	mi	el	no	no
M17		yes	wt	wt	yes	yes
M18		no	mi	el	no	no
M19		yes	wt	wt	yes	yes
M20		yes	wt	wt	yes	yes
M21		yes	wt	wt	yes	yes
M22		yes	wt	wt	yes	yes
M23		yes	wt	wt	yes	yes
M24		no	mi	el	no	no
M25		yes	wt	wt	yes	yes
M26		yes	wt	wt	yes	yes
M28		yes	wt	wt	yes	yes
M30		no	mi	el	no	no
M31		no	mi	el	no	no

ID	Construct scheme	V	ML	DT	LC	BF
M32		no	mi	el	no	no
M33		no	mi	el	no	no
M35		yes	wt	wt	yes	yes
M36		yes	wt	wt	yes	yes
M37		yes	wt	wt	yes	yes
M38		no	mi	el	no	no
M39		yes	wt	wt	yes	yes
M40		yes	wt	wte	yes	yes
M41		no	mi	el	no	no
M42		no	mi	el	no	no
M43		no	mi	el	no	no
M45		yes	wt	wt	yes	yes
M46		no	mi	el	no	no
M47		no	mi	el	no	no
M48		yes	wt	wt	yes	yes
M49		yes	wt	wt	yes	yes
M50		yes	wt	wt	yes	yes
M51		yes	wt	wt	yes	yes

3.1 Protein domain analysis of the claudin Megatrachea

ID	Construct scheme	V	ML	DT	LC	BF
M52		no	mi	el	no	no
M53		no	mi	el	no	no
M54		no	mi	el	no	no
M55		yes	wt	wt	yes	yes
M56		yes	wt	wt	yes	yes
M57		no	mi	el	no	no
M58		yes	wt	wt	yes	yes
M59		yes	wt	wt	yes	yes
M60		yes	wt	wt	yes	yes
M61		yes	wt	wt	yes	yes
M62		yes	wt	wt	yes	yes
M63		yes	wt	wt	yes	yes
M64		yes	wt	wt	yes	yes
M65		yes	wt	wt	yes	yes
M66		yes	wt	wt	yes	yes
M67		yes	wt	wt	yes	yes
M68		yes	wt	wt	yes	yes
M69		yes	wt	wt	yes	yes

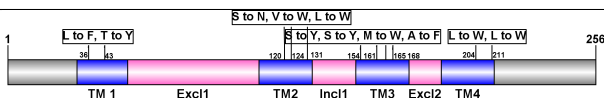
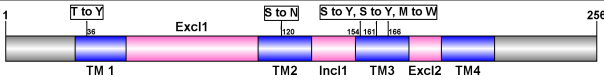
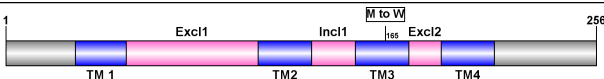
ID	Construct scheme	V	ML	DT	LC	BF
M70		no	mi	el	no	no
M71		no	mi	el	no	no
M72		no	mi	el	no	no

Table 3.1 Summary of generated synthetic *mega* mutant fly lines

Abbreviations: ID: Identification number of Mega construct, V: viability, ML: Mega localization, DT: dorsal trunk, LC: liquid clearance, BF: barrier function, el: elongated dorsal trunk, mi: Mega mislocalized, wt: wild-type.

All synthetic Mega constructs were confirmed by sequencing after integration into the fly genome. 41 homozygous mutations led to viability (V; Tab. 3.1). Stage 17 embryos of viable *mega* mutations reveal a wild-type-like tracheal network formation, wild-type-like liquid clearance (LC) and a wild-type-like barrier function. These results indicate that the viable *mega* mutant fly lines develop a normal tracheal system and functioning SJs. Unexpectedly, all 28 homozygous lethal *mega* mutant lines, which include many mutants with only a single amino acid exchange, reveal a lack-of-function *mega* phenotype and display intracellular Mega mislocalization. Therefore, interaction analysis of mutated Mega with SJ components within the lateral cell membrane was not possible.

For a more detailed analysis lethal lines with mutations in the various Mega loop and terminal regions were chosen. In M30 the highly conserved GLW motif of the 1st extracellular loop (ECL) was substituted by three alanines. This motif was shown to be essential for claudin function in vertebrates (Krause et al., 2008). In M33 six amino acids were substituted by alanine to disturb the function of the intracellular loop (ICL). In M18 four aromatic amino acids of the 2nd extracellular loop (ECL) were substituted by alanine. It was proposed that aromatic amino acids form homophilic *trans*- interactions of two 2nd ECLs (Krause et al., 2008). In M24 the entire C-terminus of Mega was deleted. Control embryos (heterozygous embryos from *mega* mutant lines) and embryos with homozygous *mega^{attP}*, in which the *mega* locus is deleted, were analyzed for comparison with the synthetic *mega* mutant constructs.

3.1.2 Mega mutations in the 2nd extracellular loop reveal wild-type-like Mega localization in the hindgut epithelium

To investigate Mega hindgut localization in the synthetic mutant embryos, anti-Mega immunohistochemical stainings of the representative lines are depicted in Figure 3.2.

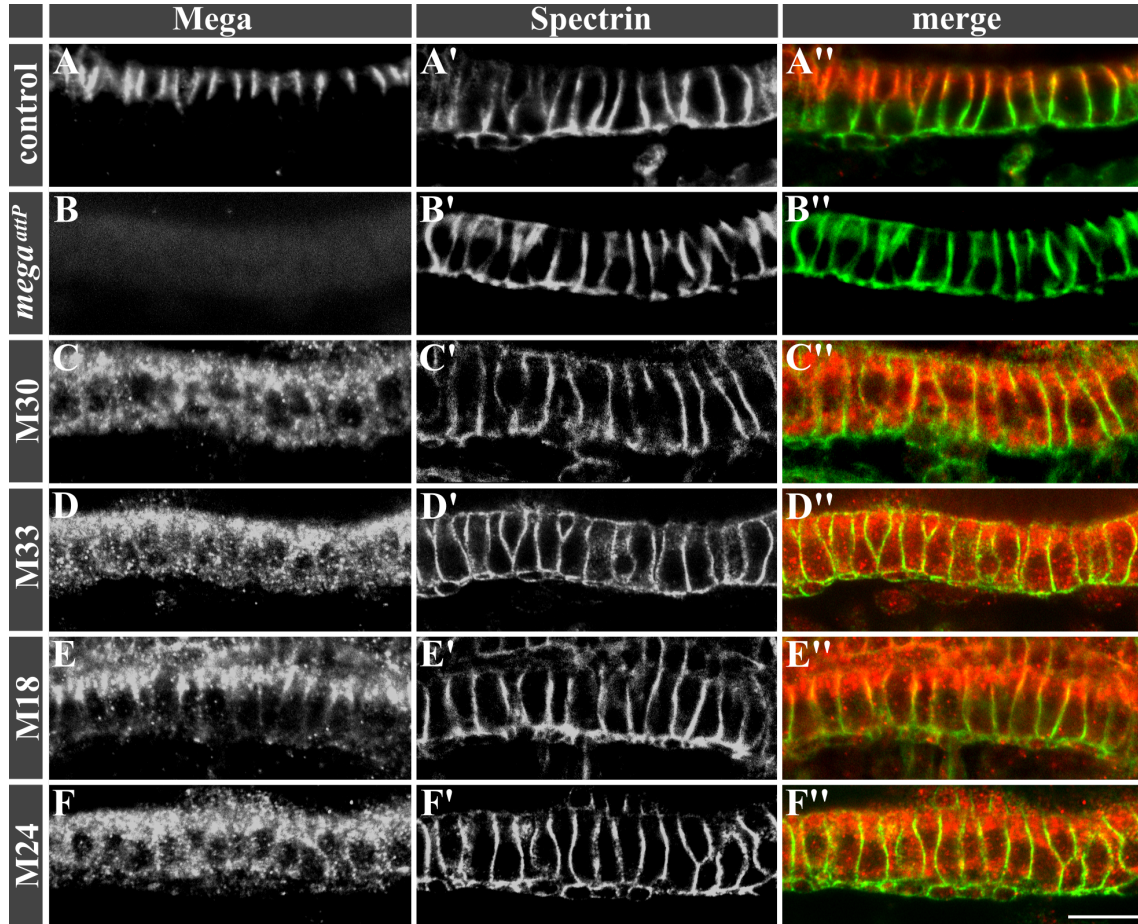


Figure 3.2 Localization of Mega in the hindgut epithelium of representative *mega* mutant lines.

Confocal images of double antibody staining in homozygous embryos of stage 16 control (A-A''), *mega^{attP}* (B-B'') and synthetic *mega* mutant constructs M30 (C-C''), M33 (D-D''), M18 (E-E'') and M24 (F-F'') embryos with anti-Mega antibody (A, B, C, D, and F) and anti-Spectrin (membrane marker) antibody (A', B', C', D', E' and F'). A'', B'', C'', D'', E'' and F'' represent the merged channels. In constructs with affected 1st ECL (M30), ICL (M33) and C-terminus (M24) Mega is mislocalized in cytoplasmic vesicles in the epithelial cells. In M18, where the 2nd ECL is affected, Mega is predominantly localized wild-type-like in apicolateral membrane regions. Scale bar indicates 10 μ m.

In the control hindgut epithelium, Mega is localized at apical-most lateral part of the lateral membrane (Fig. 3.2 A). The membrane marker Spectrin was used to visualize the epithelial cells membranes (Fig. 3.2 A', B', C', D', E' and F'). In *mega^{attP/attP}* control

embryos Mega is not detectable *via* immunofluorescence (Fig. 3.2 B), whereas embryos with constructs affecting the first ECL (M30), 2nd ECL (M33) and C-terminus (M24) reveal Mega localization within the cytoplasm including a punctated pattern (Fig. 3.2 C, D and F). The punctated pattern suggests a Mega localization within vesicles, possibly endoplasmatic reticulum (ER) and/or lysosomes. In M18 however, in which the 2nd ECL is affected, Mega is partially localized wild-type-like in the apico-lateral cell membrane (Fig. 3.2 E). These results suggest that the 1st ECL, ICL as well as the C-terminus of Mega are essential for a normal Mega localization in the hindgut epithelium, while the 2nd ECL seems not to be essential for a apico-lateral cell membrane localization of Mega.

3.1.3 Dlg and Kune show wild-type-like localization in mutant embryos affecting the 2nd extracellular loop

Mega is part of the SJ protein complex and thus, the SJ component Dlg was analyzed in order to test the SJ integrity in the various Mega domain mutant embryos.

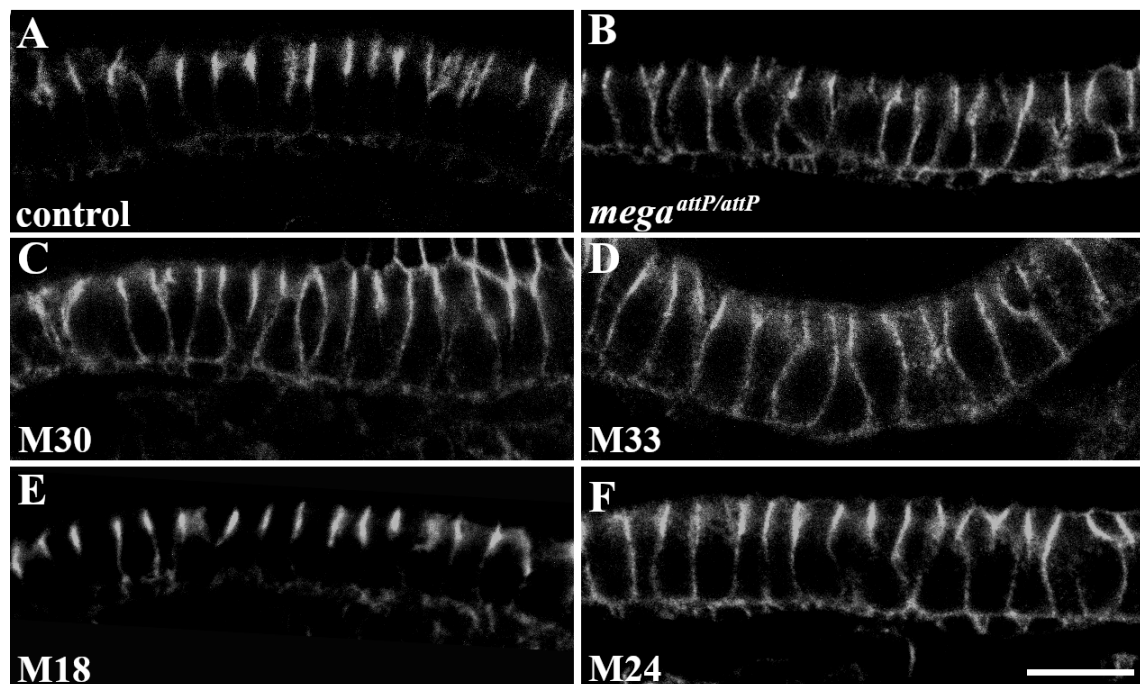


Figure 3.3 Localization of Dlg in different *mega* mutant embryos.

Confocal images of hindgut antibody stainings of Dlg in stage 16 control (A), *mega*^{attP/attP} (B), M30 (C), M33 (D), M18 (E) and M24 (F) mutant embryos. In the control hindgut epithelium Dlg is localized apicolaterally, whereas mislocalization along the lateral membrane is observed in *mega*^{attP/attP} embryos as well as in mutant embryos affecting the 1st ECL (M30), ICL (M33) and the C-terminus (M24). Dlg is localized wild-type-like in construct M18 embryos, where the 2nd ECL is affected. Scale bar indicates 10 μ m.

3.1 Protein domain analysis of the claudin Megatrachea

In control embryos, Dlg is localized at its normal apico-lateral position of hindgut epithelial cells (Fig. 3.3 A). In *mega^{attP/attP}* (Fig. 3.3 B), Dlg is mislocalized along the lateral cell membrane, indicating disrupted SJ. Similar Dlg mislocalization is observed in homozygous mutant embryos affecting the 1st ECL (M30), ICL (M33) as well as the C-terminus (M24; Fig. 3.3 C, D and F). However, in homozygous M18 construct embryos, affecting the 2nd ECL, Dlg is localized wild-type-like at apicolateral positions in epithelial cells of the hindgut (Fig. 3.3 E). This suggests, that SJ protein complexes are formed wild-type-like in mutant embryos affecting the 2nd ECL (M18).

To confirm wild-type localization of SJ core components, an immunofluorescence staining was performed using an antibody against the claudin Kune. In the control embryo hindgut epithelium as well as in the hindgut epithelium of M18 mutant embryos Kune is localized apicolaterally in hindgut cells (Fig. 3.4 A and B). Spectrin marks cell membranes (Fig. 3.4 A' and B') and merges are depicted in (Fig. 3.4 A'' and B''). This finding indicates a wild-type-like formation of the SJ complex in the hindgut epithelium of embryos, in which the 2nd ECL is affected.

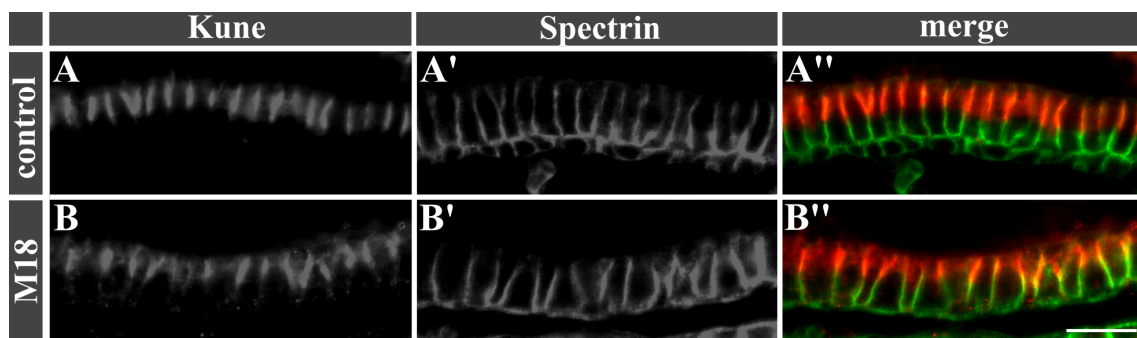


Figure 3.4 Localization of Kune in M18 mutant embryos.

Confocal images of stage 16 hindgut epithelium in double immunohistological staining using anti-Kune and anti-Spectrin antibody in stage 16 control (A-A'') and M18 mutant embryos (B-B''). In the control hindgut epithelium (A) and M18 hindgut epithelium, where the 2nd ECL is affected (B), Kune is localized apicolaterally. Spectrin (A' and B') marks cell membranes. A'' and B'' show merged channels. Scale bar indicates 10 μ m.

The finding that embryos with an affected 2nd ECL of claudin Mega may form normal SJ in the hindgut epithelium was unexpected, since such embryos reveal lack of LC and elongation of the tracheal branches, indicative of affected SJs. Thus, SJ formation and SJ function was analyzed in the tracheal system of M18 mutant embryos in more detail. In a first step localization of mutated Mega (M18) and the SJ marker Kune were analyzed. In the control tracheal epithelium Mega is localized apicolaterally in epithelial tracheal cells (Fig. 3.5 A). However, in construct M18 mutant embryos Mega is mislocalized in vesicles

filling the cells' cytoplasm (arrow in Fig. 3.5 B).

Also, the SJ marker Kune is localized at the apical-most position in the cells of the control tracheal epithelium (Fig. 3.5 C), similar to Mega localization. However, in M18 mutant embryos Kune is mislocalized along the lateral cell membrane (Fig. 3.5 D).

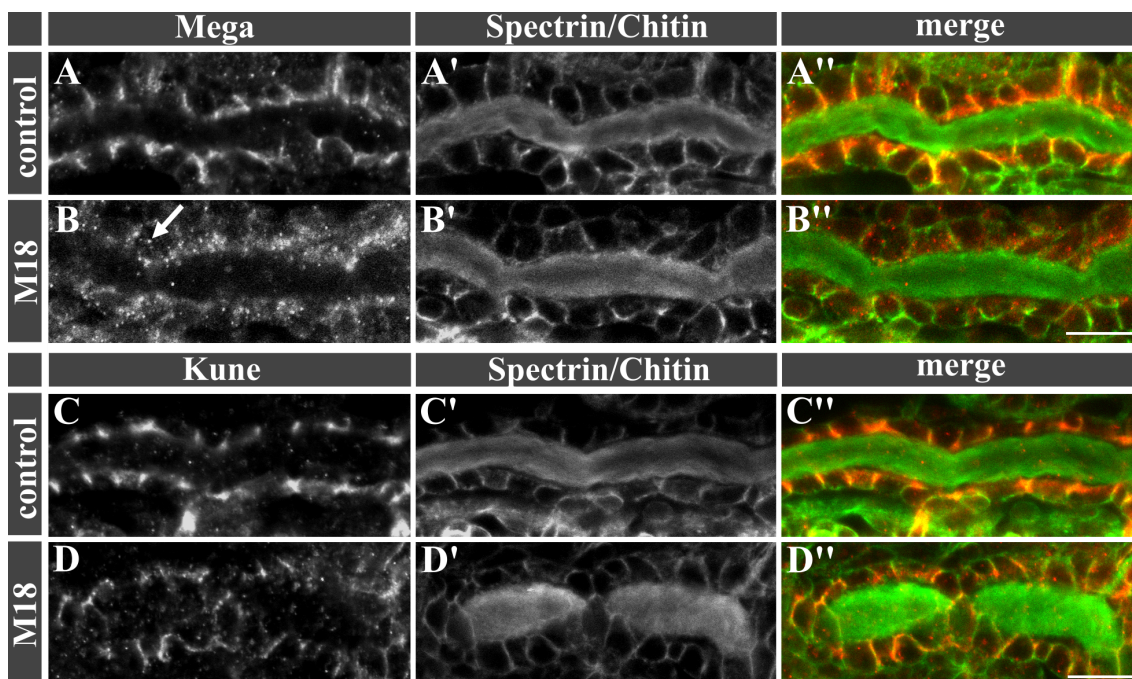


Figure 3.5 Tracheal localization of Mega and Kune in M18 mutant embryos.

Confocal images of dorsal trunks in double antibody staining using anti-Mega and anti-Spectrin antibody (A-B'') or anti-Kune and anti-Spectrin antibody (C-D'') in stage 15 control (A-A'' and C-C'') and mutant M18 (B-B'' and D-D'') embryos. In the control tracheal epithelium of the Mega staining Mega is localized apicolaterally (A), whereas in M18 mutant embryos Mega is mislocalized in cytoplasmic vesicles (arrow in B). In control tracheal epithelium of the Kune staining Kune is localized apicolaterally (C), but in the M18 tracheal epithelium Kune is mislocalized along the lateral cell membrane (D). Spectrin staining visualizes the tracheal cell membranes, whereas chitin marks the tracheal lumen (A', B', C' and D'). A'', B'', C'' and D'' show merged channels. Scale bar indicates 10 μ m.

These findings indicate that the SJ assembly and SJ marker localization is impaired in the tracheal epithelium of M18 mutant embryos. In such embryos elongated tracheal tubes and no LC was detected at the end of embryogenesis (see Tab. 3.1 M18). In order to investigate whether an epithelial barrier function is established in M18 mutant embryos, injection experiments with Texas[®] Red Dextran were performed.

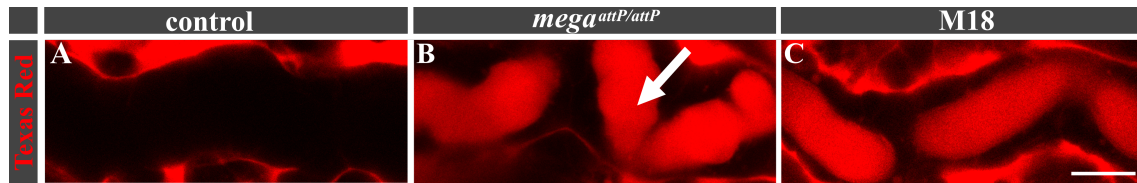


Figure 3.6 Epithelial barrier function is defective in M18 mutant embryos. Confocal images of tracheal dorsal trunks of stage 16 control (A), *mega^{attP/attP}* (B) and M18 (C) mutant embryos. In control embryos the fluorescent dye cannot pass through the tracheal epithelium and the tracheal lumen remains colorless (A). In *mega^{attP/attP}* mutant embryos the epithelial barrier is impaired and cannot prevent the dye from passing into the tracheal lumen (arrow in B). A defective epithelial barrier is also observed in M18 mutant embryos leading to red fluorescence inside the tracheal lumen. Scale bar indicates 10 μ m.

In control embryos, the fluorescent dye cannot pass the intact epithelial barrier (Fig. 3.6 A). In *mega^{attP/attP}* mutant embryos the epithelial barrier is disrupted and the Texas[®] Red Dextran passes into the lumen of the dorsal trunk (arrow in Fig. 3.6 B). An impaired epithelial barrier is also observed for M18 mutant embryos, with affected 2nd ECL (Fig. 3.6 C). Although Mega as well as Dlg localize wild-type-like in the embryo hindgut epithelium of M18 mutant embryos, no barrier function is established in the tracheal system leading to dye filling of the tracheal lumen. The tracheal mislocalization of Mega and Kune suggests that the barrier defect is caused by disrupted SJs.

3.1.4 Exocytosis of Serpentine is affected in mutant M18 embryos

A main function of tracheal SJs is the exocytosis of Serpentine (Serp) and Vermiform (Verm) into the tracheal lumen. Serp and Verm are chitin modifying enzymes and determine the length of the breathing tubes during the embryogenesis of *Drosophila*. Both enzymes are deposited into the tracheal lumen from stage 13 onward. From stage 15 the deposition functions in a SJ dependent manner *via* exocytosis. Serp and Verm are removed from the tracheal lumen at late stage 16 of embryogenesis (Luschnig et al., 2006).

To investigate whether exocytic processes are affected in embryos carrying construct M18, immunohistological stainings (sec. 5.4.3) of Serpentine were performed (Fig. 3.7). For additional controls, Serp localization was analyzed in mutant embryos affecting the 1st ECL (M30), ICL (M33) as well as the C-terminus (M24). In stage 15 control embryos, Serp is deposited into the tracheal lumen and signal of Serp is detectable inside the tracheal lumen (Fig. 3.7 A). In contrast to control embryos, in *mega^{attP/attP}* embryos (Fig. 3.7 B) and M30 (Fig. 3.7 C), M33 (Fig. 3.7 D) and M24 (Fig. 3.7 F) mutant embryos Serp is localized inside the tracheal cells. Unexpectedly, Serp localizes inside the tracheal lumen in M18 mutant embryos (Fig. 3.7 E), indicating an at least partially functioning exocytosis.

These results indicate that exocytosis of Serp *via* SJs is partially mediated in M18 mutant embryos, suggesting no essential role of the 2nd ECL for exocytosis. Furthermore, these results indicate that exocytosis is mediated although barrier function and morphology of SJs are affected.

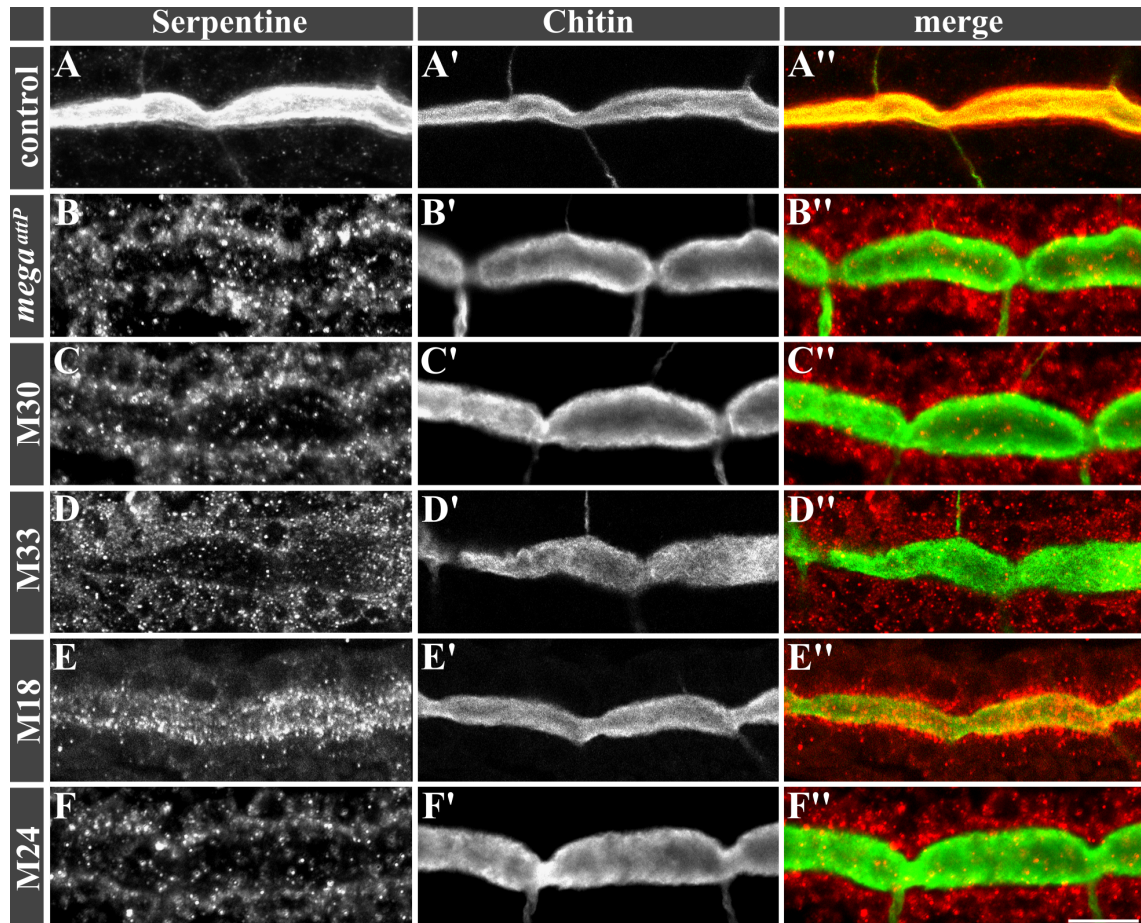


Figure 3.7 SJ mediated exocytosis is affected in tested Mega constructs.

Antibody staining of stage 15 wild-type (A-A'') embryos as well as *mega^{attP/attP}* (B-B''), M30 (C-C''), M33 (D-D''), M18 (E-E'') and M24 (F-F'') mutant embryos. A, B, C, D, E and F show the Serp staining, whereas A', B', C', D', E', and F' represent a chitin staining marking the tracheal lumen. A'', B'', C'', D'', E'' and F'' present merged channels. In control embryos Serp is deposited into the tracheal lumen (A). In mutant embryos affecting the 1st ECL (M30), ICL (M33) and the C-terminus (M24) exocytosis is impaired and Serp accumulates inside the tracheal cells. In M18 mutant embryos affecting the 2nd ECL an enrichment of Serp is observed inside the tracheal cells, however, Serp is also present inside the tracheal lumen, indicating exocytosis. Scale bar indicates 10 μ m.

3.2 Identification and characterization of *würmchen*

SJs mediate the main function of epithelial sheets by establishing the epithelial barrier and controlling the paracellular flow of ions and small molecules between neighboring cells. This barrier function allows the establishment of different physiological and chemical compartments within an organism. The SJ is a multi-protein complex, containing a core complex of at least 13 proteins and several SJ core associated proteins. During the past years, several novel SJ components have been identified (Deligiannaki et al., 2015; Hildebrandt et al., 2015). However, the defined protein composition of SJs in *Drosophila* remains puzzling.

3.2.1 Identification of Mega interaction partners *via* co-immunoprecipitation and mass spectrometry

In 2012, Jaspers et al. published a combined approach of immunoprecipitation and mass spectrometry to identify novel SJs components associated with the claudin Megatrachea (Mega; Behr et al., 2003). Bark and Crim were first identified in this approach (Jaspers et al., 2012). Due to recent advancements in the field of mass spectrometry (Kelstrup et al., 2018; Eliuk and Makarov, 2015), immunoprecipitation with the anti-Mega antibody followed by advanced mass spectrometry was performed in this work to identify novel Mega interactors, *i.e.* novel SJ components.

The anti-Mega antibody 1H10F7 is of high specificity in detecting native and denatured Mega, which makes it highly suitable for co-immunoprecipitation experiments (Jaspers et al., 2012). This method is based on the G-protein binding of anti-Mega antibody to magnetic beads and the recognition of Mega in embryo lysates by the anti-Mega antibody (detailed description in sec. 5.10.3). However, not only Mega may be bound by the antibody under the experimental conditions, but also other SJ components, which participate in the Mega protein complex. By mass spectrometry analysis of the bead-bound protein complex, novel SJ complex components may be identified.

In this work two approaches were chosen for co-immunoprecipitation:

In the first approach 100 *Drosophila* embryos staged 18-22 h were collected, encompassing the developmental stage where SJs are already established and functioning. Embryos were homogenized in 0.1 ml micro tissue grinders using 2% Nonidet P40 Substitute and 150 mM NaCl buffer. Dynabeads were prepared as described in section 5.10.2. 300 µl of 2% Nonidet P40 Substitute and 150 mM NaCl buffer and the embryo lysate were added to the beads and incubated at 4 °C over night. After incubation, four washing steps were performed with 0.1% Nonidet P40 Substitute and 600 mM NaCl buffer, in order to further denature the

protein complex. After the addition of SDS sample buffer, bound proteins were incubated at 99 °C for 10 min and loaded on a 4-20% SDS gel (BioRad). The gel was stained with Gelcode Blue staining reagent (Thermo Fisher Scientific) to visualize protein fragments. Entire PAGE lanes of immunoprecipitates as well as controls were in-gel digested and analyzed by mass spectrometry. Using 2% Nonidet P40 Substitute to solve membrane bound Mega, 857 potential Mega interactors were identified, including 2 known SJ proteins. However, in control experiments using anti-Flag antibody for immunoprecipitation, also several SJ components were identified, suggesting an unspecific binding of the antibody to transmembrane proteins. The results from this approach are not further discussed. However, the experiment was repeated using less stringent conditions.

In the second approach five main experimental steps were altered: 1. Nonidet P40 Substitute was used in a 0.1% concentration, 2. 3 x 100 embryos were used in 3 separate measurements, 3. washing steps occurred with 300 mM NaCl, 4. Protein complexes were trypsin-digested in solution and 5. liquid chromatography was performed before mass spectrometric measurements. Anti-Flag antibody for immunoprecipitation was used as control. In this approach 231 potential Mega interactors, including 17 known SJ components, were identified (label-free-quantification (LFQ) summarized in Tab. B.1). No SJ components were found to be enriched in control immunoprecipitation using anti-Flag antibody, allowing the conclusion that the binding in less stringent detergent conditions was more specific.

3.2.2 Expression and knockdown phenotypes of potential Megatrachea interaction partners

All 214 potential Mega interactors were screened for exclusive ectodermal and/or tracheal expression and, if available, protein localization (www.flybase.org, www.uniprot.org). Eight potential Mega interactors, except the known SJ components, and the corresponding coding genes were found, that reveal restricted ectodermal expression during embryonic development. To gain preliminary insight in the putative gene functions, trachea specific gene knockdowns of the eight potential Mega binding partners were performed using the UAS/Gal4 expression system and RNA interference (RNAi; *b1t*-Gal4 > RNAi). Results after tracheal knockdown are summarized in Tab. 3.2. Embryos resulting from tracheal specific knockdowns were staged and analyzed for viability, morphological phenotypes of the tracheal system and affected LC. *CG31195* and *CG9796* are lethal during pupation, but did not show an affected tracheal network formation in embryos. The tracheal knockdown of *CG13043*, *CG13063*, *CG10217*, *CG10206* and *CG12781* led to viable flies and showed

3.2 Identification and characterization of *würmchen*

a wild-type-like tracheal system. However, tracheal knockdown of *CG43780* is embryonic lethal, lacks LC and shows an abnormal tracheal network (see Fig. 3.8).

CG number	VDRC or BDSC ID	Viability after <i>btl</i> -Gal4 RNAi	TP	LC
<i>CG31195</i>	v104743	lethal during pupation	-	-
<i>CG9796</i>	b63015	lethal during pupation	-	-
<i>CG13043</i>	v102215	viable	-	-
<i>CG13063</i>	v14232	viable	-	-
<i>CG10217</i>	v38357	viable	-	-
<i>CG10206</i>	v330534	viable	-	-
<i>CG12781</i>	v27069	viable	-	-
<i>CG43780</i>	v100677	embryonic lethal	+	+

Table 3.2 Tracheal gene knockdown of potential Mega interactors.

Eight potential Mega interactors were identified in mass spectrometry analysis and tracheal knockdown was performed using *btl*-Gal4 and UAS-RNAi fly lines. Abbreviations: TP, tracheal phenotype; LC, impaired liquid clearance; VDRC, Vienna *Drosophila* Research Center; BDSC, Bloomington *Drosophila* Stock Center.

The tracheal knockdown of *CG43780* results in phenotypes reminiscent of phenotypes characteristic for SJ mutant embryos and thus the tracheal knockdown of *CG43780* was

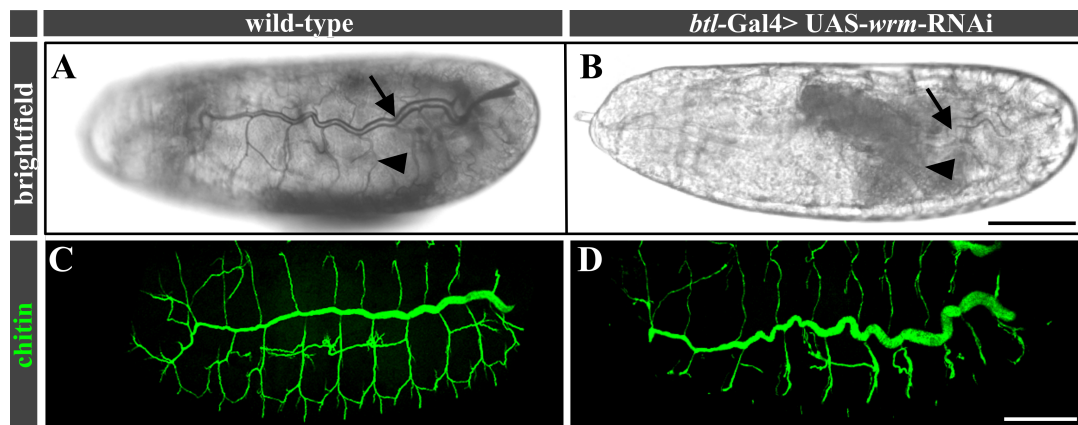


Figure 3.8 LC and tracheal branch morphology are affected in *CG43780* tracheal knockdown.

Brightfield light microscopic images of wild-type (A) and *btl*-Gal4, UAS-RNAi-v100677 mutant embryo (B). Confocal Z-projections of CBP stainings in wild-type (C) as well as *btl*-Gal4, UAS-RNAi-v100677 mutant embryo (D). Gas filling of the dorsal trunk (arrow in A) and a smaller branch (arrowhead in A) of the tracheal system is indicated in the wild-type control embryo, whereas in the *btl*-Gal4, UAS-RNAi-v100677 mutant embryo LC is impaired (arrow and arrowhead in B). In contrast to the wild-type embryo (C), tracheal knockdown of *CG43780* leads to an elongation of the tracheal tubes resembling little worms (D). Therefore the chosen gene name is *würmchen*. Scale bar indicates 100 μ m.

analyzed in more detail. Wild-type embryos show a LC of the entire tracheal system including the dorsal trunk and all other smaller tracheal branches (arrow and arrowhead in Fig. 3.8 A). In contrast, tracheal *CG43780* knockdown embryos reveal liquid-filled branches of all sizes (arrow and arrowhead in Fig. 3.8 B). Furthermore, visualization of the tracheal network by CBP (chitin binding probe) shows straight branches of wild-type embryos (Fig. 3.8 C), while *CG43780* knockdown tracheal branches show an elongated and convoluted phenotype (Fig. 3.8 D). Thus, *CG43780* was named *würmchen* (*wrm*), which means little worm in German resembling the worm-like tracheal phenotype of *CG43780* after tracheal knockdown.

3.2.3 Genomic organization of *würmchen* and Würmchen protein structure

wrm is located on the left arm of the third chromosome at position 65F5 and consists of 3 exons and 2 introns (Fig. 3.9 A). *wrm* is bicistronic, meaning it encodes for two distinct proteins. The larger of both proteins, termed Wrm1, is located 5' to the translation start of the smaller protein Wrm2. The open reading frame (ORF) of Wrm2 starts and ends in exon 3. The ORFs are separated by 6 base pairs, indicating that both proteins are encoded in frame.

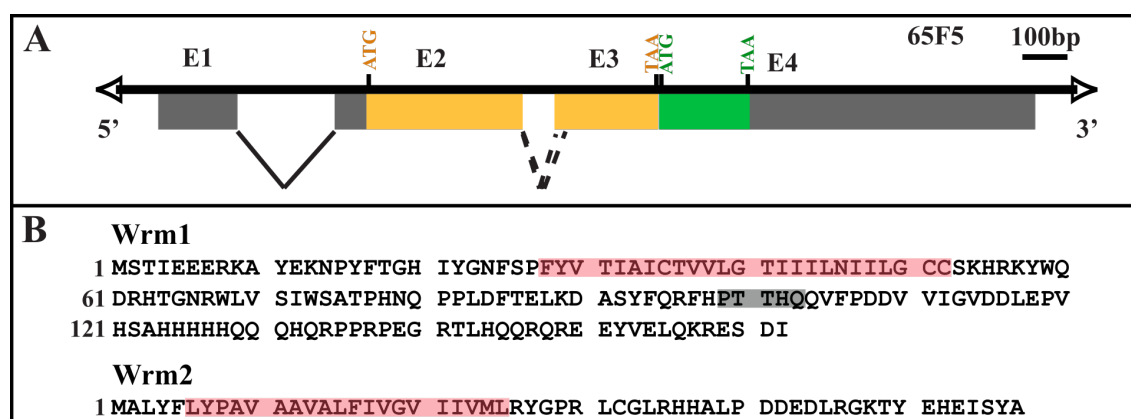


Figure 3.9 Genomic organization of *wrm* and protein sequences encoded by *wrm*.

(A) The *wrm* gene consists of 3 exons (colored parts represent coding sequence, in which yellow represents the sequence coding for Wrm1 and green represents the sequence coding for Wrm2, grey parts represent UTRs). *wrm* has one alternative splice variant marked by dotted lines, leading to the deletion of five amino acids (highlighted in grey). (B) The predicted Wrm1 protein sequence has 157 aa (152 aa) and contains a transmembrane domain (highlighted in pink), whereas the predicted Wrm2 protein sequence has 57 aa and also contains a transmembrane domain (highlighted in pink).

In silico analysis reveals single transmembrane domains in Wrm1 (aa 28-52) and Wrm2 (aa 6-25; Fig. 3.9 B, highlighted in pink) and the longer C-terminal parts of both proteins face intracellularly as predicted by TMHMM Server v. 2.0 (DTU Bioinformatics,

3.2 Identification and characterization of *würmchen*

Department of Bio and Health Informatics). No further domains have been annotated for both Wrm1 and Wrm2.

Wrm1 and Wrm2 are highly conserved within *Drosophila* species, however, only Wrm1 is also conserved within non-Dipteran insects. No orthologs have been identified in vertebrates (www.flybase.org).

3.2.4 *würmchen* is expressed in ectodermal tissues during embryonic development

A Digoxigenin-labelled antisense probe from cDNA clone LD47606 (DGRC; see sec. 5.5.1) was used to analyze *wrm* expression in *Drosophila* embryos.

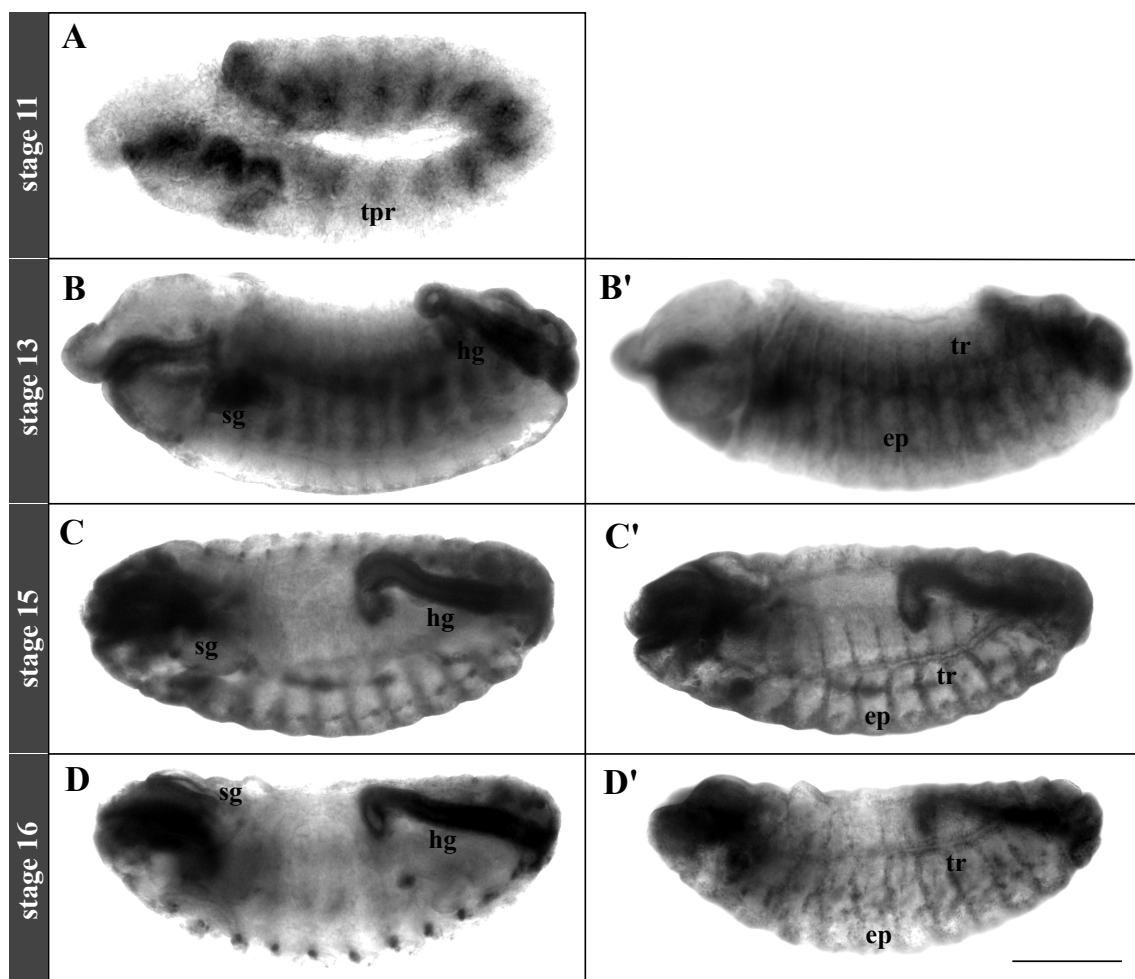


Figure 3.10 Expression pattern of *wrm* transcript during embryogenesis.

Lateral view of *in situ* hybridization with *wrm* antisense-RNA-probe (clone LD47606) in stage 11 (A), stage 13 (B, B'), stage 15 (C, C') and stage 16 (D, D'). B', C' and D' are different focal planes of embryos shown in B, C and D, respectively. In stage 11, *wrm* is expressed in tracheal placodes (tpr in A). From stage 13 until stage 16 *wrm* is detected in ectodermally derived tissues of the trachea (tr), epidermis (ep; B', C', D'), hindgut (hg) and salivary gland (sg; B, C, D). Scale bar indicates 100 μ m.

wrm expression in embryos is first detected in tracheal placodes in stage 11 (Fig 3.10 A). Ectodermal expression in the tracheal epithelium and epidermis (Fig 3.10 B') as well as the hindgut and salivary gland epithelium (Fig 3.10 B) is detected in stage 13. The expression in ectodermally derived tissues stays consistent throughout embryonic development (Fig. 3.10 D and D'). Thus, *wrm* transcript expression is restricted to ectodermally derived tissues during embryogenesis.

3.2.5 Generation of *würmchen* mutant alleles

To verify the RNAi-mediated *wrm* phenotype described in section 3.2.2, which displays convoluted elongated tracheal tubes as well as no LC, I generated mutant *wrm* alleles via the CRISPR/Cas9 technology.

In order to generate a deletion of the *wrm* locus (*wrm*^{ΔattP} allele), DNA regions flanking the *wrm* gene were cloned into the *pHD-dsRed-attP* vector, which contains a *dsRed* marker, *loxP* sites and the *attP* site (Fig. 3.11 A). Additionally, two gRNAs at the 5' and 3' region of the *wrm* locus were cloned into the *pBFv-U6.2B* vector (red arrows in Fig. 3.11 A) to mediate CRISPR/Cas9-directed homology repair. Both vectors were injected into *Drosophila* embryos expressing *vasa-cas9* (BDSC# 56552). Flies with integrated vector DNA were selected by appearance of the *dsRed* marker. Sequencing revealed only a partial integration of the *attP-dsRed* construct, thus the 3' *loxP* site did not integrate into the genome and thus preventing the deletion of the *dsRed* marker by genetic tools. Sequencing revealed that all coding and non-coding sequences of *wrm* were deleted except a small region of the *wrm* 3' UTR at the 3' end of the *dsRed* marker (Fig. 3.11 B). This *wrm*^{ΔattP} allele mimics the tracheal knockdown phenotype of *wrm*, including embryonic lethality and was used for direct integration of rescue constructs as well as a Strep-tagged versions of Wrm1. Furthermore, *wrm*^{ΔattP} was used as *wrm*⁻ control for further experiments.

To rescue the *wrm* phenotype the *wrm* gene locus was first amplified via PCR from wild-type DNA. The PCR product was cloned into the *pGE-attB* vector containing the *white*⁺ marker, following injection of the rescue construct into the *wrm*^{ΔattP} embryos (Fig. 3.11 C). A vector coding for *phiC31* integrase was co-injected to mediate recombination between *attP* and *attB* sites. The *white*⁺ marker was excised using *Cre* recombinase, generating *wrm*^{ΔattP}-*wrm* rescue. This fly line is viable and fertile, indicating full rescue of *wrm*^{ΔattP} by the *wrm* DNA. Furthermore, this result shows that outside the *wrm* gene no essential gene function is affected in *wrm*^{ΔattP} flies. Also, the integration of the *dsRed* marker near by the *wrm* gene locus has no effect for normal development.

3.2 Identification and characterization of *würmchen*

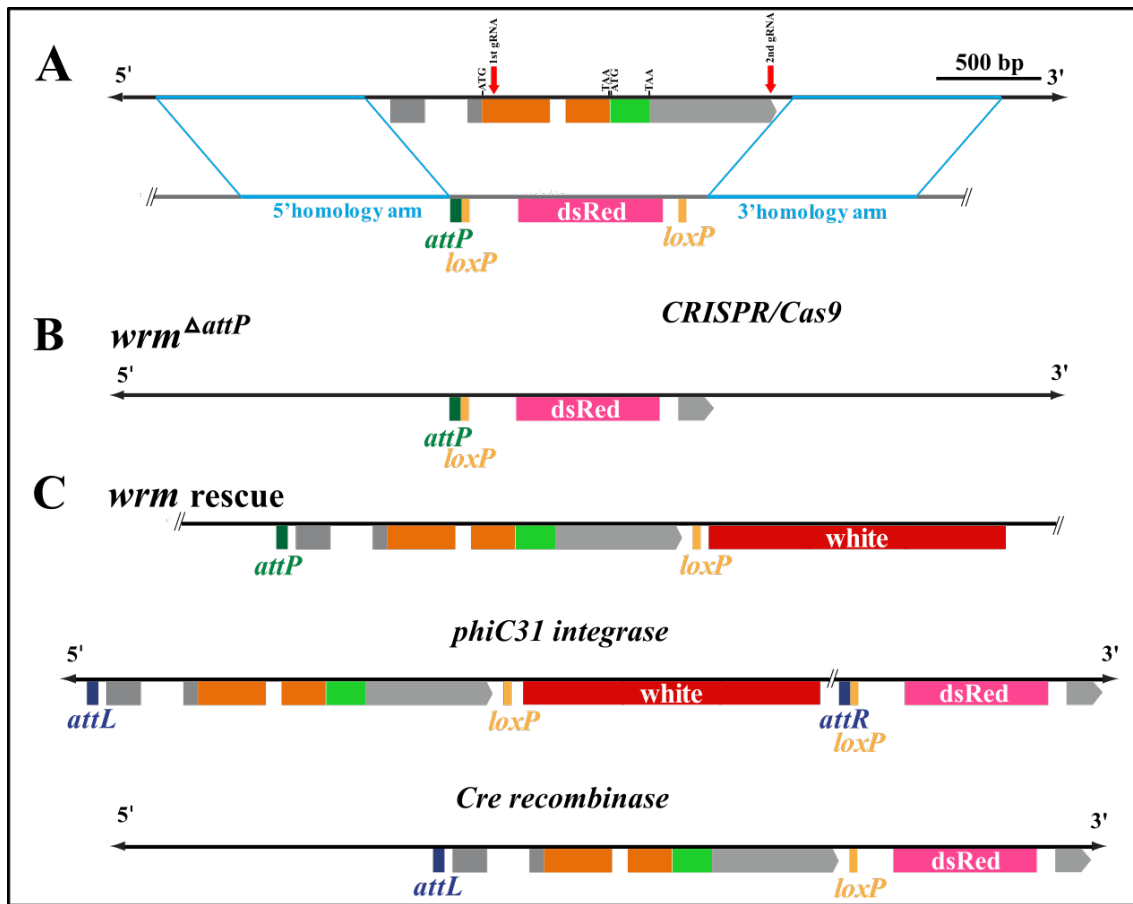


Figure 3.11 Generation of the *wrm^{ΔattP}* allele.

DNA regions flanking the *wrm* gene (orange encoding Wrm1, green encoding Wrm2; UTRs are depicted in grey) were cloned into the *pHD-dsRed-attP* vector, which contains a *dsRed* marker, *loxP* sites and the *attP* site (A). This vector was injected into fly line BDSC #56552. Additionally, a vector containing two gRNAs (red arrows in A) in the *wrm* locus was co-injected for CRISPR/Cas9-directed homology repair. The *wrm* locus is not deleted completely, but a part of the *wrm* 3' UTR remained at the 3' end of the *dsRed* marker (B). Injection of the *wrm* rescue construct into the fly line carrying the *wrm^{ΔattP}* allele is depicted in C.

As described in section 3.2.3, the *wrm* gene encodes two proteins, Wrm1 and Wrm2. To investigate, how Wrm proteins may affect SJ formation, *wrm* mutations in the *wrm* coding region of Wrm1 (Fig. 3.12 A) and Wrm2 (Fig. 3.13 A) were generated. Therefore, gRNAs were designed at the 5' translation start of Wrm1 and Wrm2 for CRISPR/Cas9 mediated double strand DNA breaks. Cells initiate DNA repair after such breaks, but repair is imprecise and often result in insertions and/or deletions at the breaking point with the potential of generating loss-of-function-mutations.

The resulting *wrm* mutant lines affecting Wrm1 contain either a 4 bp deletion and 4 bp insertion generating *wrm^{IA}* (an in frame stop codon) or a 2 bp deletion (a frameshift mutation), which is termed *wrm^{IE}* (Fig. 3.12 B). The resulting protein Wrm1^{IA} is severely

shortened, whereas the frame shift in the translation start of protein Wrm1^{1E} results in a shortened altered protein in comparison to wild-type Wrm (Fig. 3.12 C). Both *wrm* mutant alleles affecting Wrm1 are lethal during embryogenesis.

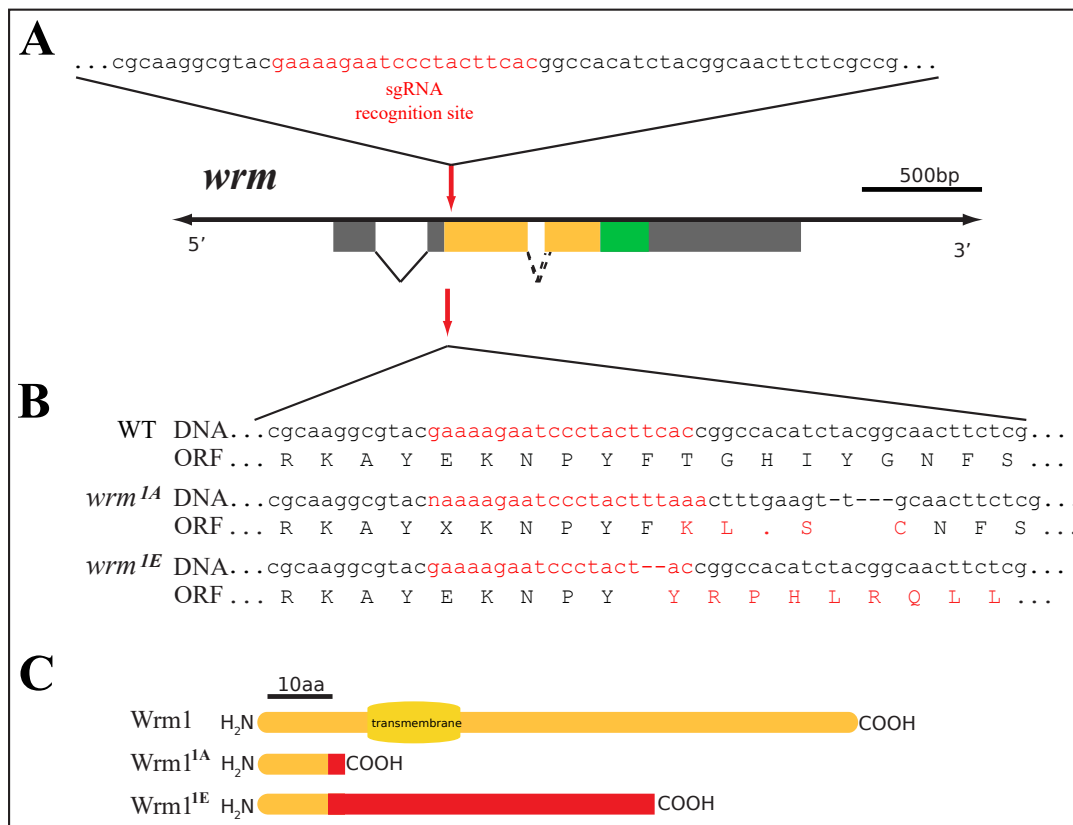


Figure 3.12 Genomic alterations in the *wrm* mutant alleles and schemes of affected Wrm1 proteins.

Schematic representation of the wild-type genomic *wrm* DNA region (A) and single guide (sg) RNA recognition site (top red arrow) at the translation start of Wrm1 (yellow). *wrm* mutant alleles affecting Wrm1 are termed *wrm*^{1A}, which contains a 4 bp deletion as well as 4 bp insertion generating a stop codon, and *wrm*^{1E}, which contains a 2 bp deletion (B). Resulting proteins Wrm1^{1A} and Wrm1^{1E} are shortened (red) in comparison to wild-type (dark yellow in C) and lack the transmembrane domain (light yellow in C).

Mutant lines affecting Wrm2 contain a 282 bp (*wrm*^{2A}), a 3 bp (*wrm*^{2N}) as well as a 6 bp (*wrm*^{2R}) deletion (Fig. 3.13 B). The resulting protein Wrm2^{2A} is similar in size when compared to wild-type Wrm2, whereas Wrm2^{2N} and Wrm2^{2R} contain deletions of one or two amino acids in the transmembrane domain leaving the remaining protein unchanged (Fig. 3.13 C). All three mutant *wrm* alleles affecting Wrm2 are not lethal during embryogenesis, but cause lethality during larval development.

3.2 Identification and characterization of *würmchen*

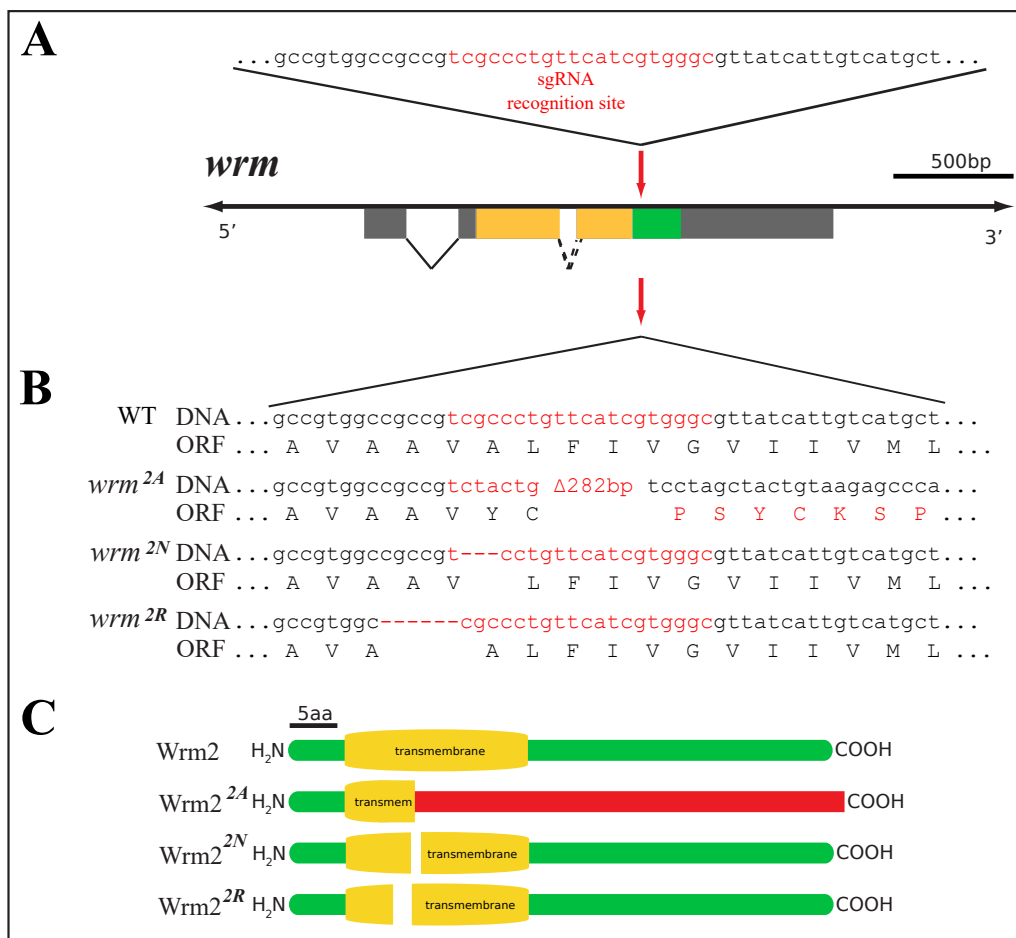


Figure 3.13 Genomic alterations in the *wrm* mutant alleles and schemes of affected Wrm2 protein.

Schematic representation of the genomic *wrm* region in wild-type (A) and single guide (sg) RNA recognition site (top red arrow) at the translation start of Wrm2 (green). *wrm* mutant alleles affecting Wrm2 are termed *wrm*^{2A}, *wrm*^{2N} and *wrm*^{2R} (B). Resulting protein Wrm^{2A}, which contains a 282 bp deletion, generating an altered Wrm protein (red) with similar size to wild-type Wrm (C). Wrm^{2N} and Wrm^{2R} contain a 1 and 2 amino acid deletion respectively, resulting in alterations of the transmembrane domain.

To determine the time point of lethality, 50 homozygous *wrm*^{2A} and *wrm*^{2R} embryos staged 18-22 h were collected and placed in a vial containing fresh fly food. The development of the embryos was observed and lethal time points of each animal were determined. Figure 3.14 depicts that most larvae die during 2nd instar larval stage. However, lethality is also elevated in embryos (Fig. 3.14 see embryo) and first instar larvae (Fig. 3.14 see L1) when compared with wild-type.

However, no SJ specific phenotypes, including morphology and gas-filling of the

tracheal system, were observed in *wrm* alleles affecting Wrm2 during larval development.

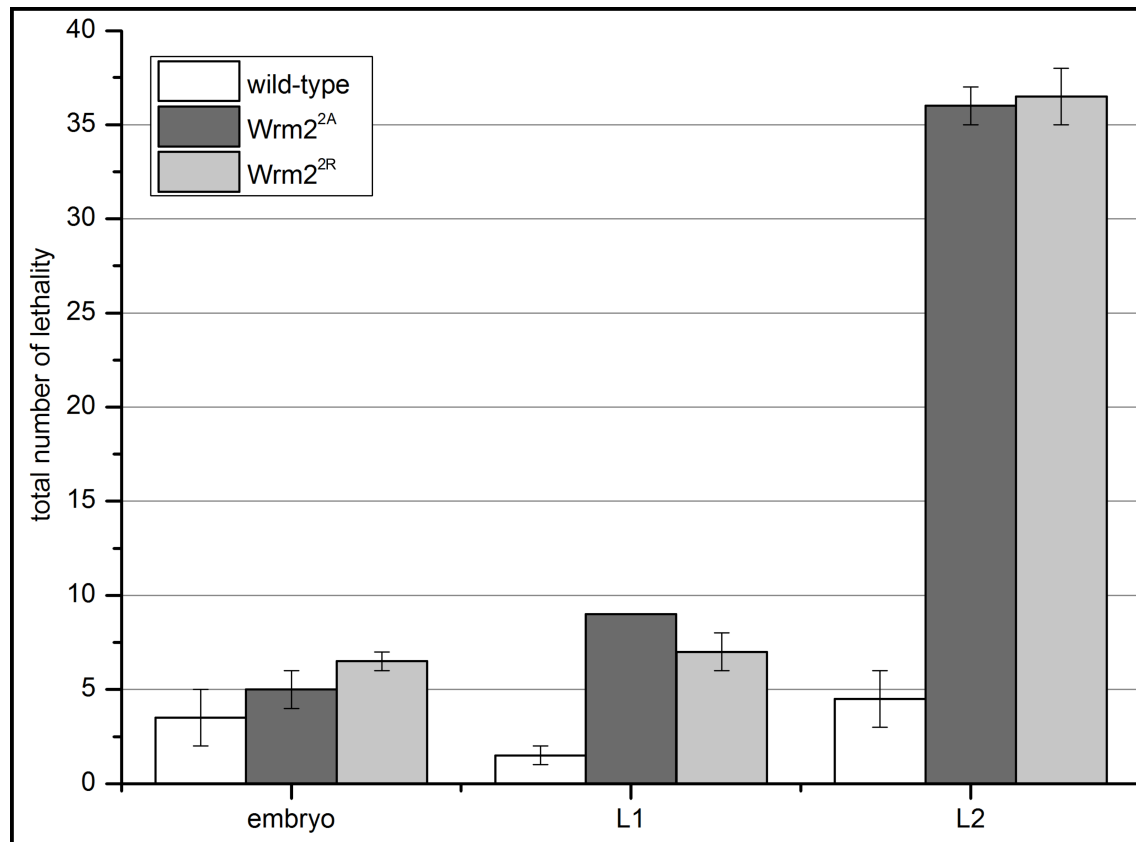


Figure 3.14 *wrm* mutant embryos affecting Wrm2 are lethal during 2nd instar larvae.

Graphic representation of lethality in wild-type (white columns) and mutant embryos homozygous for *wrm^{2A}* (dark grey columns) as well as *wrm^{2R}* (light grey columns), which affect Wrm2. Lethal time points of 2 separate experiments with 50 homozygous embryos of each line were analyzed. Lethality is shown on the y axis as total numbers. 75% of *wrm* mutant larvae affecting Wrm2 die as 2nd instar larvae, however, lethality rates are also enhanced during embryogenesis and 1st instar larval stage. Error bars were calculated by the standard error of mean. Abbreviations: L1, 1st instar larvae; L2, 2nd instar larvae.

3.2.6 Würmchen1 and Würmchen2 are two functionally independent proteins

The *wrm* gene encodes two proteins, namely Wrm1 and Wrm2. In wild-type DNA sequence of the *wrm* locus, only 6 bp separate the coding regions of Wrm1 and Wrm2, suggesting the possibility of a simultaneous in frame translation of both proteins. A stop codon read-through has been reported in *Drosophila*, where two differently sized isoforms are generated by UAG readthrough (Klagges et al., 1996; Robinson and Cooley, 1997).

To investigate if Wrm1 and Wrm2 are interdependent, mutant virgin *wrm^{1ΔTM3}* female flies, affecting Wrm1 were crossed to male *wrm^{2ΔTM3}* flies, affecting Wrm2. The same approach was used to cross mutant flies carrying *wrm* alleles *wrm^{1E/TM3}* and *wrm^{2R/TM3}*. If

Wrm1 and Wrm2 expression depend on each other, no *wrm^{IA/2A}* flies will hatch. However, if Wrm1 and Wrm2 function are independent of each other, the transheterozygous combination *wrm^{IA/2A}* as well as *wrm^{IE/2R}* will be viable. Analysis of the F1 generation of both crosses revealed viable and fertile *wrm^{IA/2A}* and *wrm^{IE/2R}* flies. These results suggest the independency of Wrm1 and Wrm2. These results also indicate that *wrm* alleles affecting Wrm1 and Wrm2 complement each other, suggesting that the mutations affect only Wrm1 or Wrm2. Also, the frame shift mutation in the ORF of Wrm1 in the allele *wrm^{IA}* does not affect Wrm2 expression. Thus, a simultaneous in frame translation (Klagges et al., 1996; Robinson and Cooley, 1997) of Wrm1 and Wrm2 is highly unlikely.

3.2.7 Würmchen1 is expressed in SJs of ectodermal tissues during embryonic development

The *wrm* gene is expressed in ectodermal tissues, such as the hindgut, epidermis and trachea during embryonic development of *Drosophila* as shown in Figure 3.10. To identify tissues with Wrm1 expression, a Wrm1::Strep3' construct was generated. The Strep tag is localized at the 3' end of Wrm1 directly before the stop codon.

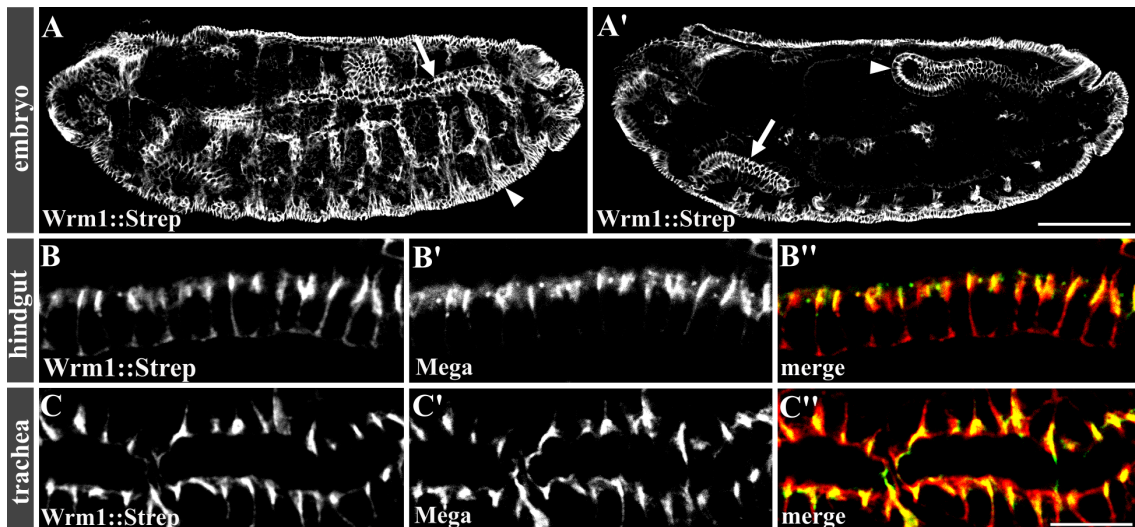


Figure 3.15 Expression pattern of Wrm1.

Confocal images of stage 16 *Wrm1::Strep3'/+* embryos using anti-Strep (A, A', B, C) and anti-Mega antibody (B' and C'). A and A' depict different focal planes of the same embryo. Merges of channels are shown in B'' and C''. *Wrm1::Strep3'* is localized in the trachea (arrow in A), epidermis (arrowhead in A) as well as salivary gland (arrow in A') and hindgut (arrowhead in A'). Close up images of hindgut (B-B'') and trachea (C-C'') show co-localization of *Wrm1::Strep3'* (B, C) and Mega (B', C'). Scale bar indicates 10 μ m in C'' and 100 μ m in A'.

This synthetic DNA was cloned into the *pGE-attB* vector and injected into embryos carrying the *wrm^{attP}* allele, to enable *attP/attB* recombination. Transformants were identi-

fied by the *white*⁺ marker and implemented recombination was confirmed by sequencing. *Wrm1::Strep3'* flies are homozygous viable and fertile, which indicates that *Wrm1::Strep3'* mediates wild-type-like *Wrm1* function. *Wrm1::Strep3'* embryos were stained using anti-Strep antibody and anti-Mega antibody to investigate co-localization of *Wrm1* and *Mega* (Fig. 3.15). *Wrm1* is expressed in ectodermally derived tissues including the embryonic trachea (arrow in Fig. 3.15 A) and epidermis (arrowhead in Fig. 3.15 A) as well as the salivary gland (arrow in Fig. 3.15 A') and hindgut (arrowhead in Fig. 3.15 A'). Merged channels of *Mega* and *Wrm1::Strep3'* in the hindgut (Fig. 3.15 B'') and the trachea (Fig. 3.15 C'') indicate that *Wrm1* is localized apicolaterally in epithelial cells in both tissues and co-localizes with *Mega*. These results indicate that *Wrm1* is localized in SJs of ectodermally derived tissues during embryogenesis.

3.2.8 Lack of *Würmchen1* affects tracheal morphology

To elucidate lack of function phenotypes of both *Wrm1* and *Wrm2*, stainings with CBP of various *wrm* alleles were performed to visualize the embryonic tracheal system for confocal imaging. The CBP binds to chitin, which is present in the tracheal lumen during embryonic development and mediates the control of length as well as diameter growth of the tubes (Luschnig et al., 2006). Figure 3.16 shows the CBP stainings in homozygous *wrm*^{ΔattP}, *wrm*^{IA}, *wrm*^{IE}, *wrm*^{2A}, *wrm*^{2N}, as well as transheterozygous *wrm*^{IA/IE} and *wrm*^{2N/2R} mutant embryos. The control embryo has straight tracheal tubes (Fig. 3.16 A), whereas all mutant alleles affecting *Wrm1* show an elongated and convoluted tracheal network (Fig. 3.16 B-E), similarly as found after RNAi mediated tracheal knockdown of *wrm* (see Fig. 3.8 D). However, mutant embryos affecting *Wrm2* show straight wild-type like tubes (Fig. 3.16 F-H). These findings are in agreement with the different lethal phases of the various *wrm* alleles. Alleles affecting *Wrm1* show an embryonic phenotype and are embryonic lethal. Alleles that affect *Wrm2* show no embryonic phenotype and die during subsequent larval development.

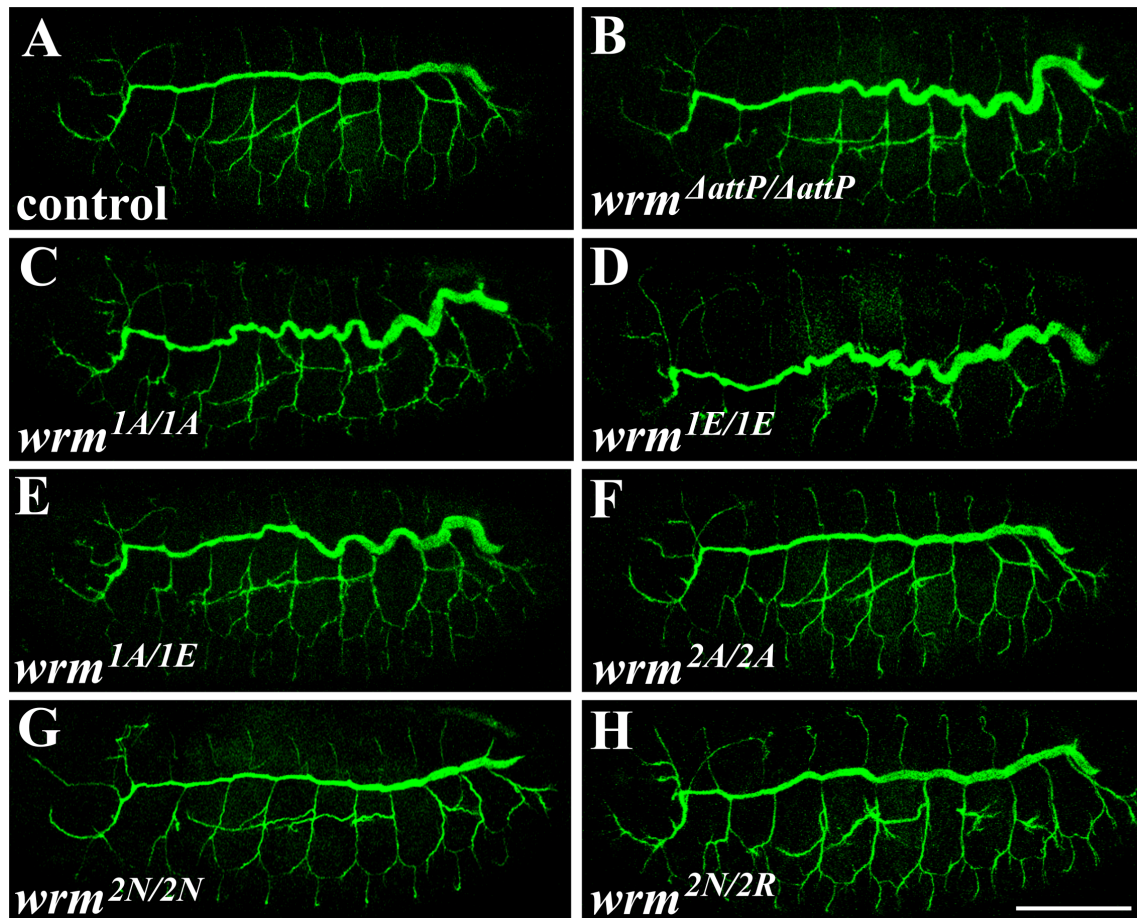


Figure 3.16 Tracheal phenotype of *wrm* mutant alleles.

Confocal Z-projections of homozygous stage 16 control (wild-type; A), *wrm*^{ΔattP} (B), *wrm*^{1A} (C), *wrm*^{1E} (D), *wrm*^{2A} (F) and *wrm*^{2N} (G) mutant embryos as well as transheterozygous embryos *wrm*^{1A/1E} (E) and *wrm*^{2N/2R} (H) embryos. Wild-type straight tracheal tubes are visible in control embryos as well as in *wrm* mutant embryos affecting Wrm2 (F-H). In contrast, elongated tracheal trunks and branches are detected in *wrm* mutant embryos affecting Wrm1 (B-E). Scale bar indicates 100 μm.

3.2.9 *würmchen* mutant embryos affecting Würmchen1 show affected liquid clearance

The elongated tracheal network and embryonic lethality described in section 3.2.8 of *wrm* mutant embryos affecting Wrm1 is reminiscent of a SJ mutant phenotype. To elucidate whether these embryos perform LC, which is impaired in bona fide SJ component mutant embryos, *wrm* mutant embryos were staged and light microscopic imaging of living stage 17 embryos was performed. Control embryos (wild-type) undergo LC and gas filling of the tracheal tubes, visualized by the gas-liquid phase contrast (arrow in Fig.3.17 A). Analysis of the LC process of embryos with mutated alleles affecting Wrm1 do not show LC and gas filling at the end of embryogenesis (arrows in Fig. 3.17 B and C). In contrast to Wrm1

affecting alleles, *wrm*^{2E} mutant embryos affecting Wrm2 perform LC and gas filling of the tracheal tubes (arrow in Fig. 3.17 D). Thus, these results suggest that Wrm1 is essential for establishing the barrier function.

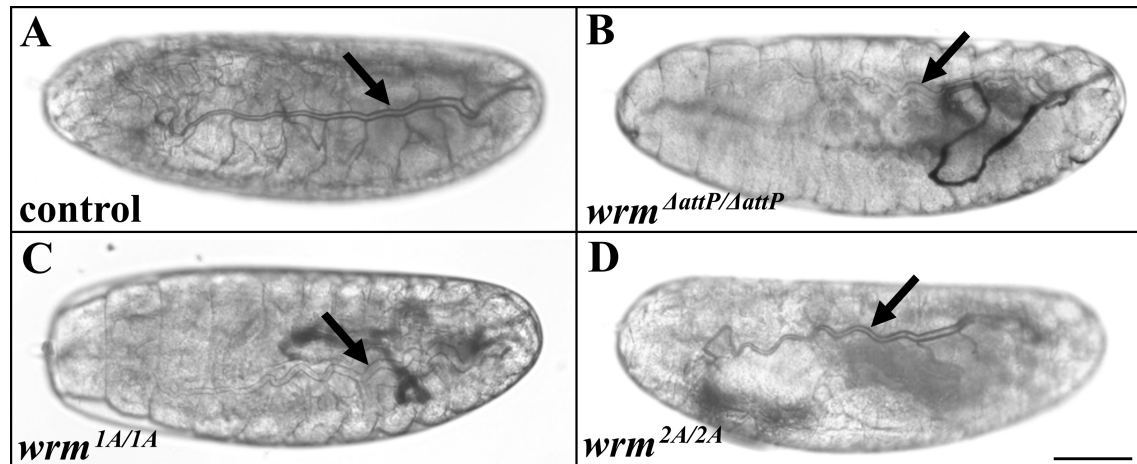


Figure 3.17 LC is impaired in *wrm* alleles affecting Wrm1.

Brightfield light microscopic images of stage 17 control (wild-type; A), homozygous *wrm*^{ΔattP} (B), *wrm*^{1A} (C) and *wrm*^{2A} (D) embryos. Gas filling is depicted in control embryos (arrow in A) as well as homozygous *wrm*^{2A} mutant embryos affecting Wrm2 (arrow in D), whereas no gas filling of the tracheal tubes is detected in *wrm*^{1A} and *wrm*^{ΔattP} mutant embryos affecting Wrm1 (arrows in B and C). Scale bar indicates 100 μm.

3.2.10 Würmchen1 is essential for epithelial barrier function

The main function of SJs is the establishment of a functioning barrier of epithelial tissues in order to restrict paracellular flow of molecules and ions. Wrm1 is a putative interaction partner of the SJ core complex protein Mega and the Wrm1 phenotype is reminiscent of the phenotype caused by the lack of function of bona fide SJ components. Thus, analysis was conducted to investigate whether the lack of Wrm1 also affects the transepithelial barrier function in *wrm* mutant embryos.

The epithelial barrier function is tested by injecting a fluorescent dye of distinct size into the haemocoel of stage 16 embryos (Lamb et al., 1998). In wild-type embryos, the fluorescent dye cannot pass the epithelial barrier. However, when the barrier function is impaired the dye passes the paracellular barrier and accumulates inside the lumina of trachea, central nervous system (CNS), hindgut and salivary gland. Confocal imaging was used to visualize the accumulation of fluorescent dye in the lumina of the tracheal tubes and CNS. 10 kDa Texas[®] Red Dextran and 70 kDa Fluorescein Dextran were co-injected to investigate possible gap size differences of the paracellular barrier.

In heterozygous *wrm*^{1A/TM3} (control) and mutant *wrm*^{2A/2A} embryos affecting Wrm2 no

3.2 Identification and characterization of *würmchen*

fluorescence is detected inside the tracheal lumina (arrow in Fig. 3.18 A), indicating an intact barrier function (Fig. 3.18 A-A'' and D-D''). In homozygous *wrm*^{ΔattP} as well as *wrm*^{1A} mutant embryos affecting Wrm1 10 kDa Texas[®] Red Dextran (arrow in Fig: 3.18 B) as well as 70 kDa Fluorescein enter the tracheal lumen and are visible after injection (Fig. 3.18 B-C''). Merges of both confocal channels are depicted in Figure 3.18 A'', B'', C'' and D''. Thus, the results indicate that Wrm1 is essential for the transepithelial barrier function, while Wrm2 does not affect the tracheal barrier.

To investigate the barrier function of *wrm* mutants in another organ system, the CNS barrier function was analyzed.

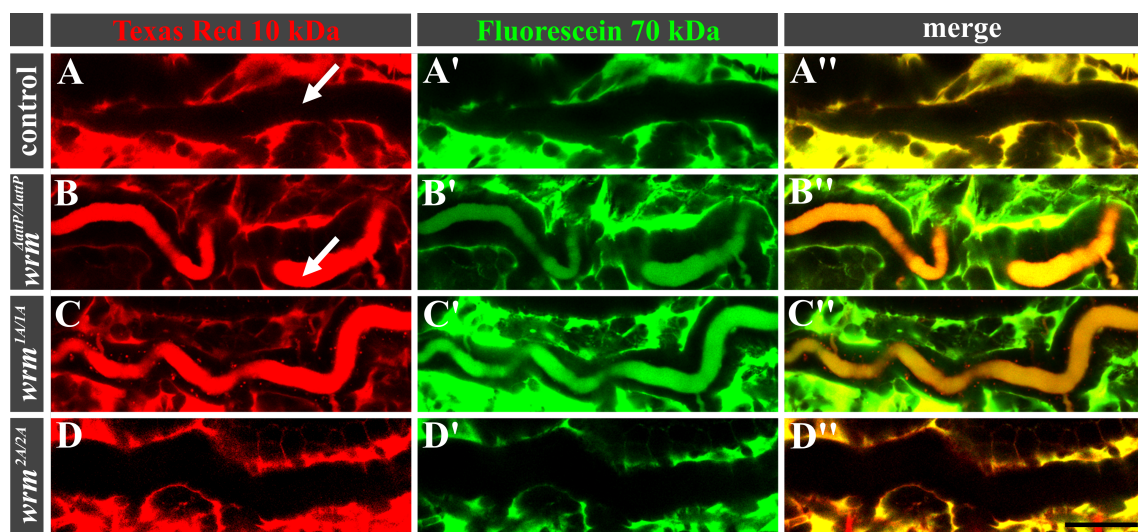


Figure 3.18 Tracheal barrier function is defective in *wrm* mutant embryos affecting Wrm1. Confocal images of stage 16 tracheal tubes of heterozygous *wrm*^{1A/TM3} embryos (control, A-A''), mutant homozygous *wrm*^{ΔattP/ΔattP} (B-B''), *wrm*^{1A/1A} (C-C'') and *wrm*^{2A/2A} (D-D'') embryos after co-injection of 10 kDa Texas[®] Red Dextran and 70 kDa Dextran Fluorescein into the haemocoel. A, B, C and D represent the fluorescence channel visualizing co-injections with Texas[®] Red Dextran and A', B', C' and D' represent the channel showing injections with Fluorescein. Merges of both channels are depicted in A'', B'', C'' and D''. In heterozygous *wrm*^{1A/TM3} as well as in homozygous mutant *wrm*^{2A/2A} embryos, which affect Wrm2, the intact epithelial barrier prevents the fluorescent dyes from passing into the tracheal lumen (arrow in A). In *wrm*^{ΔattP/ΔattP} and *wrm*^{1A/1A} mutant embryos however, 10 kDa (arrow in B) as well as 70 kDa fluorescent dyes are visible inside the tracheal lumen, indicating a impaired barrier function. Scale bar indicates 20 μm.

The paracellular barrier of the *Drosophila* CNS epithelium is also mediated by SJs (Deligiannaki et al., 2015). Therefore, this organ system was also used to determine intact or impaired barrier function. Stage 16 heterozygous control embryos, transheterozygous embryos mutant for *wrm*^{1A/1E} as well as *wrm*^{2R/2N} were co-injected with 10 kDa Texas[®] Red Dextran as well as 70 kDa Fluorescein and the barrier function was analyzed (Fig. 3.19

A-C’’).

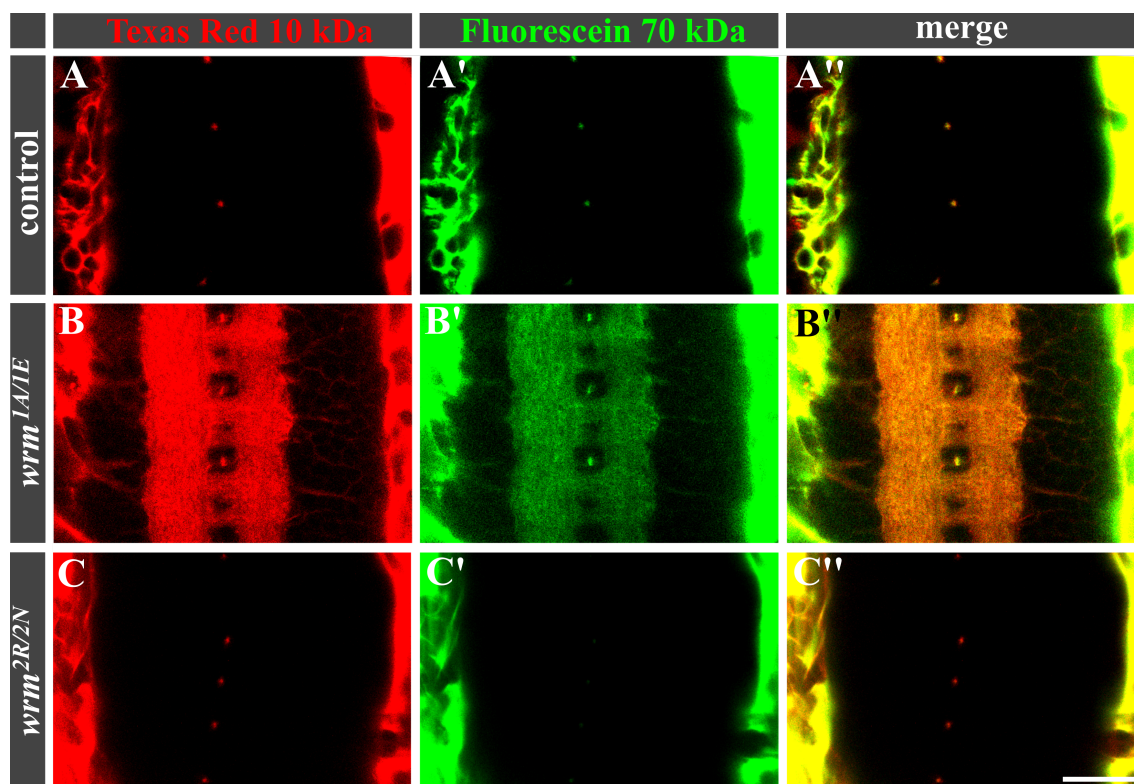


Figure 3.19 CNS barrier function is defective in *wrm* mutations affecting Wrm1.

Confocal images of stage 16 CNS of heterozygous control embryos (A-A’), embryos transheterozygous for *wrm*^{1A/1E} (B-B’’) and embryos transheterozygous for *wrm*^{2R/2N} (C-C’’) after co-injection of Texas[®] Red Dextran and 70 kDa Fluorescein into the haemocoel. A, B, and C represent the fluorescence channel visualizing co-injections with 10 kDa Texas[®] Red Dextran whereas A’, B’, and C’ represent the channel showing injections with 70 kDa Dextran Fluorescein. Merges of both channels are depicted in A’’, B’’, and C’’. In control embryos as well as in transheterozygous embryos carrying *wrm*^{2R/2N} mutant alleles, which affects Wrm2, the intact epithelial barrier prevents the fluorescent dyes from passing into the CNS. In embryos transheterozygous for *wrm*^{1A/1E} however, 10 kDa as well as 70 kDa fluorescent dyes are visible inside the CNS, indicating an impaired barrier function. Scale bar indicates 20 μ m.

In *wrm* mutant embryos affecting Wrm1 the barrier function is impaired, leading to the accumulation of 10 kDa and 70 kDa in the CNS (Fig. 3.19 B-B’). In contrast, control embryos (Fig. 3.19 A-A’’) and mutant embryos affecting Wrm2 (Fig. 3.19 C-C’), no dye is detected in the CNS, indicating an intact epithelial barrier. These findings are in agreement with findings from injection experiments into the tracheal epithelium and confirm that Wrm1 is necessary for the establishment of the epithelial barrier function in both the trachea and the CNS.

3.2.11 The localization of SJ core components depends on *Würmchen1*

The SJ protein complex is restricted to the apicolateral domain of the epithelial cell and its normal localization depends on single complex components. Lack of one SJ component leads to the mislocalization of all other components along the full length of the lateral cell membrane (Behr et al., 2003). In addition, normal SJ formation depends not only on correct component localization, but also on SJ protein level. For example, the overexpression of *mega* in hindgut cells leads to mislocalization of Cora and NrxF and a disruption of the SJ complex (Behr et al., 2003).

Localization of SJ components in the *wrm* mutant embryos was investigated by performing immunohistological stainings of SJ components.

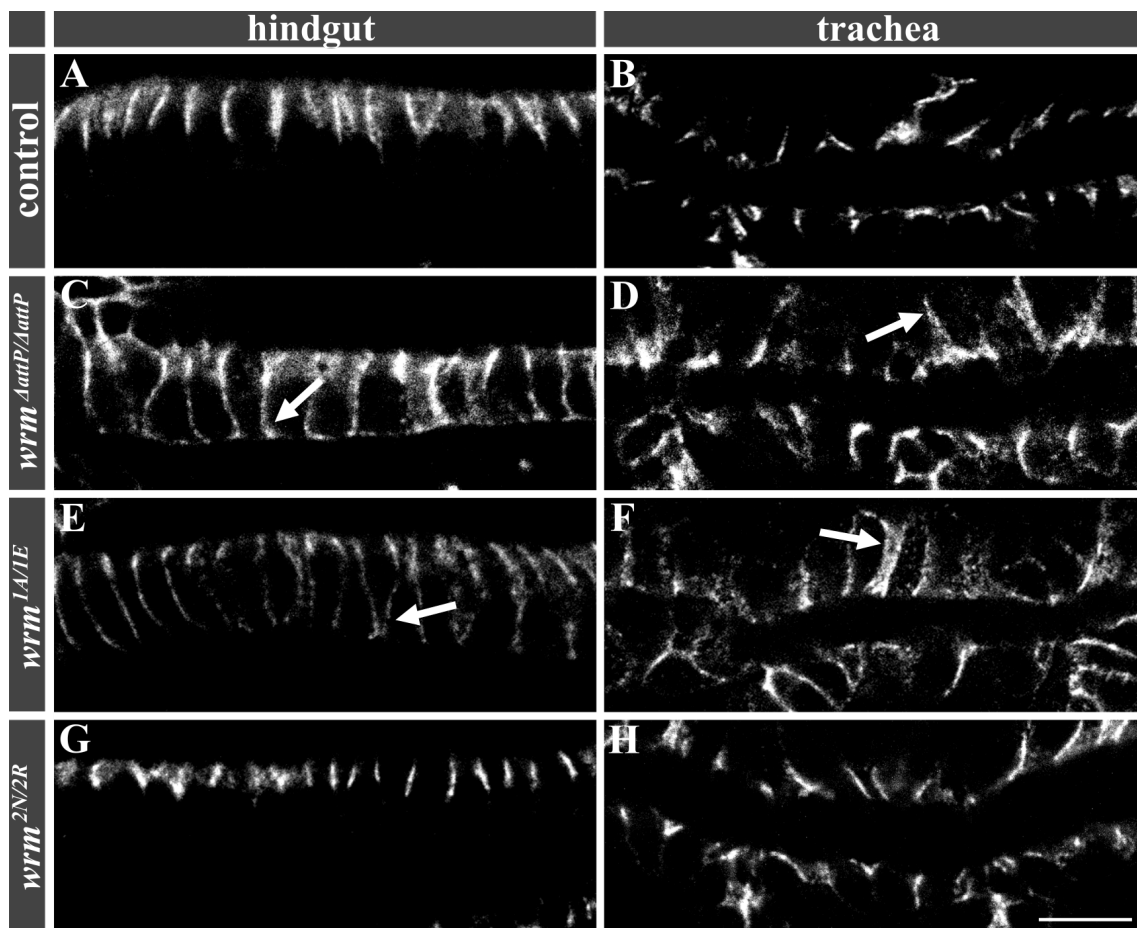


Figure 3.20 Wrm1 is essential for the normal localization of Mega.

Anti-Mega antibody staining of stage 16 hindgut epithelium (A, C, E, G) as well as stage 15 tracheal epithelium (B, D, F, H) in heterozygous *wrm^{1A/1E}* control (A and B), homozygous *wrm^{ΔattP}* (C and D), transheterozygous *wrm^{1A/1E}* (E and F) and *wrm^{2R/2N}* (G and H) mutant embryos. The correct localization of Mega is affected in *wrm* mutations affecting Wrm1 (arrows in C-F), whereas it is not distinguishable from control embryos (A and B) in *wrm* mutations affecting Wrm2 (G-H). Scale bar indicates 10 μ m.

A normal apicolateral membrane localization of Mega is found in stage 16 hindgut of heterozygous control embryos (Fig. 3.20 A) as well as in transheterozygous *wrm^{2N/2R}* mutant embryos (Fig. 3.20 G). Also stage 15 tracheal cells of control (Fig. 3.20 B) as well as transheterozygous *wrm^{2N/2R}* embryos (Fig. 3.20 H) reveal a normal Mega localization. In contrast, in homozygous mutant embryos carrying *wrm^{ΔattP}* (Fig. 3.20 C and D) and transheterozygous *wrm^{1A/1E}* mutant embryos (Fig. 3.20 E and F) Mega is mislocalized along the lateral membrane of the hindgut (Fig. 3.20 arrows in C and E) and tracheal epithelium (Fig. 3.20 arrows in D and F). These results indicate that Wrm1 is essential for a normal localization of the SJ core component Mega, while Wrm2 is not essential for Mega localization. The mislocalization of a SJ core component, such as Mega, suggests a

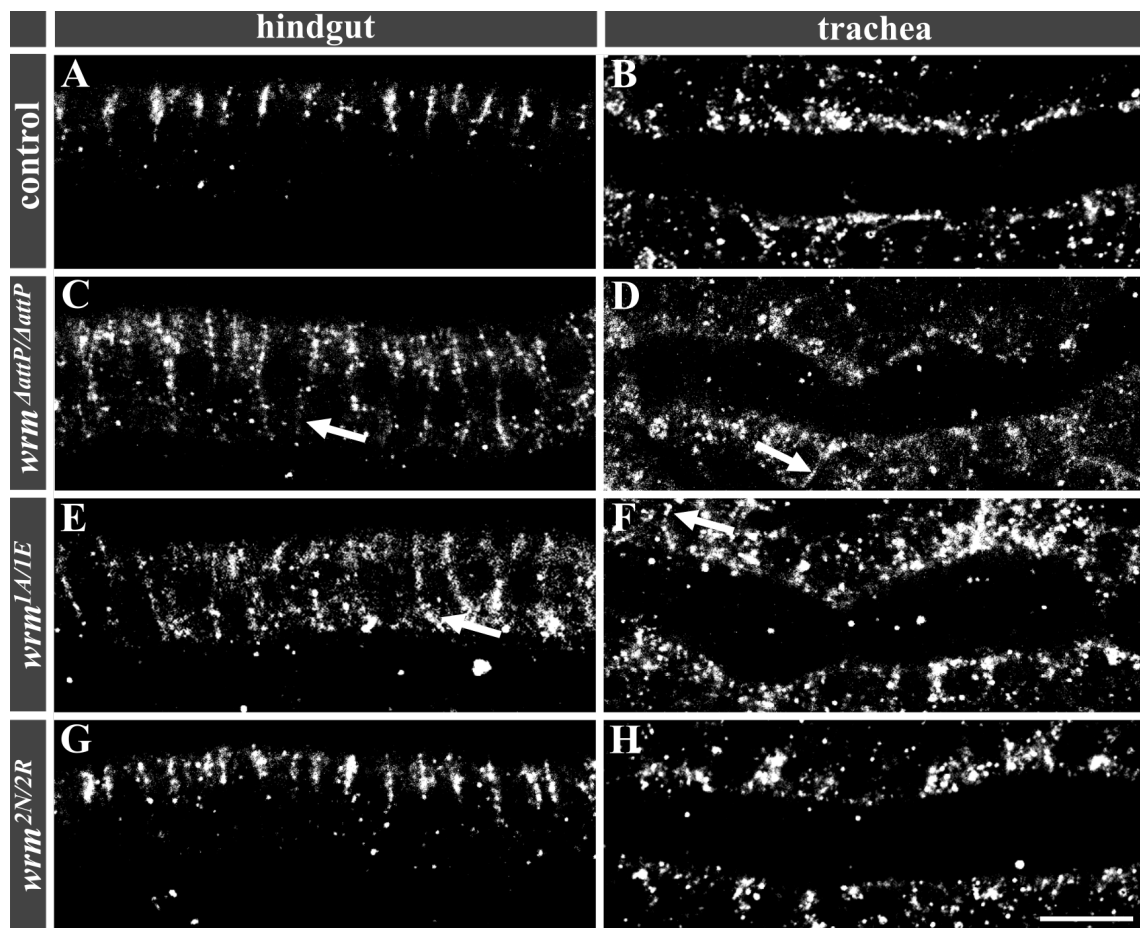


Figure 3.21 Wrm1 is essential for the normal localization of Kune.

Anti-Kune antibody staining of stage 16 hindgut epithelium (A,C,E,G) and stage 15 tracheal epithelium (B, D, F, H) in heterozygous *wrm^{1A/TM3}* control embryos (A and B), embryos homozygous for *wrm^{ΔattP}* (C and D) as well as embryos transheterozygous for *wrm^{1A/1E}* (E and F) and *wrm^{2N/2R}*. The correct localization of Kune is affected in *wrm* mutations affecting Wrm1 (arrows in C-F), whereas it is not distinguishable from control embryos (A and B) in *wrm* mutations affecting Wrm2 (G-H). Scale bar indicates 10 μ m.

3.2 Identification and characterization of *würmchen*

disrupted SJ core complex. To test this assumption the localization of an additional SJ core component, namely Kune, was analyzed.

Kune is restricted to its normal apicolateral domain in the hindgut as well as the tracheal epithelium in control (Fig. 3.21 A and B) as well as transheterozygous *wrm^{2N/2R}* mutant embryos (Fig. 3.21 G and H). However, in lack of Wrm1 function homozygous *wrm^{ΔattP}* and transheterozygous *wrm^{1A/1E}* mutant embryos, Kune is mislocalized along the full length of the lateral membrane in the hindgut (arrows in Fig. 3.21 C and E) and tracheal epithelium (arrows in Fig. 3.21 D and F). These findings suggest that Wrm1 is an essential component for the establishment of the SJ complex, while Wrm2 is non essential for the SJ complex localization.

3.2.12 Würmchen1 does not affect cell polarity

The *wrm* mutations affecting Wrm1 lead to the mislocalization of the two SJ core components Mega and Kune. To elucidate the impact of *wrm* mutations on cell polarity, immunohistological stainings of the polarity marker Crumbs were performed. Crumbs is a cell membrane marker restricted to the apical membrane in wild-type embryos.

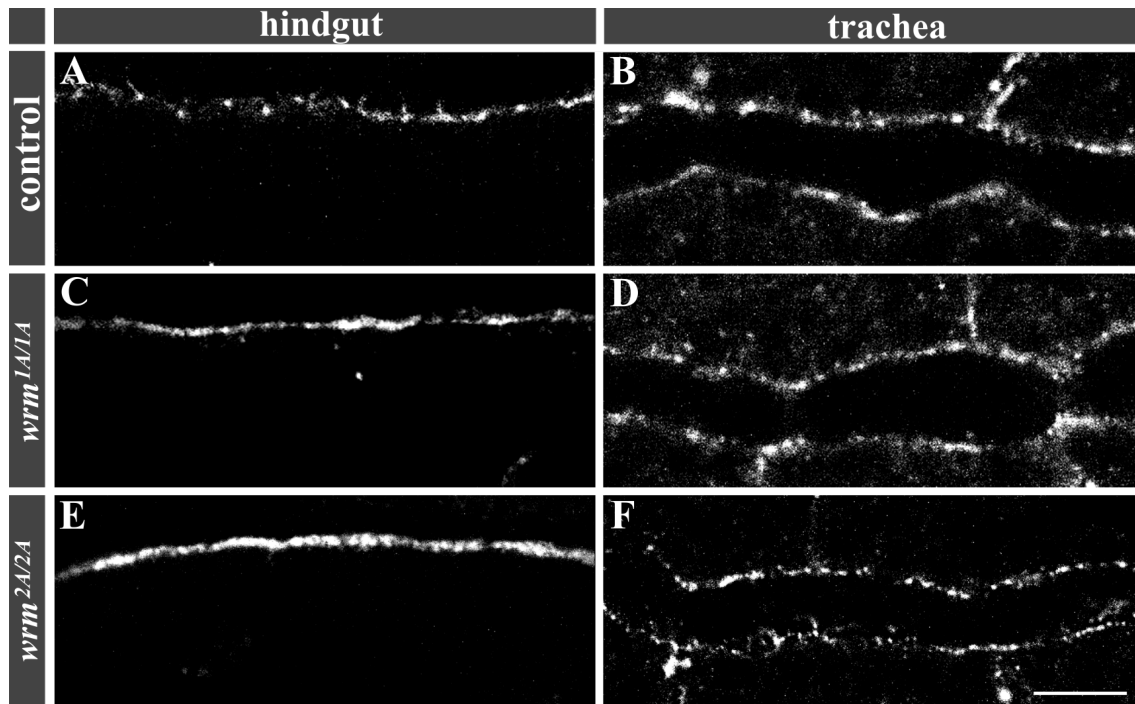


Figure 3.22 Wrm1 and Wrm2 are not essential for the localization of Crumbs.

Anti-Crumbs antibody staining of stage 16 hindgut epithelium (A, C, E) and stage 15 tracheal epithelium (B, D, F) in heterozygous control embryos (A and B), mutant *wrm^{1A/1A}* (C and D) and *wrm^{2A/2A}* embryos (E and F). Crumbs localization is not dependent by *wrm* mutations affecting Wrm1 or Wrm2. Scale bar indicates 10 μ m.

In heterozygous control embryos as well as mutant *wrm^{1A/1A}* and *wrm^{2E/2E}* embryos, Crumbs is localized wild-type-like in the hindgut (Fig. 3.22 A, C, E) as well as the tracheal epithelium (Fig. 3.22 B, D, F). These findings suggest that neither Wrm1 nor Wrm2 are essential for a normal cell polarity.

3.2.13 Würmchen1 is necessary for exocytosis of Serpentine

An essential function of the SJ is to mediate the exocytosis of Serpentine (Serp) and Vermiform (Verm). During embryonic development chitin is deposited into the tracheal lumen and forms a cylinder-like structure. The subsequent modification of chitin is important for diameter and length control of tracheal tubes. Serp and Verm are chitin deacetylases that modify chitin. Serp is expressed in the fat body, taken up by tracheal

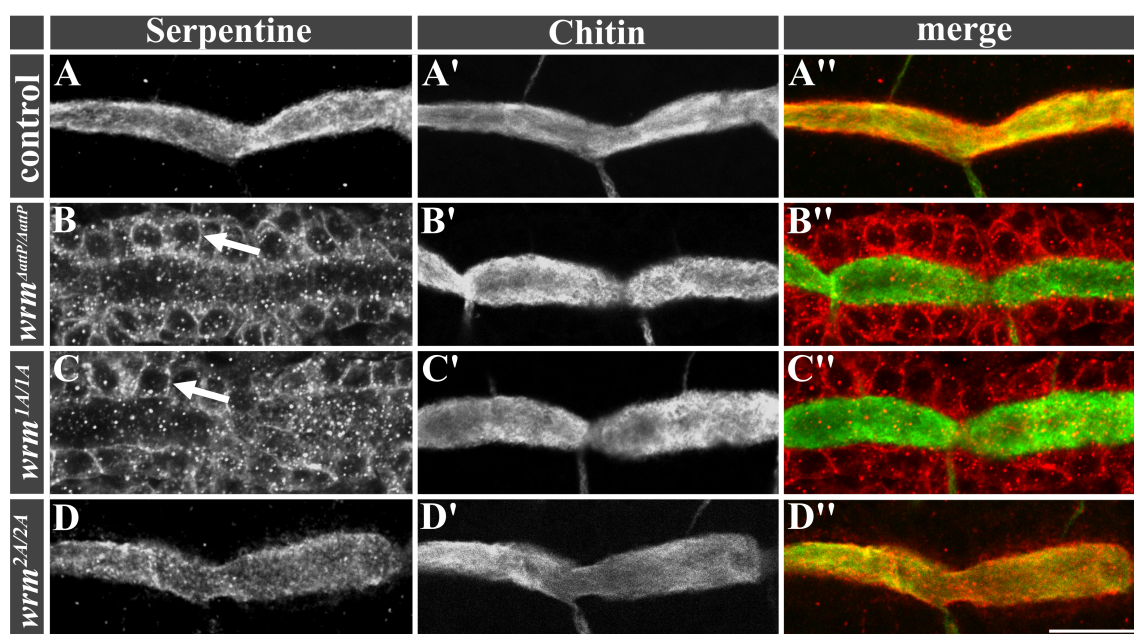


Figure 3.23 Exocytosis is impaired in *wrm* mutant embryos affecting Wrm1.

Confocal images of antibody stainings of Serp in tracheal tubes in stage 15 heterozygous control (A-A''), mutant *wrm^{ΔattP/ΔattP}* (B-B'') and *wrm^{1A/1A}* (C-C'') embryos as well as in mutant *wrm^{2A/2A}* (D-D'') embryos. In A, B, C and D Serp localization is shown, whereas in A', B', C' and D' Chitin is depicted labelling the tracheal lumen. Merges of both channels are shown in A'', B'', C'' and D''. The exocytosis of Serp is affected in *wrm* mutations affecting Wrm1, in which Serp accumulates in the cells' cytoplasm (arrows in B and C). The exocytosis of Serp in *wrm* mutant embryos affecting Wrm2 (D) is not distinguishable from control embryos (A). Scale bar indicates 10 μm.

cells and secreted into the lumen mediated by SJs from stage 13 throughout stage 16 of embryonic development (Luschnig et al., 2006; Dong et al., 2014).

In order to facilitate the visualization of the tracheal lumen, immunohistological double

stainings of Serp and Chitin, a tracheal luminal marker, were performed. Serp is present in the tracheal lumen in stage 15 heterozygous control embryos (Fig. 3.23 A) as well as in *wrm^{2A/2A}* mutant embryos (Fig. 3.23 D) affecting Wrm2, as revealed by the Serp and Chitin co-localization (Fig. 3.23 A' and D'). In contrast, Serp is not secreted into the tracheal lumen of homozygous *wrm^{ΔattP/ΔattP}* (Fig. 3.23 B) and *wrm^{1A/1A}* (Fig. 3.23 C) mutant embryos, which both affect Wrm1. In these mutants, Serp is present inside the cytoplasm of tracheal cells (arrows in Fig. 3.23 B and C). These results indicate that Wrm1 is essential for the exocytosis of Serp into the tracheal lumen, which is in agreement with the disrupted luminal secretion of Serp caused by lack of SJ components, such as Mega and Varicose (Behr et al., 2003; Wu et al., 2007).

3.2.14 SJ and taenidial folds morphology is compromised in *würmchen* mutant embryos affecting Würmchen1

The convoluted tracheal branches including affected taenidial folds, the impaired barrier function as well as the mislocalization of Mega and Kune indicate an impaired SJ morphology in *wrm* mutant embryos affecting Wrm1. High resolution imaging was used to analyze SJ morphology and taenidial folds in more detail.

In wild-type embryos the tracheal epithelium is characterized by regular and well ordered taenidial folds, which form a continuous spiral spanning the apical side of tracheal cells (arrows in Fig. 3.24 B). Regular taenidial folds are also present in *wrm* mutant embryos affecting Wrm2 (arrows in Fig. 3.24 F). In *wrm* mutant embryos affecting Wrm1, however, the taenidial folds appear irregular and crooked (arrows in Fig. 3.24 D), indicating an impact of Wrm1 on taenidial folds formation. Additionally, distinct electron-dense ladder-like structures of septae in between two plasma membranes of adjacent epithelial cells are displayed in wild-type embryos (arrowheads in Fig. 3.24 A). Similar electron dense septae are observed in *wrm* mutant embryos affecting Wrm2 (arrowheads in Fig. 3.24 E). However, in *wrm* mutant embryos affecting Wrm1 the ladder-like septae between neighboring tracheal cells are highly reduced and irregularly distributed (arrowhead in Fig. 3.24 C). Interestingly, the space between two plasma membranes in *wrm* mutants affecting Wrm1 remains parallel and wild-type-like. These results indicate that Wrm1 is essential for the formation of correct number and organization of septae, which is in line with results from dye injection experiments showing a non functional epithelial barrier.

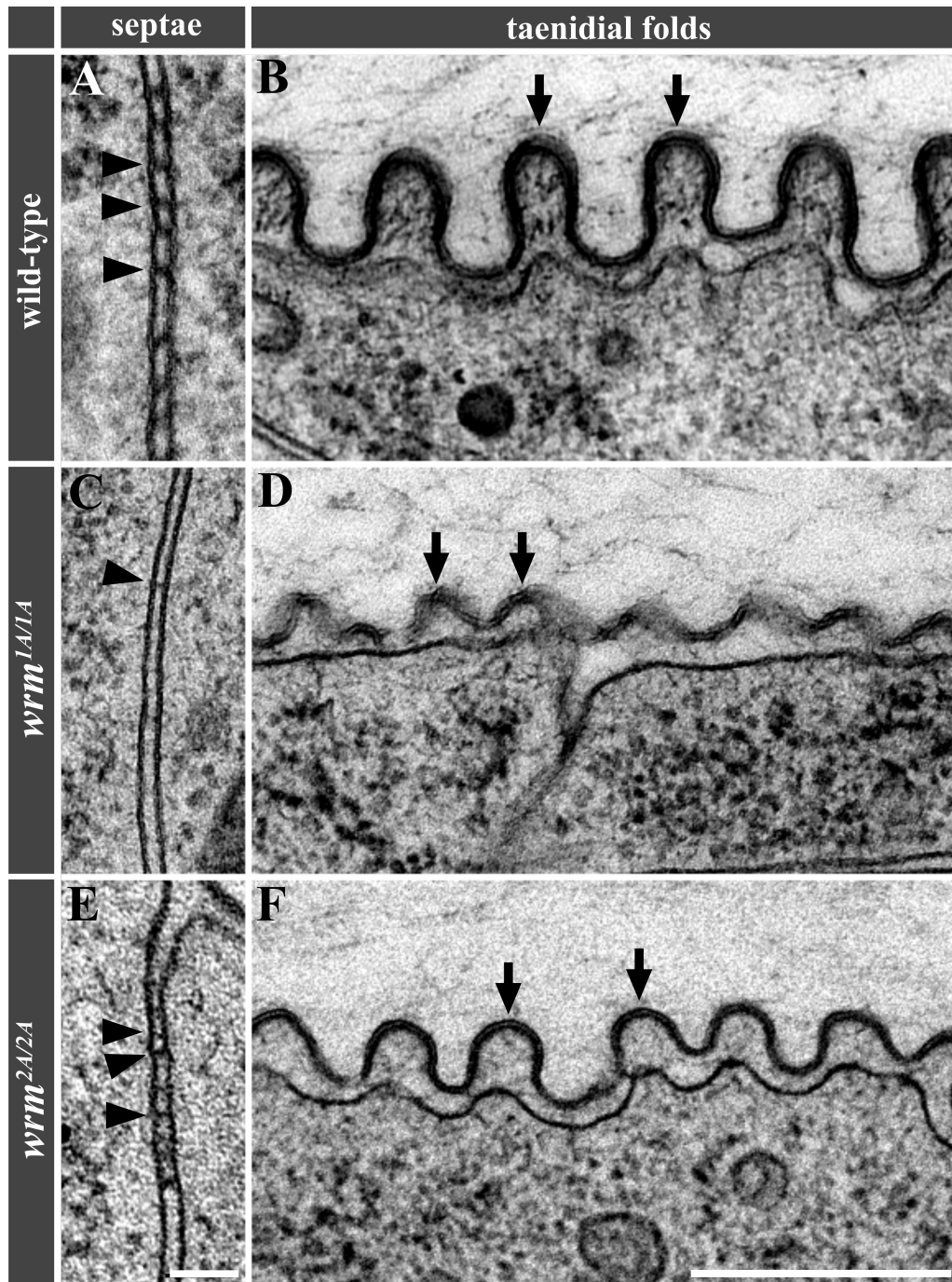


Figure 3.24 *wrm* mutant embryos affecting Wrm1 display SJ and taenial folds defects.

Electron microscopic images of tracheal cells in stage 17 wild-type (A, B), mutant *wrm^{1A/1A}* (C, D) as well as mutant *wrm^{2A/2A}* embryos (E, F). The electron-dense ladder-like septae of the SJ are established in wild-type (arrowheads in A) and *wrm* mutant embryos affecting Wrm2 (arrowheads in E). However, in *wrm* mutant embryos affecting Wrm1, electron-dense material is reduced between two plasma membranes (arrowhead in C). Wild-type as well as *wrm* mutant tracheal cells affecting Wrm2 show ordered and regular taenial folds (arrows in B and F). In contrast to wild-type, *wrm* mutant tracheal cells affecting Wrm1 display a crooked and irregular morphology of taenial folds (arrows in D). Scale bars indicates 100 nm in A, C, E and 500 nm in B, D, F. The images were kindly provided by Dietmar Riedel.

3.2.15 *Würmchen1* is essential for SJ core complex stability

SJ assembly begins during stage 13 of embryonic development in *Drosophila*, however, a functional paracellular barrier is first established during stage 16. During stage 13 SJ components are localized along the lateral cell membrane and become localized to the apicolateral membrane region in stage 16. Fluorescent recovery after photobleaching (FRAP) analysis revealed a low mobility of SJ components after the establishment of the barrier function in stage 16, indicating a stable high molecular weight core complex throughout embryonic development. This core complex stability is affected in embryos mutant for SJ core components (Laval et al., 2008). In embryos with affected core components a fast recovery rate is observed of GFP-tagged core components, indicating a disassociation of the core complex (Oshima and Fehon, 2011).

As described before, Mega and Kune mislocalize along the lateral membrane in *wrm* mutant embryos affecting Wrm1 (see sec. 3.2.11). In addition, 10 kDa as well as 70 kDa fluorescent dextran dyes cross the transepithelial barrier in *wrm* mutant embryos affecting Wrm1, indicating a impaired barrier function. To investigate whether Wrm1 is part of the SJ core complex, FRAP experiments were performed. To analyze the recovery rate of SJ components in *wrm* mutant embryos, GFP-tagged versions of the core complex members NeurexinIV (NrxIV) and Na⁺, K⁺-ATPase α -subunit (ATP α) were analyzed in *wrm*^{1A/1A} as well as *wrm*^{1E/1E} mutant embryos. Bleaching experiments of GFP-tagged core components were performed in the epidermis of wild-type embryos (Fig. 3.25 A), mutant embryos of the bona fide SJ core component Vari (Fig. 3.25 C) as well as homozygous *wrm*^{1E/1E} mutant embryos, which affects Wrm1 (Fig. 3.25 B). Recovery rates were measured at one bleached region per embryo. The FRAP kinetics of the GFP-tagged SJ core components differ from each other, depending on the mutant background. The fluorescence of NrxIV::GFP in wild-type (negative control) recovers less than 10% of the original fluorescence intensity in 13 min after photobleaching. The recovery rate of NrxIV::GFP in *vari* mutant embryos reaches 30% of its original prebleach intensity 13 min after bleaching (positive control). Also in *wrm*^{1E/1E} the recovery rate of NrxIV::GFP reaches almost 40% 13 min after bleaching (Fig. 3.25 D).

The recovery rate of ATP α ::GFP in *mega* mutant embryos reaches 25% of its original intensity (positive control), whereas less than 10% of the original intensity are reached in wild-type ATP α ::GFP embryos (negative control). However, in *wrm*^{1A/1A} mutant embryos affecting Wrm1 the fluorescence recovers 30% of its original intensity (Fig. 3.25 E). In embryos lacking the SJ core components Mega and Vari the fluorescence recovers within the first 5 min after photobleaching. In *wrm* mutant embryos affecting Wrm1, the recovery

rate of Nr x IV::GFP and ATP α ::GFP is similar to the recovery rate of Nr x IV::GFP and ATP α ::GFP in *mega* and *vari* mutant embryos.

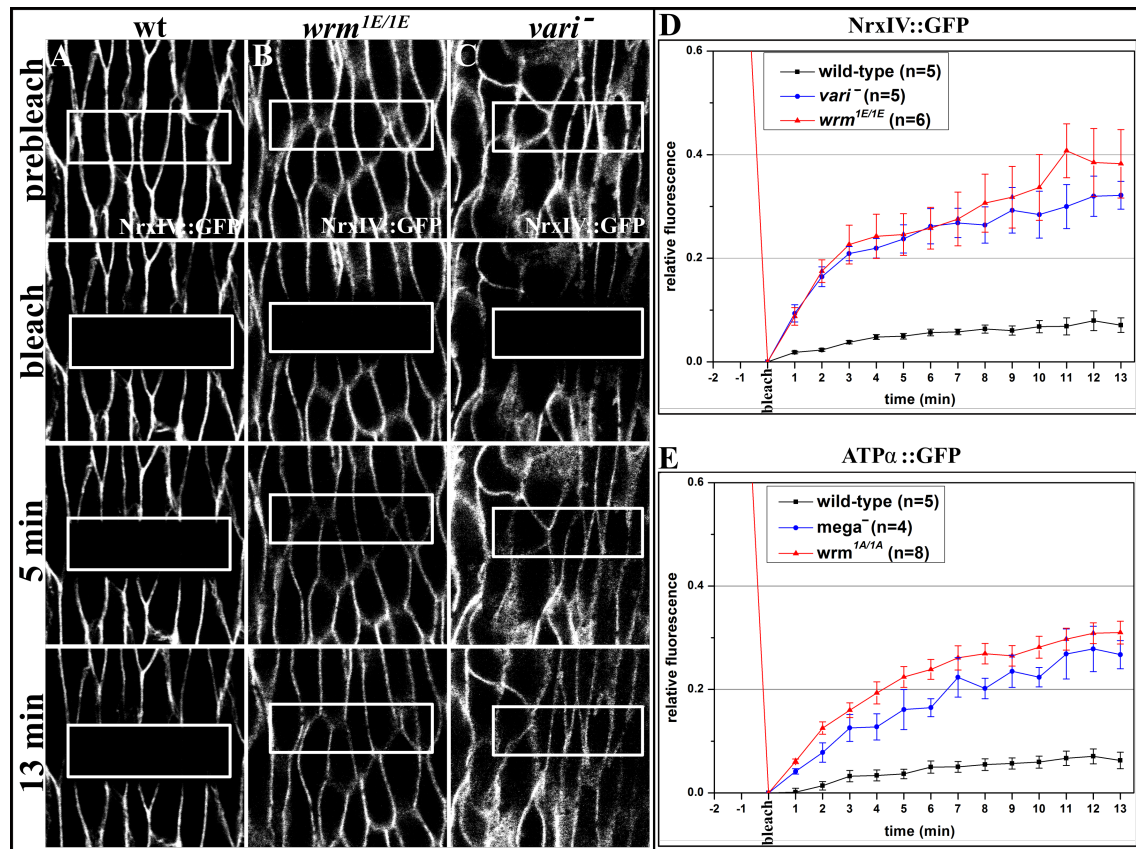


Figure 3.25 W \ddot{u} rmchen1 is essential for SJ core complex stability.

Time series of confocal imaging of FRAP experiments in early stage 16 wild-type (A), *wrm* mutant embryos affecting Wrm1 (B) as well as *vari* (C) or *mega* mutant embryos expressing GFP-tagged Nr x IV or ATP α . Photobleaching was performed across several epidermal cells and photobleached regions are indicated by white rectangles in A-C. The average relative fluorescence after photobleaching for GFP-tagged Nr x IV in wild-type and *wrm* mutant embryos were plotted. (D) In wild-type embryos Nr x IV::GFP fluorescence recovery reaches less than 10% after 13 min while in *vari*⁻ mutant embryos fluorescence is recovered to 30% after 13 min. The fluorescence recovery rate in *wrm* mutant embryos affecting Wrm1 is similar to the recovery rate of GFP-tagged Nr x IV in the *vari* mutant background, reaching 40% of its original intensity. (E) In *wrm* mutants affecting Wrm1 with GFP-tagged ATP α the recovery rate of the fluorescence reaches 30% of its original intensity, and recovers similarly to ATP α *mega* mutants embryos (25% recovery). The error bars indicate the standard error of mean.

Thus, the similar recovery rates of the SJ core components ATP α and Nr x IV in embryos mutant for *mega*, *vari* and *wrm*^{1A/1A} indicate that Wrm1 represents a genuine SJ core component as Mega and Vari.

3.2.16 Tracheal-specific overexpression of Würmchen1 leads to elongated tracheal tubes

The normal formation of a SJ core complex critically depends on the concentration of single core components. Not only the lack of a core component, but also its overexpression leads to a disruption of the complex (Behr et al., 2003). Thus, the tracheal overexpression of Wrm1 using the UAS-Gal4 system in combination with the *btl*-Gal4 driver line was analyzed.

In embryos with ectopic overexpression of Wrm1 in the developing embryonic trachea, no LC is detected (arrow and arrowhead in Fig. 3.26 B), which is in contrast to gas-filled trachea of wild-type embryos (arrow and arrowhead in Fig. 3.26 A). Also, stainings with CBP reveal a convoluted and tortuous tracheal network in embryos with tracheal overexpressed Wrm1 (compare Fig. 3.26 D to Fig. 3.26 C). Thus, the overexpression of Wrm1 in the embryonic trachea mimics the phenotype of *wrm* alleles affecting Wrm1, indicating that the correct level of Wrm1 is essential for a normal SJ formation.

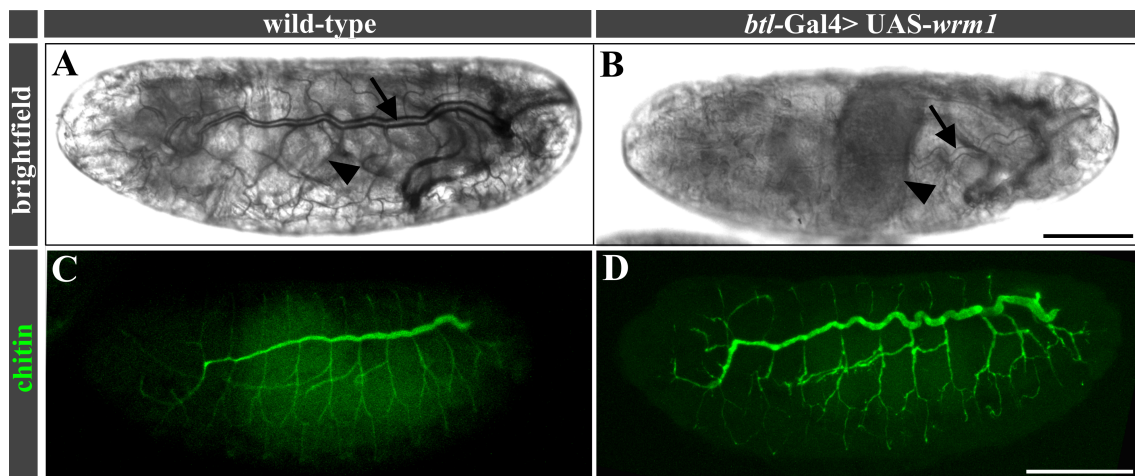


Figure 3.26 Tracheal specific overexpression of Wrm1 leads to elongated tracheal branches and impaired LC.

Brightfield light microscopic images of wild-type (A) and *btl*-Gal4, UAS-*wrm1* mutant embryos with overexpressed Wrm1 (B). Confocal Z-projections of CBP stainings in wild-type (C) and *btl*-Gal4, UAS-*wrm* mutant embryos, with overexpressed Wrm1 (D). Gas filling in tracheal tubes of different sizes is indicated in the wild-type embryo (arrow and arrowhead in A), however, no gas filling occurs in the *btl*-Gal4, UAS-*wrm1* mutant embryo (arrow and arrowhead in B). Elongation of the tracheal network is shown after tracheal knockdown (D), in contrast to straight branches in the wild-type embryo (C). Scale bar indicates 100 μ m.

3.2.17 Würmchen1 binds to *Drosophila* claudins

Wrm1 was discovered in co-immunoprecipitation (co-IP) experiments, which show Wrm1 binding to the *Drosophila* claudin Mega. Furthermore, FRAP experiments indicate that

Wrm1 is a SJ core component. To test whether Wrm1 not only binds to Mega, but also to other SJ components, *in vitro* co-IPs were performed with GFP-Trap beads against GFP-tagged forms of SJ components in cell culture. GFP-tagged SJ components were single- or co-expressed with Strep-tagged Wrm1 to investigate the interaction between

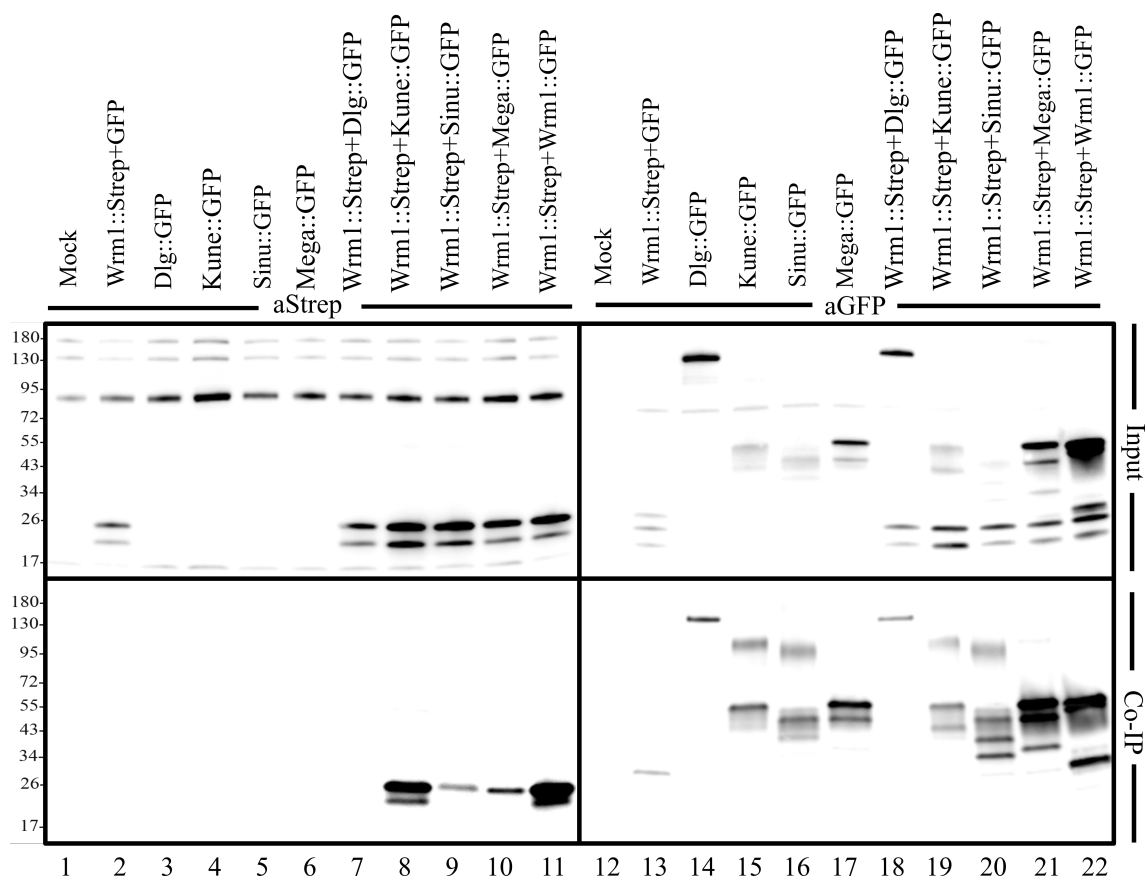


Figure 3.27 Wrm1 binds to claudins as well as itself *in vitro*.

In vitro co-IP of GFP-fusion proteins Dlg::GFP, Kune::GFP, Sinu::GFP, Mega::GFP as well as Wrm1::GFP (bottom row) using GFP-Trap beads, followed SDS PAGE and western blotting analysis stained for anti-Strep-HRP (aStrep; lanes 1-11) or anti-GFP (aGFP; lanes 12-22) following anti-rabbit-HRP antibody. The top row shows the corresponding inputs after staining of anti-Strep antibody (top row lanes 1-11) and anti-GFP (top row lanes 12-22), whereas Mock represents a negative control without prior transfected DNA. Full length Wrm1::Strep (22.5 kDa) is detected in co-IP probes Wrm1::Strep+Kune::GFP (bottom row lane 8), Wrm1::Strep+Sinu::GFP (bottom row lane 9), Wrm1::Strep+Mega::GFP (bottom row lane 10) as well as Wrm1::Strep+Wrm1::GFP (bottom row lane 11). A weaker fragment signal of full length Wrm1::Strep is detected after co-IP of Wrm1::Strep+Sinu::GFP and Wrm1::Strep+Mega::GFP when compared to co-IPs of Wrm1::Strep+Kune::GFP and Wrm1::Strep+Wrm1::GFP. The western blot anti-GFP staining after co-IP (bottom row, lanes 12-22) shows full length GFP (lane 13, 27.1 kDa), Dlg::GFP (lane 14 and 18, 116 kDa), Kune::GFP (lane 15 and 19, 57 kDa), Sinu::GFP (lane 16 and 20, 55 kDa), Mega::GFP (lane 17 and 21, 57.2 kDa) and Wrm1::GFP (lane 22, 46.6 kDa) fusion proteins.

Wrm1 and the corresponding GFP-tagged SJ component. Co-IP, SDS PAGE and

western blot analysis stained for Strep (aStrep; Fig. 3.27 lanes 1-11) as well as GFP (aGFP; Fig. 3.27 lanes 12-22) were performed subsequently. Figure 3.27 also shows inputs (top row) and corresponding probes after co-IP (bottom row). No Wrm1::Strep (22.5 kDa) fragment is visible after co-IP in Figure 3.27 lane 7 indicating that Wrm1 does not bind to Dlg::GFP (Fig. 3.27 lane 18). In contrast, Wrm1::Strep is detectable in Figure 3.27 lane 8-11 after co-IP with Kune::GFP (Fig. 3.27 lane 19), Sinu::GFP (Fig. 3.27 lane 20) and Mega::GFP (Fig. 3.27 lane 21). Furthermore, a strong Wrm1::Strep fragment signal is visible in Figure 3.27 lane 11, indicating that Wrm1 not only binds to *Drosophila* claudins, but also to itself. These results indicate that Wrm1 binds to the SJ core components Kune, Sinu and Mega as well as itself, but not to the SJ protein Dlg.

3.2.18 Würmchen2 binds to Mega

Wrm2 might be an essential SJ component during larval stages of *Drosophila* and might therefore interact with other SJ components. To test whether not only Wrm1 but also Wrm2 binds to the *Drosophila* claudin Mega, fusion proteins Wrm1::GFP as control and Wrm2::GFP were expressed in S2R+ cells, followed by co-IPs using GFP-Trap magnetic beads. Subsequent SDS PAGE as well as western blot analysis were conducted followed by anti-Mega (Fig. 3.28 lanes 1-6) or anti-GFP (Fig. 3.28 lanes 7-12) stainings. Inputs are depicted in the top row, whereas probes after co-IP are shown in the bottom row of Figure 3.28. Full length Mega (29.6 kDa) is detected in co-IP probes after co-expression of Wrm1::GFP (Fig. 3.28 lane 5) as well as Wrm2::GFP (Fig. 3.28 lane 6) fusion constructs. These result indicate an interaction between Mega and Wrm1 as well as Mega and Wrm2. However, the Mega fragment is more prominent in the co-IP probe after binding to Wrm1, suggesting a stronger interaction between Mega and Wrm1 than Mega and Wrm2.

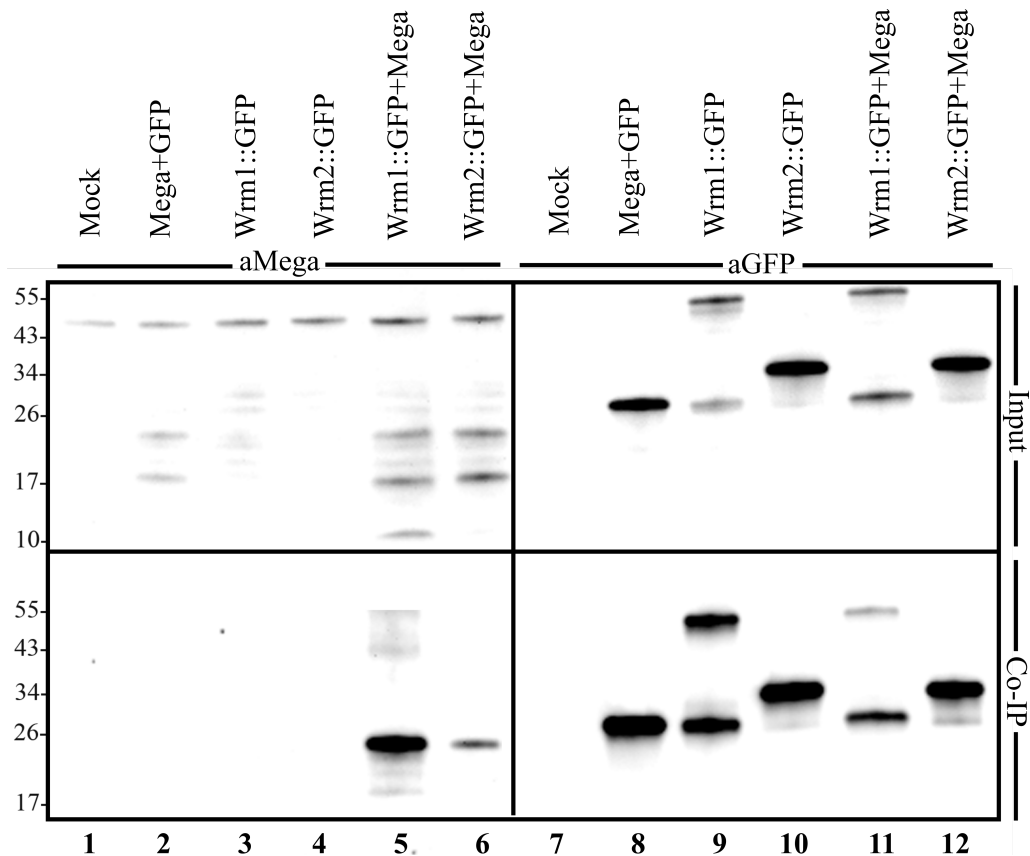


Figure 3.28 Wrm1 and Wrm2 bind to Mega *in vitro*.

In vitro co-IP of GFP-fusion proteins Wrm1::GFP as well as Wrm2::GFP (bottom row) using GFP-Trap beads, followed SDS PAGE and western blotting analysis stained for anti-Mega (aMega; lanes 1-6) or anti-GFP (aGFP; lanes 7-12) following anti-mouse-HRP or anti-rabbit-HRP antibody. The top row shows the corresponding inputs, whereas Mock represents a negative control without prior transfected DNA. Full length Mega (29.6 kDa) is detected in co-IP probes Mega+Wrm1::GFP (bottom row, lane 5) as well as Mega+Wrm2::GFP (bottom row, lane 6). A weaker fragment signal of full length Mega is detected after co-IP of Mega-Wrm2::GFP when compared to co-IP of Mega-Wrm1::GFP. The western blot anti-GFP staining after co-IP (bottom row, lanes 7-12) indicates full length Wrm1::GFP fusion protein (lane 9 and 11; 46.6 kDa) and from the fusion protein disintegrated GFP, which is detected as a single GFP fragment (lanes 9 and 11; 27.1 kDa). Wrm2::GFP fusion proteins are present as 33.9 kDa fragments (bottom row, lane 10 and 12).

3.2.19 Würmchen1 binds to Würmchen2

Wrm1 as well as Wrm2 bind to Mega, however the interaction between Mega and Wrm2 is weaker when compared to the interaction of Mega and Wrm1. To test *in vitro* whether Wrm1 and Wrm2 bind to each other or the interaction might be mediated by Mega, Wrm1::Strep as well as Wrm2::GFP constructs were co-transfected into S2R+ cells with

3.2 Identification and characterization of *würmchen*

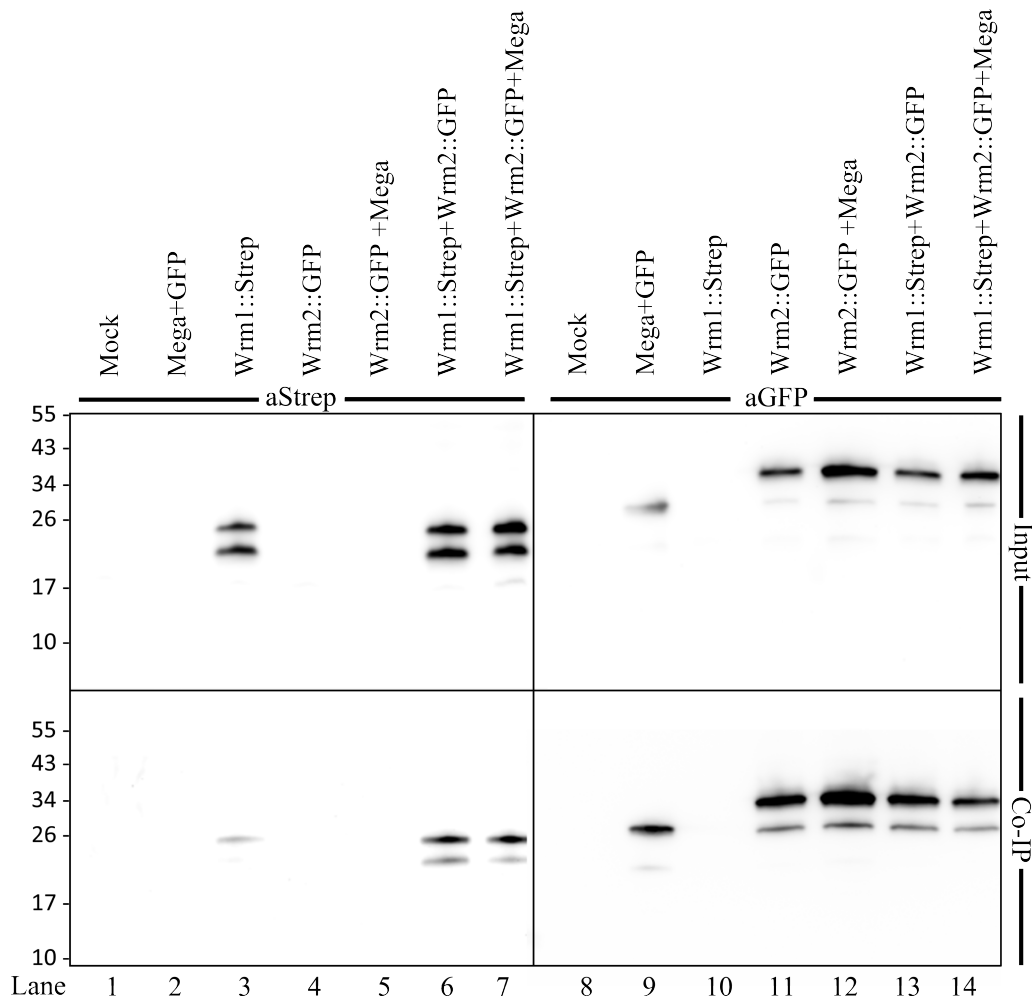


Figure 3.29 Wrm1 binds to Wrm2 *in vitro*.

In vitro co-IP of GFP-or Strep fusion proteins Wrm1::Strep and Wrm2::GFP (bottom row) using GFP-Trap beads, followed SDS PAGE and western blotting analysis stained for anti-Strep-HRP (aStrep; lanes 1-7) or anti-GFP (aGFP; lanes 8-14) following anti-rabbit-HRP antibody. The top row shows the corresponding inputs, whereas Mock represents a negative control without prior transfected DNA. Full length Wrm1::Strep (22.5 kDa) is detected in co-IP probes Wrm1::Strep +Wrm2::GFP (bottom row, lane 6) and Wrm1::Strep+Wrm2::GFP+Mega (bottom row, lane 7). The western blot anti-GFP staining after co-IP (bottom row, lane 8-14) shows full length GFP (lane 9; 27.1 kDa) and Wrm2::GFP (lane 11, 12, 13 and 14; 33.9 kDa). Additionally, in lanes 11, 12, 13 as well as 14 GFP is detected (27.1 kDa), which disintegrated from the corresponding fusion protein.

or without Mega, followed by co-IP using GFP-Trap beads, SDS PAGE and western blot analysis stained for Strep (Fig. 3.29 lanes 1-7) and GFP (Fig. 3.29 lanes 8-14). Inputs are depicted in Figure 3.29 top row, whereas probes after co-IP are visible in Figure 3.29 bottom row. Full length Wrm1::Strep (22.5 kDa) is visible after co-IP with Wrm2::GFP (Fig. 3.29 bottom row lane 6) as well as Wrm2::GFP+Mega (Fig. 3.29 bottom row lane 7). The anti-GFP staining in Figure 3.29 (lanes 8-14) show the Wrm2::GFP fusion fragment (33.9 kDa) in lane 11-14, but also an additional single GFP fragment (27.1 kDa) due to

fusion protein degradation. A single GFP fragment is also detected in Figure 3.29 lane 9 after expression of Mega and GFP. These results indicate Wrm1 binds to Wrm2 and this interaction is not mediated by Mega. The results also suggest that Wrm2 is at least a transient binding partner of SJ core components.

3.2.20 Würmchen1 and Würmchen2 expressing S2R+ cells lack homophilic adhesion capability

A single transmembrane domain, is predicted for both Wrm1 and Wrm2. However, Wrm2 showed no effect on the localization of tested SJ core components, but it may still associate with the SJ complex in later larval development. Therefore, the adhesion capacity was tested for Wrm1 and Wrm2.

One SJ protein, FasciclinIII (FasIII), was shown to have adhesion capability *in vitro* (Snow et al., 1989). FasIII was used as positive control in the cell aggregation assay. S2R+ cells were transfected with *fasIII* and upon incubation time of 24 h, the cells expressed FasIII. After the aggregation assay and subsequent fixation an immunohistological staining of FasIII was performed and cell clusters were observed in FasIII expressing cells (Fig. 3.30 A) due to the adhesion capability of FasIII. The same approach was performed using S2R+ cells expressing Mega (Fig. 3.30 B), GFP-tagged Wrm1 (Fig. 3.30 C) and Wrm2 GFP-tagged (Fig. 3.30 D). An additional staining with DAPI, marking cell nuclei, was conducted (Fig. 3.30 A', B', C' and D') and merges of both channels are depicted in Figure 3.30 A'', B'', C'' as well as D''. In contrast to cell clusters in FasIII expressing cells, only single cells were observed after the expression of Mega (Fig. 3.30 B), Wrm1::GFP (Fig. 3.30 C) and Wrm2::GFP (Fig. 3.30 D). In summary, the aggregation assay using S2R+ cells indicates no evidence of homophilic cell adhesion in cells expressing Mega, Wrm1 and Wrm2. These results suggest that neither Wrm1 nor Wrm2 mediate homophilic cell adhesion *in vitro*.

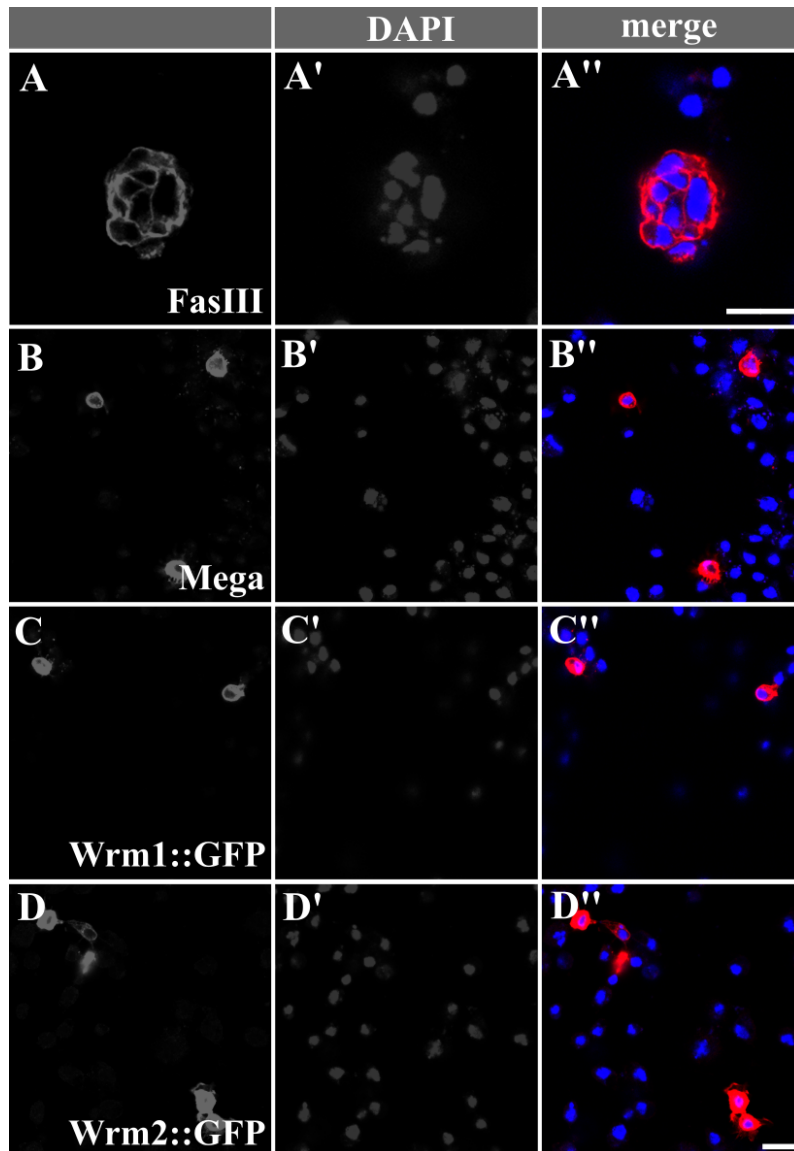


Figure 3.30 Mega, Wrm1 and Wrm2 show no cell adhesion capability in S2R+ cells.

Confocal images of *Drosophila* S2R+ cells expressing FasIII (A-A''), Mega (B-B''), Wrm1::GFP (C-C'') and Wrm2::GFP (D-D'') stained with anti-FasIII antibody (A), anti-Mega antibody (B) as well as anti-GFP antibody labelling Wrm1 (C) and Wrm2 (D), respectively. FasIII expressing cells form large cell clusters, in contrast to Mega, Wrm1-GFP and Wrm2-GFP, where no cell clusters are observed. Scale bar indicates 20 μ m in A'' and 10 μ m in D''.

4 Discussion

SJ are large protein complexes that control the transepithelial flow of solutes and thereby establish different physiological compartments in the invertebrate body. This work describes the identification and characterization of the essential and novel SJ core component, called Würmchen1 (Wrm1). Wrm1 is encoded together with Wrm2 by the bicistronic *wrm* gene locus. Wrm2 is also a SJ component and essential during larval development. Furthermore, this work describes the generation of synthetic mutant constructs of the core component Megatrachea (Mega), a member of the claudin family, and their *in vivo* functional analysis during SJ formation.

4.1 Functional domain analysis of the claudin Megatrachea

Vertebrate claudins have been extensively studied *in vitro*. A highly conserved motif, GLW-C-C in the 1st extracellular loop (ECL1), was shown to be essential for claudin function in vertebrates (Krause et al., 2008). Additionally, the GLW triplet of amino acids is a receptor for the hepatitis C virus (HCV) in vertebrates (Cukierman et al., 2009). Individual mutation of the GLW residues in claudin-1 prohibit HCV binding and mutants are able to traffic to the plasma membrane normally. However, the ability to model *trans*-interactions may be impaired, whereas *cis*-interactions are formed normally. In vertebrate claudin-2, mutations of all three GLW residues to alanine (GLW to AAA) prevented the protein to reach the plasma membrane. Despite the substitution of GLW to three alanines, mutants are still able to form dimers detected in native PAGE, same as wild-type claudin-2 (Van Itallie et al., 2011). Mutations of all three GLW residues to alanine individually or all three exchanged together to alanine in the *Drosophila* claudin Mega in this work abolish the ability of the proteins to reach the plasma membrane (see Tab. 3.1 constructs M30, M52, M53 and M54), as observed for vertebrate claudin-2. These results indicate that the conserved GLW motif plays an essential role in stabilizing the correct folded structure of ECL1 not only in vertebrates, but also in invertebrates and hence having a common function in vertebrates and invertebrates.

Another feature of the claudin signature motif is a pair of cysteines located shortly

after the GLW sequence in the ECL1 of vertebrate claudin 1-24. Individual mutations of either conserved cysteines in claudin-1 prevents HCV binding (Cukierman et al., 2009). Mutations of one or both conserved cysteines in claudin-5, lead to loss of the ability to form a barrier for small ions, however, still retaining its ability to reach the plasma membrane and localize correctly (Wen et al., 2004). Mutations of either cysteine has the same functional phenotype and mutations of both cysteines has no additive effect suggesting that they may form an intracellular disulfide bond (Günzel and Yu, 2013). In *Drosophila* mutations of both conserved cysteines in the claudin Mega lead to viable flies (see Tab. 3.1 construct M17), suggesting that the cysteines are not involved in stabilizing folded Mega and the C-C function is not conserved between vertebrates and invertebrates.

It was discovered in vertebrates, that the net charge of the second half of the ECL1 plays a critical role in paracellular charge selectivity (Van Itallie et al., 2003). A model was developed, where the ECL1 forms a pore and several specific residues face into the lumen of the pore. These pore-facing residues are specifically charged and therefore act as a charge filter for diffusing molecules (Günzel and Yu, 2013). Mutations of several residues in the second half of the ECL1 in the claudin Mega in *Drosophila* (see Tab. 3.1 construct M40, M48, M60, M62, M64 and M67-M69), result in viable flies, indicating that the mutations do not affect Mega function essentially. However, it cannot be excluded that these mutations do change or reverse charge selectivity of the presumable forming pore of ECL1, but Mega function is not essentially impaired and therefore SJs are functional. Differences between vertebrate and invertebrate findings concerning the charge selectivity of ECL1 might also be explained by the fact that vertebrate experiments were conducted *in vitro*, leading to the question of how altered charge selectivity may affect viability of such vertebrates.

Ultimately, a highly conserved arginine residue is found at the very end of the ECL1, which leads to low expression levels in claudin-4 and -16 when mutated. Mutation of this residual arginine leads to the retention of claudin-4 and -16 to the endoplasmic reticulum, indicating a function of this residue in global claudin folding (Günzel and Yu, 2013). Mutation of this conserved arginine at the very end of the ECL1 of Mega in *Drosophila* (see Tab. 3.1 construct M56) leads to viable flies indicating no essential function for protein folding as well as SJ formation in *Drosophila*.

In vertebrates, the ECL2 is highly conserved among claudins and it was previously shown that the ECL2 is not involved in determination of the paracellular permeability (Günzel and Yu, 2013), but rather mediates claudin-claudin interaction (Blasig et al., 2006). Mutations

of individual residues of the ECL2 in claudin-5 and transfection into HEK cells, led to mutants, in which the wild-type-like localization of claudin-5 at cell contacts is affected and a distribution along the plasma membrane was observed. FRET measurements indicate that *cis*-interactions of claudin-5 is wild-type-like, however, *trans*-interactions are affected in mutants, in which claudin-5 is mislocalized (Piontek et al., 2008). Modeled ECL2 structure reveals a helix-turn-helix motif, in which three residues mediate *trans*-interaction. The three residues, F147, Y148 and Y158 form an aromatic core that may be involved in hydrophobic interactions with the aromatic core of a second ECL2 on the other side of the TJ. Mutations of F147, Y148 and Y158 disrupted the *trans*-interaction and cause loss of barrier function in MDCKII cells (Piehl et al., 2010). A similar aromatic motif is found in the ECL2 of Mega in *Drosophila* (see Tab. 3.1 construct M18). Individual mutations of all four aromatic amino acids of the motif lead to viability of the flies (see Tab. 3.1 construct M19, M35-M37). Also mutations of all four aromatic amino acids to alanines (YWYF to AAAA) lead to wild-type-like localization of Mega in the hindgut, indicating that Mega folding and trafficking is not affected in this tissue. Additionally, the SJ components Dlg and Kune are localized wild-type-like in the hindgut, indicating wild-type-like SJ assembly. However, in the tracheal epithelium of M18 mutant embryos Mega and Kune are localized only partially wild-type-like. Also, the loss of barrier function for 10 kDa and 70 kDa fluorescent dextran dyes and an elongated and convoluted tracheal network indicate impaired function of tracheal SJs. However, the exocytosis of the chitin modifying enzyme Serp is mediated in such embryos. Thus, the partially normal localization of Mega and Kune may indicate the formation of a limited number or rudimentary SJs, which still mediate exocytosis, but lack an epithelial barrier function.

Based on data from vertebrates, which suggest that ECL2 may be involved in *trans*-interactions, the same may be analogous in *Drosophila*. The *cis*-interactions of ECL2 in Mega may not be affected in the hindgut and tracheal epithelium leading to correct formation and function of SJ. However, loss of *trans*-interactions of Mega ECL2 may lead to loss of a bridge that spans two plasma membranes and therefore the barrier in the tracheal epithelium may be impaired. In conclusion, I propose that the ECL2 is also essential for *trans*-interactions of Mega, but the persistence of *cis*-interaction is sufficient for at least limited wild-type-like Mega folding, trafficking, localization and function.

The C-terminus of claudins differs in length, is divergent in sequence and predicted to be disordered (Günzel and Yu, 2013). In *Drosophila*, several Mega constructs affecting the C-terminus were designed and analyzed. Interestingly, serial adjacent deletions of

the Mega C-terminus did not affect viability (see Tab. 3.1 constructs M9, M10 and M21), indicating no essential motif for Mega function. The highly conserved PDZ-binding motif at the very 3' end of the C-terminus also displayed no impaired Mega. In vertebrates the PDZ motif of claudins is highly conserved and binds to TJ scaffolding protein ZO1, ZO2 and ZO3 as well as MUPP1 (Itoh et al., 1999; Hamazaki et al., 2002), but the biological effect of the interaction is unclear.

In vertebrate claudin-1, -5, -6 and -16 truncation of the cytoplasmic tail was discovered to impair trafficking to TJ and affected claudins remained intracellularly, mostly in the endoplasmic reticulum (ER; Arabzadeh et al., 2006; Müller et al., 2006; Ruffer and Gerke, 2004), followed by degradation *via* the proteasome (Müller et al., 2006). ER retention may be explained by the binding of the cytoplasmic tail to different proteins, which enable exit of claudins from ER. Truncations of the PDZ-binding motif in claudin-1 and -5 did not impair trafficking and deletions of most of the C-terminus was needed to have an effect on trafficking. In *Drosophila*, the deletion of the entire Mega C-terminus led to retention of Mega in vesicles of the cytoplasm, mimicking the vertebrate phenotype for truncated C-termini in claudin-1 and -5. These results indicate that the cytoplasmic C-terminus has an essential role in trafficking from the ER to the plasma membrane to TJs as well as SJs, thus, the C-terminus is essential for claudin function in vertebrates and invertebrates.

In addition, several Mega constructs have been designed and analyzed affecting the ICL of Mega. All constructs that are homozygous lethal, led to the retention of Mega in vesicles inside the cytoplasm. One amino acid, E147, was identified to be essential in normal Mega folding. Exchange of the motif YWL to three alanines led to viable flies (see Tab. 3.1 construct M20), however, the additional substitution of glutamic acid E147 to alanine (see Tab. 3.1 construct M41), revealed affected Mega folding trafficking and localization, leading to an impaired barrier function and convoluted tracheal tubes. Thus, the ICL may be essential for normal Mega folding and localization.

In summary, synthetic *mega* constructs were either viable (see Fig. 4.1) or lethal (see Fig. 4.2). However, it was not possible to assign a distinct function to a certain Mega domain due to partial overlapping of substitutions or deletions within viable and lethal mutant lines and the retention of Mega presumably within the ER of epithelial cells in lethal lines.

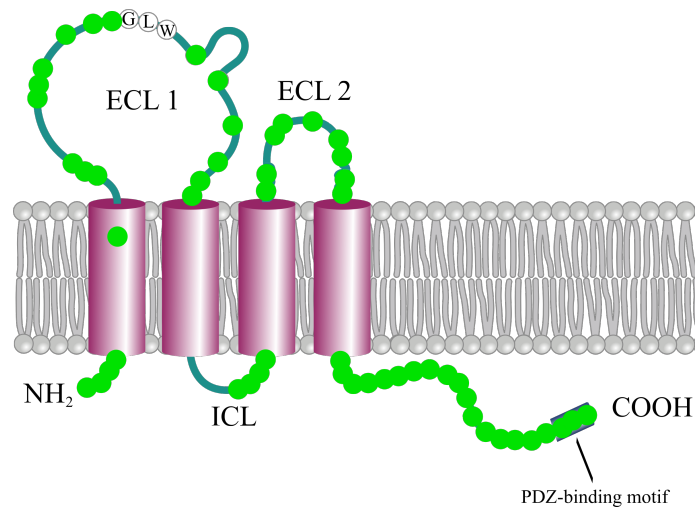


Figure 4.1 Scheme of viable mutations in Mega.

Model of Megatrachea consisting of N-terminus, two extracellular loops (ECLs), one extracellular loop (ICL) and a C-terminus as well as four transmembrane domains. Green dots indicate positions of mutations of single amino acids or groups of amino acids as well as deletions.

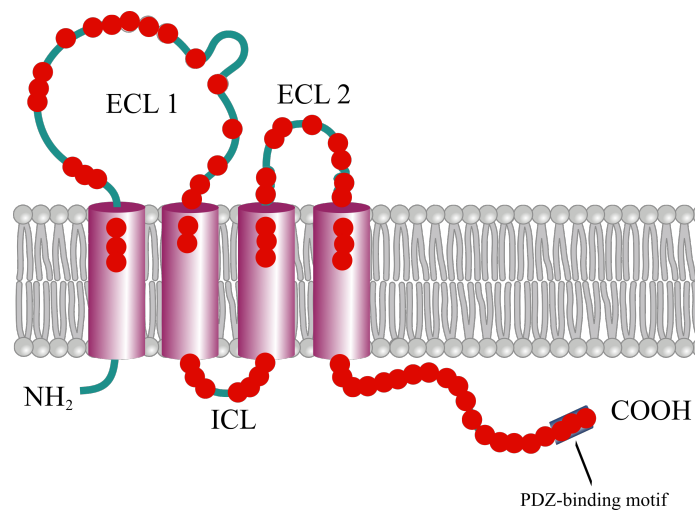


Figure 4.2 Scheme of lethal mutations in Mega.

Model of Megatrachea consisting of N-terminus, two extracellular loops (ECLs), one extracellular loop (ICL) and a C-terminus as well as four transmembrane domains. Red dots indicate positions of mutations of single amino acids or groups of amino acids as well as deletions.

4.2 Functional analysis of the bicistronic gene *wrm*

Wrm1 was identified in co-immunoprecipitation experiments, followed by mass spectrometry analysis as a putative binding partner of the claudin Mega (see sec. 3.2.1). Further analysis of the *wrm* locus revealed that it encodes two proteins, Wrm1 and Wrm2. The open reading frames (ORFs) of Wrm1 and Wrm2 are separated by 6 base pairs and are therefore in frame. Thus, there might be the rare case of a stop codon readthrough in the *wrm* gene. Stop codon readthrough has been proposed in different organisms including yeast, in which readthrough as well as frameshifting is epigenetically controlled by a prion protein state. This feature enables yeast to adapt the translation of new domains at low rates during normal development and simultaneously allowing higher translation rates when exposed to stress (True and Lindquist, 2000; Baudin-Baillieu et al., 2014). Moreover, stop-codon-readthrough has also been reported for the *Drosophila* genes *synapsin* and *kelch*, generating differently sized isoforms (Klagges et al., 1996; Robinson and Cooley, 1997).

Complementation tests, which include frameshift mutations in *wrm1*, indicate that Wrm1 and Wrm2 are expressed independently of each other. At least the essential functions of Wrm1 and Wrm2 for viability and tracheal development are not compromised by the lack of either one or the other Wrm protein.

4.2.1 Würmchen1 is an essential SJ core component

In embryos mutant for *wrm* affecting Wrm1, SJ organization was shown to be impaired. Ultrastructure analysis revealed lack of septae at cell-cell contacts, suggesting the requirement of Wrm1 for SJ organization. Strikingly, Wrm1 is not required for septae formation per se, since single septae distributed between plasma membranes are detectable. This is in strong contrast to *nrxIV*, *cor* as well as *mega* mutant embryos, where no septae were discovered between plasma membranes (Baumgartner et al., 1996; Lamb et al., 1998; Behr et al., 2003). In mutant embryos with affected Wrm1 the number of septae is strongly reduced as reported in *sinu* mutant embryos (Wu et al., 2004), indicating that Wrm1 is not only required for SJ establishment but also for the formation of the correct number of septae. The remaining ability of *wrm* mutant embryos affecting Wrm1 to form morphologically normal septae may result from the presence of all three *Drosophila* claudins as well as several other transmembrane components.

Recent studies revealed a highly stable and high molecular weight SJ core complex using fluorescence recovery after photobleaching (FRAP). The SJ core complex is exceptionally immobile in wild-type conditions, but disassociates in embryos mutant for

SJ core components, resulting in a fast redistribution of SJ core components along the cell membrane. The fast recovery rate of the tagged core components in *wrm* mutant embryos affecting Wrm1 strongly indicate that Wrm1 represents a bona fide SJ core component. However, the recovery rate of the tagged core components is faster in *wrm1* mutant embryos as compared to mutants of the claudin core component Mega. This difference in recovery may be explained by the disassociation of the SJ core complex into distinct subcomplexes in different mutant backgrounds leading to a faster recovery rate for smaller subcomplexes. This speculation leads to the assumption that the SJ core complex disassociates into different and smaller subcomplexes in *wrm* mutant embryos affecting Wrm1 than in *mega* mutant embryos. Further analysis with other GFP-tagged SJ core components is necessary to address this hypothesis.

In summary, Wrm1 is a putative novel SJ core component essential for proper SJ formation as well as function and co-localizes with known SJ core components at apicolateral regions of epithelial cells (Fig. 4.3).

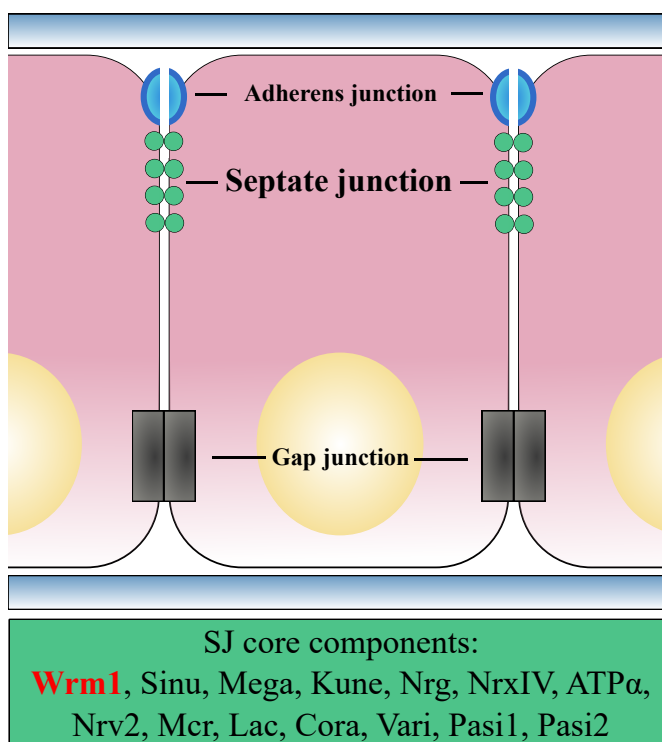


Figure 4.3 Scheme of an ectodermally derived epithelium in *Drosophila*.

Wrm1 is a member of the SJ core complex and co-localized with known SJ core components in ectodermally derived epithelial tissues of *Drosophila*.

4.2.2 Würmchen1 is involved in tracheal morphology and function during embryogenesis

The regulation of tube length and size has been extensively studied in the tracheal system of *Drosophila* (Wu et al., 2004; Behr et al., 2003; Moussian et al., 2005; Arau et al.,

2005). Two phenotypic categories can be deduced from genes regulating tube size: genes essential for controlling tube length and genes for regulating tube diameter. Mutations in SJ core components, such as *Mega*, *Kune*, *Sinu* as well as *ATP α* lead to an elongated and tortuous tracheal network with unaffected tube diameter (Behr et al., 2003; Wu et al., 2004; Nelson et al., 2010; Paul et al., 2003). However, mutations in the SJ core component *Vari* result in enlarged tube diameter (Moyer and Jacobs, 2008) mimicking the phenotype of mutations of *cystic* and *mummy* as well as *krotzkopf verkehrt* (Moussian et al., 2005; Arau et al., 2005). Tracheal phenotype of double *vari/sinu* mutant embryos appears worse than the phenotype in single *vari* and *sinu* mutant embryos, suggesting that these SJ core component act in different tube size controlling pathways (Wu et al., 2004).

In *wrm* mutant embryos, which affect *Wrm1*, tracheal tubes are elongated and convoluted, however, tube diameter is unchanged. These finding indicates that *Wrm1* acts in the same tube size regulatory pathways as the claudins *Mega*, *Kune* and *Sinu*.

Tube length is restricted by the putative chitin deacetylases *Serp* and *Verm* (Luschnig et al., 2006). However, apical exocytosis is required to accumulate *Serp* and *Verm* inside the tracheal lumen. This process is mediated by the SJs, and is disturbed in bona-fide SJ mutants (Behr et al., 2003; Nelson et al., 2010; Wu et al., 2004). Luminal accumulation of *Serp* was analyzed in *wrm* mutant embryos affecting *Wrm1* and *Wrm2*. *Serp* is exocytosed into the tracheal lumen in lack of *wrm2* embryos, whereas accumulation of *Serp* inside the tracheal cells and therefore an impaired exocytosis was observed in lack of *wrm1* embryos. Thus, *Wrm1* is essential for SJ mediated exocytosis.

The function of *Wrm1* was further analyzed in overexpression experiments in wild-type conditions. The overexpression of the essential SJ core component *Mega* leads to mislocalized *Mega* in the hindgut, convoluted tracheal network and impaired LC. It was proposed that *Mega* level is critical for the correct assembly of the SJ protein complex (Behr et al., 2003). Overexpression of *Mega* leads to a higher *Mega* level and might disrupt SJ complex due to competitive binding during complex assembly. Also, embryos with overexpressed *Wrm1* mimic the *Mega* overexpression phenotype, including a morphologically different tracheal system, impaired LC as well as embryonic lethality. This *Wrm1* overexpression phenotype may be explained in a similar manner: the higher than wild-type level of *Wrm1* may prevent the assembly of the SJ protein complex due to competitive binding of the SJ core components to each other and therefore affecting the establishment of SJs.

In vitro analysis showed that *Wrm1* binds to all *Drosophila* claudins, indicating that *Wrm1* may play a key role in the composition of the SJ complex. Most importantly, *Wrm1*

binds to itself, revealing the possibility of more than one Wrm1 protein existing within one SJ complex, which might additionally mediate binding between other SJ core components. These results suggest an essential function of Wrm1 interaction to SJ components, and thus, Wrm1 may provide a protein connecting and stabilizing function within the SJ core complex.

4.2.3 Würmchen2 is a putative transient binding partner of SJ core components

Wrm2 was shown to bind to the SJ core components Mega as well as Wrm1 *in vitro*, suggesting the involvement of Wrm2 in SJ assembly and/or maintenance. However, Wrm2 showed no essential function during embryonic development, but mutations in *wrm2* led to lethality in larval stages. Surprisingly, affected larvae did not display abnormal tracheal morphology or LC defects, indicating a normal barrier function. These findings suggest that Wrm2 is not directly involved in the establishment of the SJs and the resulting barrier function, but Wrm2 may have an essential function for viability *via* binding or transient interaction with the core components Mega and Wrm1 during larval stages.

The deletion of one or two amino acids in the predicted transmembrane domain of Wrm2 led to the lack of function and thus, lethality in larval stages. Transmembrane proteins play essential roles in cell function and therefore minimal alterations in the transmembrane anchor of proteins may lead to severe consequences, such as function alterations or loss of function (Prusiner, 1994; Kwok et al., 2000). A lack of function was also found in Mega, when substituting methionine at position 165 to the bulky residue tryptophan (see Tab. 3.1 construct M72) in the 3rd transmembrane domain, presumably preventing correct protein folding and integration into the membrane. These findings suggest that small changes in the composition of transmembrane domains have dramatic consequences for protein folding and trafficking. It is therefore highly likely that the deletion of one or two amino acids in the transmembrane domain of Wrm2 is sufficient to impair processing and thus, cause complete lack of Wrm2 function.

5 Materials and methods

5.1 Material

5.1.1 Chemicals

All chemicals used in this thesis were obtained from Fluka, Invitrogen, Merck, Roche, Roth, Sigma-Aldrich and VWR, if not indicated otherwise.

5.1.2 Enzymes

Restriction endonucleases and DNA polymerases were ordered from NEB. Shrimp Alkaline Phosphatase was obtained from Affimetrix.

5.1.3 Suppliers

Table 5.1 List of suppliers

Name	Location
Abcam	Cambridge, USA
Addgene	Watertown, USA
Affimetrix	Santa Clara, USA
Agilent Technologies (Stratagene)	Waldbronn, Germany
Applied Biosystems GmbH	Darmstadt, Germany
Becker's Bester GmbH	Lütgenrode, Germany
Best Gene Inc.	Chino Hills, USA
BioRad	Hercules, USA
Biozym Scientific GmbH	Hessisch Oldendorf, Germany
Bloomington Drosophila Stock Center (BDSC)	Bloomington, USA
Carl Roth GmbH & Co. KG	Karlsruhe, Germany
Chromotek	Planegg-Martinsried, Germany
Colgate-Palmolive	Hamburg, Germany
Cornexo GmbH & Co. KG	Freimersheim, Germany

Table 5.1 – *Continued from previous page*

Name	Location
Developmental Studies Hybridoma Bank (DSHB)	Iowa City, USA
DMS Bakery Ingredients	Dordrecht, Netherlands
Enzo Life Science GmbH	Lörrach, Germany
Eppendorf AG	Hamburg, Germany
Fermentas	St. Leon-Rot, Germany
Fluka	Neu-Ulm, Germany
GE Healthcare Buchler GmbH & Co. KG	Braunschweig, Germany
Gibco	Eggenstein, Germany
Gilson International B.V.	Den Haag, Netherlands
Grafschafter Krautfabrik	Meckenheim, Germany
Greiner Bio One	Nürtingen, Germany
Invitrogen Life Technologies	Darmstadt, Germany
Jackson ImmunoResearch	West Grove, USA
Leica Microsystems	Wetzlar, Germany
Macherey-Nagel GmbH & Co. KG	Düren, Germany
MatTek	Ashland, USA
MeisterMarken Ulmer Spatz	Bingen am Rhein, German
Merck KGaA	Darmstadt, Germany
Microsynth AG	Göttingen, Germany
Millipore	Darmstadt, Germany
Molecular Probes	Eugene, USA
MWG	Ebersberg, Germany
New England Biolabs (NEB)	Frankfurt, Germany
Perkin Elmer	Boston, USA
Phillips Deutschland GmbH	Erlangen, Germany
Pierce Biotechnology	Rockford, USA
Promega	Madison, USA
Qiagen GmbH	Hilden, Germany
Roche Diagnostics GmbH	Basel, Switzerland
Sarstedt AG & C.	Nürnbrecht, Germany
Sartorius Stedim Biotech GmbH	Göttingen, Germany
Schott AG	Mainz, Göttingen
Schleicher and Schüll	Dassel

5.1 Material

Table 5.1 – *Continued from previous page*

Name	Location
Sigma-Aldrich Chemie GmbH	Taufkirchen, Germany
Soja Austria	Vienna, Austria
Stratagene	See Merck
Synaptic Systems	Göttingen
Thermo Fisher Scientific	Schwerte, Germany
USB	Staufen, Germany
Vector Labs	Burlingame, USA
VWR International	Leuven, Belgium
Zeiss AG	Jena, Germany

5.1.4 Commercially available kits

Table 5.2 List of commercially available kits

Name	Source
NucleoSpin [®] Extract II Kit	Macherey-Nagel
NucleoSpin [®] Plasmid Kit	Macherey-Nagel
Qiagen [®] Plasmid Plus Midi Kit	Qiagen
TOPO TA Cloning [®] Kit for Sequencing	Invitrogen
NEBuilder [®] HiFi DNA Assembly Master Mix	NEB
DIG RNA Labeling Kit (SP6/T7)	Merck KGaA
HotStarTaq DNA Polymerase Kit	Qiagen
Quick Ligation Kit	NEB
WesternBright Chemilumineszenz Substrat Sirius	Biozym

5.1.5 Reagents

Table 5.3 List of reagents

Name	Company
10x blocking buffer	Sigma-Adrich
Ammonium hydrogen carbonate (ABC)	Thermo Fisher Scientific
BS3	Pierce

Table 5.3 – *Continued from previous page*

Name	Company
Desoxynucleotide (dNTPs)	NEB
Dithiothreitol (DTT)	BioRad
Dynabeads® Protein G	Thermo Fisher Scientific
ECL Western Blotting-Substrat	Thermo Fisher Scientific
Effectene Transfection Reagent	Qiagen
GelCode blue stain reagent	Thermo Fisher Scientific
Goat Serum	Sigma-Aldrich
Nitrocellulosemebrane BA85	Schleicher and Schüll
Polynukleotid kinase	Roche
ProLong Gold antifade mountant	Invitrogen
ProLong Diamond antifade mountant	Invitrogen
Protease Inhibitor Cocktail	Roche
Shrimp Alkaline Phosphatase	USB
Vectashield mounting medium with DAPI	Vector Labs

5.1.6 Solutions and buffers

Water was filtered with a Milli-Q-System (Millipore) and sterilized in an autoclave at 120 °C for 45 min. All buffers and solutions were stored in bottles (Schott), tubes (Sarstedt) or in Eppendorf reaction tubes at room temperature unless indicated otherwise.

Table 5.4 List of solutions and buffers

Name	Chemical composition
Alkaline-phosphatase buffer	100 mM Tris/HCL, 100 mM NaCl, 50 mM MgCl ₂ , 1 mM Levamisole, 0.1% (v/v) Tween 20; pH 9.5
BBS (10x), stored at –20 °C	100 mM Tris, 550 mM NaCl, 400 mM KCl, 70 mM MgCl ₂ , 50 mM CaCl ₂ , 200 mM Glucose, 500 mM Sucrose; pH 7.0
BBT (1x)	BBS (1x), 0.1% (w/v) BSA, 0.1% (v/v) Tween 20

5.1 Material

Table 5.4 – *Continued from previous page*

Name	Chemical composition
BCIP, stored at $-20\text{ }^{\circ}\text{C}$	8% (w/v) in DMSO
Bleach for dechoriation (protected from light exposure)	50% (v/v) DanKlorix (Colgate-Palmolive)
Blocking solution, stored at $-4\text{ }^{\circ}\text{C}$	BBT (1x), 2% (v/v) Goat-Serum
Calcium chloride stock solution	100 mM CaCl
Carbonate buffer (2x)	120 mM Na_2CO_3 , 80 mM NaHCO_3 , pH 10.5
A. Co-IP NP40 buffer for embryos	50 mM Tris-Cl, 150 mM NaCl, 0.1% Nonidet P40 Substitute, 1x Protease Inhibitor Cocktail (Roche); pH 7.4
B. Co-IP NP40 buffer for embryos	50 mM Tris-Cl, 150 mM NaCl, 2% Nonidet P40 Substitute, 1x Protease Inhibitor Cocktail (Roche); pH 7.4
Co-IP wash buffer	50 mM Tris, 150 mM NaCl, 1x Protease Inhibitor Cocktail (Roche); pH 8.0
Co-IP lysis buffer for cell culture	50 mM Tris-Cl, 150 mM NaCl, 0.5% Nonidet P40 Substitute, 1x Protease Inhibitor Cocktail (Roche); pH 7.4
Co-IP wash buffer for cell culture	10 mM Tris-Cl, 150 mM NaCl, 0.5 mM EDTA; pH 7.5
DNA loading buffer, stored at $-4\text{ }^{\circ}\text{C}$	0.25% (w/v) Bromphenol-Blue, 0.25% (w/v) Xylene-Cyanol, 30% (v/v) glycerol
EDTA	0.5 M; pH 8
Dilution buffer for GFP-Trap [®]	10 mM Tris-Cl, 150 mM NaCl, 0.5 mM EDTA; pH 7.5
Hepes solution, stored at $-4\text{ }^{\circ}\text{C}$	100 mM Hepes, 2mM MgSO_4 , 1 mM EDTA; pH 6.8

Table 5.4 – Continued from previous page

Name	Chemical composition
Hybridization solution, stored at $-20\text{ }^{\circ}\text{C}$	50% (v/v) formamide (deionized), 5x SSC, 200 $\mu\text{g/ml}$ ss DNA, 10 $\mu\text{g/ml}$ tRNA, 50 $\mu\text{g/ml}$ heparin; pH 5.0
Na_3PO_4 buffer (1 M)	77.4 ml 1 M Na_2HPO_4 , 22.6 ml 1 M NaH_2PO_4 ; pH 7.4
Lämmli buffer (1x)	625 mM Tris-HCL, 5% SDS, 10% Glycerol, 0.001% Bromphenolblue, 25 mM DTT; pH 6.8
Levamisol solution, stored at $-20\text{ }^{\circ}\text{C}$	50 mM
Magnesium chloride solution	1 M MgCl_2
Magnesium sulfate solution	1 M MgSO_4
NBT solution, stored at $-20\text{ }^{\circ}\text{C}$	4-Nitro-Blue-Tetrazolium-Chloride, 75 mg/ml in 70% (v/v) dimethylformamide
Nipagin solution	15% (v/v) Nipagin in ethanol (95%)
PBS (10x)	1.3 M NaCl, 100 mM Na_2HPO_4 -buffer; pH 7.4
PBTw (1x)	PBS (1x), 0.1% (v/v) Tween 20
Pre-hybridization solution, stored at $-20\text{ }^{\circ}\text{C}$	50% (v/v) Formamide (deionized), 5x SSC
ProteinaseK solution, stored at $-20\text{ }^{\circ}\text{C}$	5 mg/ml ProteinaseK
RNA-Fix solution	10% (v/v) paraformaldehyde in PBS, 50 mM EGTA; pH 7.0
SDS buffer (10x)	250 mM Tris-HCL, 1.92 M glycine, 1% SDS; pH 8.8
SDS sample buffer (4x)	240 mM Tris, 40% w/v glycerol, 8% w/v SDS, 0.004% bromphenolblue
Sodium acetate	3 M NaAc; pH 6-7

5.1 Material

Table 5.4 – *Continued from previous page*

Name	Chemical composition
Squishing buffer	10 mM TrisCl, 1 mM EDTA, 25 mM NaCl; pH 8.5
SSC buffer (20x)	3 M NaCl, 0.3 M Sodium citrate; pH 7
TAE (Tris/Acetate/EDTA)-buffer (50x)	2 M Tris, 1 M acetic acid, 50 mM EDTA; pH 8.4
Western blot transfer buffer (1x)	2.4 g Tris-HCl, 11.2 g glycine, 160 ml methanol
X-Phosphate solution (BCIP), stored at -20 °C	5-Bromo-4-Chloro-3-Indolyl-Phosphate, 50 mg/ml in dimethylformamide

5.1.7 Nutrient media

Table 5.5 List of nutrient media for cell culture

Name	Chemical composition
Schneider's <i>Drosophila</i> cell culture medium, stored at -20 °C	Invitrogen
Cell culture medium with fetal calf serum and Pen Strep (Thermo Fisher)	own production

Table 5.6 List of nutrient media for cloning

Name	Chemical composition
LB (Luria Bertani)-medium	0.5% (w/v) NaCl, 0.5% (w/v) Yeast-Extract, 0.1% (w/v) Glucose; pH 7
LB-medium with ampicillin	100 µ/ml ampicillin-solution (-20 °C) in LB-medium
LB plates with ampicillin	15 g agar in 1 L LB-ampicillin-solution
LB-medium with kanamycin	50 µg/ml kanamycin-solution (-20 °C) in LB-medium

Table 5.6 – Continued from previous page

Name	Chemical composition
LB plates with kanamycin	15 g agar in 1 L LB-kanamycin-solution
LB-medium with chloramphenicol	30 µg/ml chloramphenicol-solution (–20 °C) in LB-medium
LB plates with chloramphenicol	15 g agar in 1 L LB-chloramphenicol-solution

Table 5.7 List of nutrient media for fly work

Name	Chemical composition
Fly food	0.63% agarose, 1.8% inactive dry Yeast, 1% soy bean powder (Soja Austria), 8% cornmeal, 2.2% light corn syrup, 8% malt extract, 0.63% propionic-acid, 0.15% nipagin-solution, in dH ₂₀
Apple juice agar plates	33% apple-juice (Becker's Bester GmbH), 3.3% sucrose, 2.8% agarose, 1.3% nipagin-solution

5.1.8 *Drosophila melanogaster* strains

Table 5.8 *Drosophila melanogaster* strains

Genotype	Description	Source
<i>w¹¹¹⁸</i>	Reference strain (wild type)	BDSC ¹
<i>w⁻/w⁻, Baz/FM7i-dfd-eYFP;;</i>	Balancer for X chromosome	BDSC ¹
<i>w⁻/w⁻;; Dr/TM3, Sb^l</i>	Third multiple 3; Balancer for 3rd chromosome	Reinhard Schuh ²
<i>Dr^{Mio}/TM3,P{GAL4-twi.G}2.3 P{UAS-2xEGFP}AH2.3 Sb^l Ser^l</i>	YFP marked balancer used for identification of homozygous embryos (chromosome 3)	BDSC ¹

5.1 Material

Table 5.8 – Continued from previous page

Genotype	Description	Source
$w^-/w^-; P\{KK107175VIE-260B\}$	RNAi of <i>wrm</i> (CG43780)	VDRC ³
$w^-/w^-; P\{Gal4-btl\}/P\{Gal4-btl\}$	Gal4 driver line used for tracheal specific expression and knockdown	BDSC ¹
$w^-/w^-; wrm^{1A}/TM3-dfd-eYFP$	<i>wrm1</i> mutant allele	This thesis
$w^-/w^-; wrm^{1E}/TM3-dfd-eYFP$	<i>wrm1</i> mutant allele	This thesis
$w^-/w^-; wrm^{2A}/TM3-dfd-eYFP$	<i>wrm2</i> mutant allele	This thesis
$w^-/w^-; wrm^{2N}/TM3-dfd-eYFP$	<i>wrm2</i> mutant allele	This thesis
$w^-/w^-; wrm^{2R}/TM3-dfd-eYFP$	<i>wrm2</i> mutant allele	This thesis
$w^-/w^-; wrm^{\Delta attP}/TM3-dfd-eYFP$	<i>wrm</i> mutant allele	This thesis
$w^-/w^-; P\{w[+mC]=PTT-GA\}Nrx-IV[CA06597]/P\{w[+mC]=PTT-GA\}Nrx-IV[CA06597]$	Homozygous line expressing NrxFIV-GFP, used for FRAP	BDSC ¹
$w^-/w^-; P\{w[+mC]=PTTGA\}ATP\alpha[ZCL1792]/P\{w[+mC]=PTTGA\}ATP\alpha[ZCL1792]$	Homozygous line expressing ATP α -GFP, used for FRAP	BDSC ¹
$w^-/w^-; wrm^{1A}/TM3-dfd-eYFP, P\{w[+mC]=PTTGA\}ATP\alpha[ZCL1792]/P\{w[+mC]=PTTGA\}ATP\alpha[ZCL1792]$	Homozygous line expressing ATP α -GFP, used for FRAP	BDSC ¹
$w^-/w^-; wrm^{1A}/TM3-dfd-eYFP, P\{w[+mC]=PTT-GA\}Nrx-IV[CA06597]/P\{w[+mC]=PTT-GA\}Nrx-IV[CA06597]$	<i>wrm</i> mutant line expressing NrxFIV-GFP, used for FRAP experiments	This thesis
$w^-/w^-; wrm^{1E}/TM3-dfd-eYFP, P\{w[+mC]=PTT-GA\}Nrx-IV[CA06597]/P\{w[+mC]=PTT-GA\}Nrx-IV[CA06597]$	<i>wrm</i> mutant line expressing NrxFIV-GFP, used for FRAP experiments	This thesis
$y^1 w^{1118}; PBac\{y[+]-attP-9A\}VK00014$	line for UAS- <i>wrm1</i> insertion via <i>attP</i> landing site	BDSC

Table 5.8 – Continued from previous page

Genotype	Description	Source
$w^-/w^-;;wrm1^{attL,Strep}$	line expressing Wrm1::Strep	This thesis
$w^-/w^-; UAS-wrm$	UAS-controlled Wrm1 expression	This thesis

¹Bloomington *Drosophila* Stock Center, Department of Biology, Indiana University

²Max-Planck-Institute for Biophysical Chemistry, Research Group Molecular Organogenesis, Am Fassberg 11, 37077 Göttingen, Germany

³The Vienna *Drosophila* Resource Center, Vienna, Austria

5.1.9 Cell lines

Table 5.9 List of cell lines

Identifier	Source
S2R+	DGRC ¹

¹ *Drosophila* Genomics Resource Center, 1001 E. 3rd St. Bloomington, IN 47405-7005

5.1.10 *Escherichia coli* strains

Table 5.10 List of *Escherichia coli* strains

Designation	Genotype	Source
TOP10	F- <i>mcr</i> $\Delta(mrr-hsdRMS-mcrBC)$ Φ 80 <i>lacZ</i> Δ M15 $\Delta lacZX74$ <i>recA1</i> <i>araD139</i> $\Delta(ara\ leu)$ 7697 <i>galU</i> <i>galK</i> <i>rpsL</i> (StrR) <i>endA1</i> <i>nupG</i>	Invitrogen
DH5 α	F- Φ 80 <i>lacZZMD15</i> D(<i>lacZYA-argF</i>) U169 <i>recA1</i> <i>endA1</i> <i>hsdR17</i> (rK-,mK+) <i>phoA</i> <i>supE44</i> λ - <i>thi-1</i> <i>gyrA45</i> <i>relA1</i>	Invitrogen
Xl1-Blue	<i>recA1endA1gyrA96</i> <i>thi-1</i> <i>hsdR17</i> <i>supE44</i> <i>relA1</i> <i>lac</i> $\Delta F'$ <i>proAB</i> <i>lacIqZ</i> Δ M15 Tn10 (Tetr) Δ	Stratagene
10-beta	$\Delta(ara-leu)$ 7697 <i>araD139</i> <i>fhuA</i> $\Delta lacX74$ <i>galK16</i> <i>galE15</i> <i>e14-</i> Φ 80 <i>dlacZ</i> Δ M15 <i>recA1</i> <i>relA1</i> <i>endA1</i> <i>nupG</i> <i>rpsL</i> (StrR) <i>rph</i> <i>spoT1</i> $\Delta(mrr-hsdRMS-mcrBC)$	NEB

5.1.11 Plasmids

Table 5.11 List of plasmids

Name	Purpose	Source
Actin-Gal4	Expression of proteins in cell culture	Felix Babatz ¹
<i>pOT2</i>	Initial vector for <i>in situ</i> hybridization probe production	DGRC ²
<i>pJet1.2/blunt</i>	Cloning of PCR amplicons	Fermentas
<i>pHD-DsRed-attP</i>	Vector for generating dsDNA donors for HDR	Addgene
<i>pGE-attB</i>	recombination <i>via attP/attB</i> site in <i>Drosophila</i>	DGRC
<i>pGE-wrm</i>	Rescue of <i>wrm</i>	This thesis
<i>pGX-attP</i>	vector for generating <i>mega attP</i> line	Addgene
<i>pBFv-U6.2</i>	vector for gRNA expression	Addgene
<i>pBFv-U6.2B</i>	vector for 2 gRNA expression	Addgene
<i>pUAST</i>	initial UAS-controlled expression vector	Invitrogen
<i>pUAST-GFP</i>	UAS-controlled expression of GFP	Invitrogen
<i>pUAST-attB</i>	UAS-controlled expression vector for the production of transgenic flies using <i>attP</i> landing sites	Invitrogen
<i>pUAST-wrm1</i>	UAS-controlled expression of <i>wrm</i>	This thesis
<i>pUAST-dlg-GFP</i>	UAS-controlled expression of Dlg::GFP	This thesis
<i>pUAST-kune-GFP</i>	UAS-controlled expression of Kune::GFP	This thesis
<i>pUAST-mega</i>	UAS-controlled expression of Mega	This thesis
<i>pUAST-mega-GFP</i>	UAS-controlled expression of Mega::GFP	This thesis
<i>pUAST-sinu-GFP</i>	UAS-controlled expression of Sinu::GFP	This thesis
<i>pUAST-wrm1-GFP</i>	UAS-controlled expression of Wrm1::GFP	This thesis
<i>pUAST-wrm1-Strep</i>	UAS-controlled expression of Wrm1::Strep	This thesis

Table 5.11 – Continued from previous page

Name	Purpose	Source
<i>pUAST-wrm2-GFP</i>	UAS-controlled expression of <i>Wrm2::Strep</i>	This thesis
<i>pUAST-fasIII</i>	UAS-controlled expression of <i>FasIII</i>	A.Hildebrandt ³
LD47606	cDNA template used for the production of <i>in situ</i> hybridization probes corresponding to <i>wrm</i>	DGRC
LD29359	cDNA template of <i>sinu</i>	DGRC
SD14923	cDNA template of <i>kune</i>	DGRC
GH1107	cDNA template of <i>dlg</i>	DGRC

¹University of Münster, Institute for Neuro and Behavioral Biology, Klämbt lab, Badestr. 9, 48149 Münster, Germany

²*Drosophila* Genomics Resource Center, 1001 E. 3rd St. Bloomington, IN 47405-7005, USA

³Max-Planck-Institute Biophysical Chemistry, Department Molecular Organogenesis, Am Fassberg 11, 37077 Göttingen, Germany

5.1.12 Oligonucleotides

Table 5.12 List of oligonucleotides

Name	Sequence 5'-3'	Localization	Purpose
<i>mega</i> 5' arm for	GGCGACGGGCGGCACGATCTGCT CGG	<i>mega</i>	cloning
<i>mega</i> 5' arm rev	GAGCTGAGAGCTGCTCGAAAGAA TGCC	<i>mega</i>	cloning
<i>mega</i> 3' arm for	CCCACTAGTTACACCTAATATGT TTATGTTTGCC	<i>mega</i>	cloning
gRNA <i>wrm1</i>	GAAAAGAATCCCTACTTCAC	<i>wrm</i>	CRISPR/Cas9
gRNA <i>wrm2</i>	TCGCCCTGTTTCATCGTGGGC	<i>wrm</i>	CRISPR/Cas9
gRNA 3' <i>wrm</i>	ATTTAGGGTAGTCTGTCTAC	<i>wrm</i>	CRISPR/Cas9
<i>wrm attP</i> for	CGTGTCGGGTTTTAAACATG	<i>wrm</i>	sequencing
<i>wrm attP</i> rev	GCATTGTTAACCATTCTATTTG	<i>wrm</i>	sequencing
<i>pGE attB</i> for	TTCCTACTGCAGGTAATG	<i>pGE attB</i>	sequencing

Table 5.12 – Continued from previous page

Name	Sequence 5'-3'	Localization	Purpose
<i>pGE attB</i> rev	CAAAACGAATAGAGAATAACG	<i>pGE-attB</i>	sequencing
<i>pUAST</i> for	ACTGAAATCTGCCAAGAAGTA	<i>pUAST</i>	sequencing
<i>pUAST</i> rev	TTGTGAAGGAACCTTACTTCT	<i>pUAST</i>	sequencing
<i>pBFV-U6.2</i> rev	ACCGCCTTTGAGTGAGCTGATAC C	<i>pBFV-U6.2</i>	sequencing
<i>pHD-dsRed-attp</i> for	ACGAAAGGCTCAGTCGAAAG	<i>pHD-DsRed-attp</i>	sequencing
<i>pHD-dsRed-attp</i> rev	GATGGACTTGAACTCCAC	<i>pHD-DsRed-attp</i>	sequencing
<i>pHD-dsRed-attp</i> for 3'	GGCCGCGACTCTAGATCATAATC	<i>pHD-dsRed-attp</i>	sequencing
<i>pHD-dsRed-attp</i> rev 3'	GATATCAAAATTATACATGTCAA CG	<i>pHD-dsRed-attp</i>	sequencing
<i>wrm</i> rescue for	gctccccgggcgcgctactccacT ATGTTTATAAACATTGTTTAATA TATTTAAATTC	<i>wrm</i>	<i>wrm</i> rescue
<i>wrm</i> rescue rev	agttatggtaccggcgcgccGAT TAAAAAACACAATATTATTTTGG G	<i>wrm</i>	<i>wrm</i> rescue
<i>wrm</i> 5'arm for	CCCTTCGCTGAAGCAGGTGGACC AGATCGATGATGGTC	<i>wrm</i>	<i>wrm</i> 5'arm
<i>wrm</i> 5'arm rev	ACTACGATCGCAGGTGTGCACAA TTTAAAATTAACGTATGTGCTA TTTTTG	<i>wrm</i>	<i>wrm</i> 5'arm
<i>wrm</i> 3'arm for	TACGAAGTTATAGAAGAGCAGTA GATGCTAGTGGGTAGCTTG	<i>wrm</i>	<i>wrm</i> 3'arm
<i>wrm</i> 3'arm rev	ACTCGATTGACGGAAGAGCCGAC AGCGATCCCGGAGAC	<i>wrm</i>	<i>wrm</i> 3'arm
UAS- <i>wrm1</i> for	actctgaataggaattgggATG TCCACAATCGAAGAGG	<i>wrm</i>	expression of <i>wrm</i>

Table 5.12 – Continued from previous page

Name	Sequence 5'-3'	Localization	Purpose
UAS- <i>wrm1</i> rev	ggttccttcacaaagatcctTTA GATGTCGCTCTCGCG	<i>wrm</i>	expression of <i>wrm</i>
<i>pUAST-dlg</i> for	actctgaataggggaattgggATG GATTCGGATACGGACTC	<i>dlg</i>	<i>dlg</i> -GFP tag
<i>pUAST-dlg</i> rev	ccttgctcaccataaccgccgcta gcGATGCTCGACTTACGATAGTC AG	<i>dlg</i>	<i>dlg</i> -GFP tag
<i>pUAST-kune</i> for	actctgaataggggaattgggATG GGTGCGTCCAACCGCG	<i>kune</i>	<i>kune</i> -GFP tag
<i>pUAST-kune</i> rev	ccttgctcaccataaccgccgcta gcTATATCTGTTTGAATTCCTCC TTGTACAGCG	<i>kune</i>	<i>kune</i> -GFP tag
<i>pUAST-sinu</i> for	actctgaataggggaattgggATGC AAAAACCATCCCCTTC	<i>sinu</i>	<i>sinu</i> -GFP tag
<i>pUAST-sinu</i> rev	ccttgctcaccataaccgccgctag cTCCGCGCACCAGCTCAAAT	<i>sinu</i>	<i>sinu</i> -GFP tag
<i>pUAST-mega</i> for	actctgaataggggaattgggATG CGCGAACTTAACAAGC	<i>mega</i>	<i>mega</i> -GFP tag
<i>pUAST-mega</i> rev	ccttgctcaccataaccgccgcta gcTATGTAGCCCTGCAGGCTCC	<i>mega</i>	<i>mega</i> -GFP tag
<i>pUAST-wrm1</i> for	actctgaataggggaattgggATG TCCACAATCGAAGAGGAAC	<i>wrm1</i>	<i>wrm1</i> - TwinStrep tag
<i>pUAST-wrm1</i> rev	gactccatgcactaccgccgcta gcGATGTCGCTCTCGCGCTTCC	<i>wrm1</i>	<i>wrm1</i> - TwinStrep tag
<i>pUAST-wrm1</i> for	actctgaataggggaattgggATG TCCACAATCGAAGAGGAAC	<i>wrm1</i>	<i>wrm1</i> -GFP tag
<i>pUAST-wrm1</i> rev	cttgctcaccataaccgccgctag cGATGTCGCTCTCGCGCTTC	<i>wrm1</i>	<i>wrm1</i> -GFP tag

5.1 Material

Table 5.12 – *Continued from previous page*

Name	Sequence 5'-3'	Localization	Purpose
<i>pUAST-wrm2</i> for	actctgaataggggaattgggATG GCTCTTTACTTCCTTTATCCC	<i>wrm2</i>	<i>wrm2</i> -GFP tag
<i>pUAST-wrm2</i> rev	ccttgctcaccataccgccccta gcGGCATAGCTAATCTCATGCTC ATAC	<i>wrm2</i>	<i>wrm2</i> -GFP tag
T7	TAATACGACTCACTATAGGG	T7 prom.	sequencing
Sp6	CATTTAGGTGACACTATAG	Sp6 prom.	sequencing
T3	AATTAACCCTCACTAAAGGG	T3 prom.	sequencing

5.1.13 Primary antibodies

Table 5.13 List of primary antibodies

Antigen	Host	Dilution	Source
GFP	chicken	1:500	Abcam
GFP	rabbit	1:1000	Synaptic Systems
Megatrachea	mouse	1:50 (embryo) 1:200 (western blot)	Reinhard Schuh ¹
Serpentine	rabbit	1:200	Stefan Luschnig ²
Kune kune	rabbit	1:50	Reinhard Schuh
Crumbs	mouse	1:250	DSHB ³
FasciclinIII	mouse	1:500	DSHB
Coracle	mouse	1:500	DSHB
Discs large	mouse	1:20	DSHB
Spectrin	mouse	1:50	DSHB
Strep	rabbit-HRP	1:250	Abcam

¹Max-Planck-Institute Biophysical Chemistry, Department Molecular Organogenesis, Am Fassberg 11, 37077 Göttingen, Germany

²University of Zurich, Institute of Molecular Life Sciences, Winterthurerstr. 190, 8057 Zurich, Switzerland

³Developmental Studies Hybridoma Bank University of Iowa, Department of Biology 028 Biology Building East Iowa City, Iowa 52242-1324

5.1.14 Secondary antibodies

Table 5.14 List of secondary antibodies

Antigen	Label	Host	Dilution	Source
mouse IgG	AlexaFluor488	goat	1:500	Invitrogen
mouse IgG	AlexaFluor568	goat	1:500	Invitrogen
ginea pig IgG	AlexaFluor488	goat	1:500	Invitrogen
rabbit IgG	AlexaFluor488	goat	1:500	Invitrogen
rabbit IgG	AlexaFluor568	goat	1:500	Invitrogen
chicken IgY	AlexaFluor488	goat	1:500	Jackson Immuno Research
rabbit IgY	AlexaFluor488	goat	1:500	Jackson Immuno Research
mouse IgG	HRP	goat	1:10000	Jackson Immuno Research
rabbit IgG	HRP	goat	1:10000	Jackson Immuno Research
ginea pig IgG	HRP	goat	1:10000	Jackson Immuno Research
StrepMAB- Classic	HRP	mouse	1:10000	iba
Anti-Chitin Binding Domain Serum (CBP)	Fluorescein or Rhodamine	synthetic	1:1000	NEB

5.1.15 Analysis and imaging software

Table 5.15 List of analysis and imaging software

Name	Location
Adobe Systems GmbH	Munich, Germany
DNASar Inc.	Madison, USA
Engineering Office M. Wohlwend	Sennwald, Switzerland
IBS 1.0 Illustrator	The CUCKOO Workgroup
ImageJ / Fiji	Bethesda, USA

Table 5.15 – *Continued from previous page*

Name	Location
MASCOT	Matrix Science Ltd, United Kingdom
Microsoft® Office	Redmond, USA
Perseus	MPI for Biochemistry, Planegg
Proteome Software, Inc	Portland, USA
Zen Acquisition software Zeiss	Jena, Germany

5.2 Fly protocol

5.2.1 Fly husbandry

Flies were cultivated in plastic cylinder vials (Greiner Bio One) with a diameter of 3 cm. Fly food was filled up to one third of the vial. If necessary, a folded filter (Macherey-Nagel) was inserted into the food to provide more solid surface for pupae and flies. Flies were kept on 18 °C, 22 °C or 25 °C depending in the desired generation time and transferred into newly prepared vials every two to four weeks. Transient sedation with CO₂ allowed selection of flies on the basis of their gender and chromosomal markers. Collected males and females were joined in a new vial.

5.2.2 RNAi crosses

All candidate RNAi lines were crossed to the *btl*-Gal4 driver line. Homozygous or heterozygous virgin females carrying the RNAi construct were crossed to males with *w¹¹¹⁸; P{Gal4-btl}/P{Gal4-btl}*.

The progeny was screened for lethality and further investigated molecularly.

5.2.3 Generation of transgenic fly lines

The injection of plasmids for the generation of transgenic flies was performed by the *Drosophila* embryo injection service BestGene Inc.

5.3 Generation of $\Delta attP$ mutant lines

Homology-directed repair (HDR) uses homologous DNA templates for DNA synthesis to bridge the gap of a double-strand break. Providing an excess of donor DNA template, HDR can be used to precisely modify or introduce new DNA sequences.

The *mega^{attP}* line was generated by the use of 3 kB homology region at the 5' as well

as 3' end of the *mega* locus. Homologous regions were isolated by PCR (sec. 5.9.2) and cloned into the *pGX-attP* vector. The construct was injected into *w¹¹¹⁸* line and integrated randomly into the genome. Transformants were identified by the *white* marker and crossed to Flp recombinase and ubiquitous Gal4 expressing flies, leading to mobilization and reintegration of the construct at the *mega* locus. Integration was confirmed by sequencing. Transformants were balanced using the X-chromosomal *Baz/FM7i* balancer.

The *wrm^{ΔattP}* line was generated by designing Gibson assembly oligonucleotides (Tab. 5.12) for 1 kb homology region 5' and 3' of the *wrm* locus. The 5' and 3' homology arm was isolated *via* PCR (sec. 5.9.2) and cloned into the *pHD-dsRed-attP* vector using Gibson assembly (sec. 5.9.10).

Additionally, two target sequences (gRNAs, sec. 5.9.13) were selected at the 5' and 3' end of the *wrm* locus and cloned into the *pBFv-U6.2B* vector. Both constructs were co-injected into the BDSC # 56552 line expressing *vasa-Cas9*. All injections were conducted by BestGene Inc. Obtained transformants were sequenced and balanced with the third chromosomal balancer *Dr/TM3*.

5.3.1 Balancing of transgenic flies

Transgenic larvae were sent by BestGene Inc. For CRISPR/Cas9 mutations on the third chromosome, males and females were separated and single crossed to five males or females of *w⁻/w⁻*; *Dr/TM3*, *Sb⁻* genotype after hatching. In the F1 generation, flies were selected against *Dr⁻* and for *Sb⁻* and single crossed to *w⁻/w⁻*; *Dr/TM3*, *Sb⁻* again. 10 to 25 single crosses per F1 generation vial were conducted. In the F2 generation, males and females of the same hatch were selected against *Dr⁻* and for *Sb⁻* and joint in a fresh vial. Progeny of these crosses was analyzed for lethality (only *Sb⁻* flies are present). Hatching of *Sb⁺* flies led to the discarding of the cross. Sequencing of homozygous embryos was conducted to confirm mutation at the desired locus.

For mutant lines with substitution of an *attP* site in the desired gene locus, hatched flies were selected for either *dsRed⁺* or *w⁺* after hatching, depending on the integrated construct and crossed to *yw* by Bestgene before shipping.

For *attP* insertions on the X chromosome, F1 generation females containing the selection *w⁺* were crossed to *FM7i/Y* males. Progeny was selected for the X-chromosomal marker *Bar* and hatchlings of the same cross were placed in a new vial.

For *attP* insertions on the third chromosome, F1 generation males containing the selection marker *dsRed⁺* were crossed to females of *w⁻/w⁻*; *Dr/TM3*, *Sb⁻* genotype. Progeny of this cross was selected against *Dr⁺* and for *Sb⁻* and joint in a fresh vial. Sequencing of

5.4 Histological methods for whole embryos

homozygous embryos was conducted to confirm integration into the correct locus.

5.3.2 Overexpression experiments

The ORF of *wrm* encoding Wrm1 was amplified from genomic DNA (BDSC #56552) and cloned into the *pUAST-attB* vector. This construct was used to generate transgenic fly lines by injection into BDSC fly line 9733, which contains an *attP* landing site on the second chromosome. Progeny was screened for the selection marker *w*⁺.

5.3.3 Rescue experiments

Rescue experiments were performed using the *attP* and *attB* target sequences of the integrase Φ C31 (Bateman et al., 2006). Therefore, the genomic locus of *wrm* was amplified in a PCR and cloned into the *pHD-dsRed-attP* vector via Gibson Assembly. Crosses were performed according to section 5.3.1.

5.3.4 Embryo collection

Flies were sedated and transferred into a cylindrical container with a mesh on the upper side. The bottom side was closed with an apple juice agar plate (Tab. 5.7) that was holding a drop of water-yeast mixture. Depending on further experiments, the cages were kept at 18 °C, 22 °C, 25 °C or RT. Female flies laid eggs onto the apple juice plate, which was changed at different time points, depending on the experiment. The embryos on the apple juice plates were incubated (aged) in different temperatures and for distinct time spans, until embryo development reached the desired stage.

5.3.5 Dechoriation of embryos

Using tap water and a soft brush, the embryos were carefully retrieved from the apple juice agar plate and washed into a close mesh net with tap water. Remaining yeast was rinsed off. The mesh net carrying the embryos was incubated in a petri dish containing 50% DanKlorix diluted with tap water for 3 min and extensively rinsed with tap water after the incubation time.

5.4 Histological methods for whole embryos

5.4.1 Paraformaldehyde (PFA) fixation

Dechorionated (sec. 5.3.5) embryos were transferred into a scintillation tube containing 6 ml heptane, 2 ml hepes-solution and 1 ml RNA-Fix-solution (Tab. 5.4) using a brush.

The scintillation vial was shaken at 200 rpm for 20 min. After the fixation, the lower phase was aspirated and 8 ml methanol were added. The vial was shaken extensively at 500 rpm for 1 min to detach the vitelline membrane from the embryos. After the embryos had settled on the bottom of the vial, the supernatant was aspirated, followed by eight methanol washing steps. Embryos were finally transferred into an Eppendorf cup, covered with methanol and stored at -20°C .

5.4.2 Methanol fixation

Embryos were collected from an apple juice agar plate using a soft brush and dechorinated (sec. 5.3.5). After transferring the embryos into a scintillation vial containing 5 ml heptane and 5 ml methanol, the vial was shaken for 2 min at 300 rpm. Supernatant was removed from sedimented embryos, following repeated rinsing steps with methanol until the supernatant cleared. Methanol fixed embryos were transferred into an Eppendorf cup, covered with methanol and stored at -20°C .

5.4.3 Immunofluorescence staining in whole embryos

All incubation, blocking and washing steps were conducted on a rotating wheel. Fixed embryos were transferred to a new Eppendorf tube and washed three times with BBT (Tab. 5.4) for 5 min, followed by two 15 min incubation steps with blocking solution (Tab. 5.4) to saturate unspecific immunoglobulin binding sites. Primary antibody diluted in blocking solution was added to the embryos, before over night incubation at -4°C . On the second day embryos were rinsed with BBT four times followed by treatment with two 10 min incubation steps with blocking solution. Secondary antibody diluted in blocking solution was added to the embryos and incubated at RT for 2 h. After antibody treatment, embryos were washed 8 times with PBTw (Tab. 5.4) and embedded.

5.4.4 Staining of tracheal lumen with anti-chitin binding domain serum

All incubation steps are conducted on a rotating wheel. Fixed embryos were transferred to a new Eppendorf tube and washed three times with BBT (Tab. 5.4) for 5 min. Fluorescein-labeled anti-chitin binding domain serum was added to embryos diluted in 1:1000 in blocking solution and incubated for 2 h. Finally, embryos were washed 8 times with PBTw (Tab. 5.4) and embedded.

5.4.5 Prolong Diamond embedding

Immunohistologically prepared embryos were transferred onto a microscope slide with a pipette and a cut tip. The excessive PBTw was then removed with a tissue as thoroughly as possible. 100 µl of Prolong Diamond were quickly added to the embryos, followed by equally spreading of the embryos with a pipette tip. Mounted embryos were covered with a 24 mm x 32 mm cover slip and stored in the dark at 4 °C.

5.5 Protocols for *in situ* hybridization in whole embryos

5.5.1 Synthesis of labeled RNA-probes *via in vitro* transcription

In vitro transcription was performed as previously described (Tautz and Pfeifle, 1989). The clone LD 47606 in the pOT2 vector was ordered from DGRC, containing the cDNA of *wrm*. This vector provides flanking T3 and Sp6 to the inserted fragment.

The restriction enzyme EcoRV was used to cut 5' of the transcript and linearize the vector according to the manufacturer's protocol, to produce an antisense RNA probe. The digest was purified *via* agarose gel extraction and used for RNA transcription.

10 µl *in vitro* transcription reaction were pipetted according to the manufacturer's protocol (Roche):

- 1 µg linearized vector
- 2 µl transcription buffer (5x)
- 1 µl 1µl DIG RNA labeling mix (10x)
- 1 µl RNA polymerase (T7 for antisense probes; T3 for sense probes)
- 1 µl RiboLock RNase Inhibitor
- RNase-free water

The transcription was incubated at 37 °C for 2 h. A hydrolytic digest was performed by adding 15 µl RNase-free water and 25 µl carbonate buffer to the mix and the reaction was incubated at 70 °C for 15 min. To stop the digest and start the precipitation of the RNA, following chemicals were added to the mix in this order:

- 50 µl 0.25 NaAc
- 10 µl 4M LiCl
- 10 µl tRNA (20 mg/ml)
- 300 µl ethanol

The RNA probe was incubated at -20 °C over night and spun down at 17000 g and 4 °C for 15 min. The obtained visible pellet at the bottom of the Eppendorf cup was washed

once with 500 μ l of 70% ethanol and air-dried for 15 min. Finally, the pellet was dissolved in 150 μ l hybridization-solution (Tab. 5.4) by extensive pipetting and stored at -4°C .

5.5.2 *In situ* hybridization in whole embryos

In situ hybridization allows the visualization of gene expression patterns (Tautz and Pfeifle, 1989). Therefore, *in vitro* synthesized antisense RNA probes hybridize *via* base pairing to target RNAs. A Digoxigenin (DIG) labeling of the RNA probes enable the detection by chemical techniques.

All steps were performed at RT on a rotating wheel, unless mentioned otherwise. For *in situ* hybridization, embryos were fixed as described in section 5.4.1 and transferred into a new Eppendorf cup. After three washing steps with methanol:PBTw 1:1 (v/v) for 15 min, embryos were submerged in PBTw. Subsequently, incubation occurred in RNA-fix-solution:PBTw 1:1 (v/v) (Tab. 5.4) for 20 min, followed by four time rinsing with PBTw. 10 μ l Proteinase K-solution in 1 ml PBT was added to the embryos and removed by two rinsing steps with PBTw after 3 min. Postfixation was conducted in RNA-fix-solution:PBTw 1:1 (v/v) for 20 min followed by four rinsing steps with PBTw.

After postfixation, embryos were first washed with pre-hybridization-solution:PBTw 1:1 (v/v) (Tab. 5.4), followed by incubation steps with pre-hybridization-solution and finally hybridization-solution (Tab. 5.4). Subsequently, embryos were incubated in hybridization-solution at 70°C in a water bath for 1 h. 30 μ l hybridization-solution combined with 3 μ l of DIG-labeled antisense RNA probe was added to the embryos. Hybridization occurred at 70°C in a water bath over night. On the second day, excessive antisense RNA probe was removed by three washing steps with pre-warmed hybridization-solution at 70°C for 15 min. Next, embryos were rinsed three times with PBTw, followed by three washing steps with PBTw for 15 min.

For signal detection, embryos were incubated with anti-DIG-antibody diluted in PBTw (1:1000) for 1 h, followed by four rinsing and three 20 min washing steps with PBTw to eliminate excess antibody. Embryos were rinsed with 1 ml AP-buffer once and incubated in 1 ml AP-buffer for one minute. After discarding of the supernatant, 0.5 ml of AP-buffer was added to the embryos and they were transferred into a glass dish using a cut pipette tip. 4.5 μ l NBT and 3.4 μ l BCIP (Tab. 5.4) were added to the embryos and carefully mixed by moving of the glass dish. The staining reaction was observed under a binocular and stopped with 8 washing steps with 1 ml PBTw. Stained embryos were kept in PBTw at 4°C .

5.6 Live imaging techniques

5.6.1 Texas[®]-Red-dextran injection

Depending on the experiment, stage 15, 16 or 17 embryos were dechorionated (sec. 5.3.5) and placed on an apple juice agar plate in a straight row with the dorsal site facing upwards. One side of a microscope cover slip was covered with heptane glue and was pressed carefully onto the embryos to fixate them to the slide after drying. Subsequently, embryos were covered with Voltalev oil to prevent drying-out and allow gas exchange.

Before injection, sterile Femtotips-II needles (Eppendorf) were filled with 10 µl of PBTw containing Texas-Red[®]-dextran. The injection was performed on an Eppendorf FemtoJet and sterile Femtotips-II needles (Eppendorf), with pressure adjusted to the needles' opening. Embryos were injected at the anterior side and imaged by confocal microscopy after 5-10 min incubation.

5.6.2 Fluorescence recovery after photobleaching (FRAP)

Early stage 16 embryos were dechorionated (sec. 5.3.5) and extensively washed with PBS. After embryos were transferred onto a glass bottom microwell dish (MatTek), they were covered with PBS and a cover slip. Imaging and photobleaching were performed with a LSM780 confocal microscope and Zen acquisition software (Zeiss), using a Plan-Apochromat 40x/1.4 Oil DIC M27 objective. Fluorescent protein was photobleached with 100% output of 405 nm and 100% output of 488 nm laser for 168.58 µseconds/pixel. The photobleached region was kept between 4 to 8 µm in height and 14 to 18 µm in width. The standard errors of mean (s.e.m.) were calculated using following formula with x =measurement, \bar{x} =mean average and n =sample size:

$$s.e.m. = \frac{\sqrt{\frac{\sum (x-\bar{x})^2}{n}}}{\sqrt{n}} \quad (5.1)$$

5.7 Cell culture protocol

Attached S2R+ cells were detached from the flask bottom using a cell scraper. 9 ml of room temperature cell culture medium containing 1% Pen Strep (Thermo Fisher) and 10% FBS were transferred into a sterile cell culture flask. 1 ml of cell solution from the previously used flask was added. All steps were conducted in a sterile environment of a clean bench. Cells were incubated at 25 °C for one week.

5.7.1 Transfection of S2R+ cells

24 h before transfection, confluent cells were diluted 1:6 with Schneider's medium and were transferred into a 6-well-plate with a final volume of 3 ml per well.

For transfection, 500 ng of *pUAST* vector containing *pUAST-wrm1-Strep*, *pUAST-wrm1-GFP*, *pUAST-wrm2-GFP*, *pUAST-dlg-GFP*, *pUAST-kune-GFP*, *pUAST-sinu-GFP*, *pUAST-mega-GFP* and/or *pUAST-GFP* and 500 ng of *actin5C-Gal4* vector were mixed in an Eppendorf cup. 8 µl enhancer was added to the DNA mixture, followed by vortexing for 10 sec. The reaction was incubated at RT for 5 min. 10 µl effectene reagent was added to the reaction, followed by vortexing for 10 sec and incubation at RT for 15 min. The transfection mixture was carefully pipetted directly onto the supernatant of the cells. Cells were harvested 24-48 h after transfection.

5.7.2 Cell aggregation assay

Transfected cells were detached of the bottom of the plate by pipetting. Using a Neubauer counting chamber, 10 µl of the cells in cell culture medium were counted. For the experiment, cells were resuspended to a final density of 2×10^6 cells per ml with pre-warmed serum-free cell culture medium. 1.5 ml of each suspension was transferred to a well of a new glass bottom dish. The dish was shaken at 100 rpm for 90 min at room temperature, followed by incubation at 25 °C for 45 min to assure adhesion to the glass bottom.

5.8 Histological methods for cells

5.8.1 Fixation of cells

Supernatant was removed from the cells and incubation with 5% formaldehyde in PBS (Tab. 5.4) followed at RT for 15 min. After aspiration of the formaldehyde solution, cells were washed with PBS twice for 5 min.

5.8.2 Immunofluorescence staining of cells

All steps were performed in round glass bottom dishes at RT.

Permeabilization of the cells was ensured by incubation with PBS containing 0.5% Triton-X-100 for 150 sec. After aspiration of the supernatant, cells were washed with PBS twice for 5 min. Cells were treated with blocking solution for 30 min to saturate unspecific immunoglobulin binding sites, followed incubation with the primary antibody diluted in blocking solution for 2 h. To ensure elimination of the primary antibody, two washing

steps were conducted with PBS for 5 min. The secondary antibody was diluted in blocking solution and added to the cells for 1 h. Finally, cells were washed with PBS for 5 min and mounted.

5.8.3 Mounting of stained cells

All supernatant was removed from the cells with a pipette. 15 drops of Prolong[®] Diamond were carefully pipetted on top of the stained cells and distributed equally. A cover slip covering the entire cell region in the glass bottom dish was carefully placed on top of the cells without the generation of air bubbles.

5.9 Molecular biological methods

All techniques were performed according to standard protocols (Sambrook et al., 1989), if not mentioned otherwise.

5.9.1 Generation of genomic template DNA for PCR

One fly was sedated, collected into an Eppendorf cup and sacrificed by $-20\text{ }^{\circ}\text{C}$ freezing for 15 min. 50 μl of squishing buffer was pipetted into a 0.1 ml glass micro tissue grinder (VWR), the fly was added and homogenized with the corresponding glass pistil, until no more fly structures were detectable. The homogenized fly solution was directly used as template for PCR and stored at $-20\text{ }^{\circ}\text{C}$.

5.9.2 Polymerase chain reaction (PCR)

The polymerase chain reaction (PCR) is used to amplify small amounts of DNA. Following reaction was pipetted:

Template DNA (2 μl homogenized fly, 100-500 ng genomic DNA or 0.5-10 ng plasmid-DNA)

10 μl 5x HF Phusion buffer

1 μl of each oligonucleotide (10 mM)

1 μl dNTPs (10 mM)

0.5 μl Phusion polymerase (NEB)

Water added up to a final volume of 50 μl

The PCR was conducted with following steps:

Step	Temperature	Duration	Cycles
Denaturation	98 °C	30 sec	1x
Denaturation	98 °C	10 sec	
Primer-annealing	55 – 72 °C	20 sec	30x
Elongation	72 °C	30 sec/kb (depending on the length of the target DNA)	
Elongation	72 °C	5 min	1x
Storage	4 °C	∞	1x

All PCRs were conducted in a MyCycler Thermal Cycler (Biorad). Oligonucleotides were ordered from MWG.

5.9.3 Electrophoretic separation of DNA-fragments in agarose gels

DNA-fragments were electrophoretically separated in 1% agarose gels depending on their size. 1 g agarose was added to 100 ml 1x TAE buffer (Tab. 5.4) and brought to boil, until the agarose was fully dissolved. 10 µl Midori Green (Biozym) were added to the warm agarose solution. Midori Green intercalates with DNA enabling visualization in a fluorescent reaction stimulated by UV light. The gel was filled into a gel tray and placed at 4 °C for hardening. Samples were provided with loading dye (NEB) and loaded onto the hardened agarose gel, which was submerged in 1x TAE in a gel chamber. Gene ruler ready-to-use (Fermentas) ladder was also loaded on the gel as size reference for DNA fragments. Electrophoresis was conducted at 125 V. An UV Solo TS transilluminator (Biometra) was used for visualization and documentation.

5.9.4 Purification of DNA via gel extraction

DNA fragment were cut from the agarose gel with a clean surgical blade. The NucleoSpin® Extract II kit (Macherey-Nagel) was used for extraction according to manufacturer's instructions.

5.9.5 Measuring of nucleic acid concentrations

DNA/RNA concentration is determined by the nucleic acid maximum absorption of UV light at 260 nm. An OD₂₆₀ of 1 corresponds to 47.5 µg dsDNA/ml and 37.5 µg ssDNA/ml. A NanoDrop ND-1000 spectrophotometer (PEQLAB) was used according to manufac-

turer's instructions to determine the concentrations of DNA/RNA.

5.9.6 Isolation of plasmid-DNA out of small bacterial cultures (mini prep)

Bacteria of one colony were picked from a LB-agar-plate with a pipette tip and grown in 3 ml LB medium (Tab. 5.6) at 37 °C and 180 rpm over night. Plasmid DNA was isolated with the NucleoSpin® Plasmid kit (Macherey-Nagel) according to manufacturer's instruction.

5.9.7 Isolation of plasmid-DNA out of large bacterial cultures (midi prep)

Bacteria of one colony or a smaller liquid culture were picked and grown in 200 ml LB medium at 37 °C and 180 rpm over night. Plasmid DNA was isolated with the Qiagen Plasmid Plus Midi Kit (Qiagen) according to manufacturer's instructions.

5.9.8 Restriction digest of DNA

DNA was linearized or isolated using restriction endonucleases. For plasmid DNA linearization or DNA fragment isolation 2-3 µg DNA were incubated with 1-2 µl of desired restriction endonuclease, 5 µl 10x restriction buffer, and distilled water in a total volume of 50 µl at 37 °C for 15 min according to manufacturer's instructions.

The digest was arrested by freezing at -20 °C or applying on an agarose gel for electrophoresis.

5.9.9 Ligation

DNA fragments were ligated the following using the Quick Ligation Kit (NEB):

10 µl Quick Ligase reaction buffer (2 x)

50 ng vector DNA

37.5 ng insert DNA

1 µl Quick Ligase

Water added up to a final volume of 20 µl

The ligation was incubated at RT for 5 min and chilled on ice before transformation of 50 µl chemically competent cells.

5.9.10 Gibson Assembly

Using the Gibson assembly approach, it is possible to seamlessly assembly multiple DNA fragments with different length (Gibson et al., 2009). Therefore, the NEBuilder® HiFi

DNA Assembly Master Mix was used. Oligonucleotides with appropriate overlaps to the 5' and 3' fragments were designed and a PCR was performed as described in section 5.9.2. DNA was purified *via* an agarose gel as described in section 5.9.4. Linearized vector was prepared and concentration of all fragments including the vector was determined *via* Nanodrop (sec. 5.9.5). Following reaction was pipetted to assemble 2-4 DNA fragments:

100 ng linearized vector
200-300 ng of each DNA fragment
10 µl Gibson assembly master mix
10-X µl dH₂O

The reaction was incubated at 50 °C for 15 min, when two fragments were assembled and 1 h, when 3-4 fragments were used. 10 µl of the reaction was used to transform chemically competent cells (sec. 5.9.11).

5.9.11 Transformation of chemically competent *E. coli* cells

50 µl chemically competent TOP10 or DH5 α cells (Invitrogen) were thawed on ice for 10 min. 10 µl DNA solution mix were added and the cells were incubated on ice for additional 30 min. Heat shock was performed by transferring the cell containing Eppendorf cups into a 42 °C water bath for 30 sec. Subsequently, the cell containing Eppendorf cup was transferred back on ice. Cells were shaken at 180 rpm and 37 °C for at least 30 min, after the addition of 300 µl pre-warmed LB medium (Tab. 5.6). The bacterial suspension was plated onto an LB plate containing the according antibiotic for selection. Bacteria colonies with the internalized recombinant plasmid were obtained on the plate after incubation at 37 °C over night.

5.9.12 Generation of plasmid constructs for injection

All generated PCR-products were sequenced (data not shown). Inserts were amplified with primers listed in Table 5.12 and cloned into the desired vector *via* Gibson Assembly. The success of a cloning procedure was confirmed by sequencing.

For the Mega project, all double stranded DNA fragments were synthesized by Eurofins Genomics and cloned into the *pGE-attB* vector *via* either NsiI-NdeI or XhoI-NsiI restriction sites.

5.9.13 Generation of CRISPR/Cas9 constructs

Clustered regularly interspaced short palindromic repeats (CRISPR) is a genome editing method that allows precise modification of genes. The system is involved in adaptive immunity in bacteria and archaea.

A minimal two component system able to induce site-specific cleavage of DNA was identified by (Jinek et al., 2012). FlyCRISPR Optimal Target Finder tool (<http://flycrispr.molbio.wisc.edu/>) to identify highly specific target sites in the *Drosophila* genome was used to find a target sequence in the gene of interest and design an oligonucleotide pair for Cas9 nuclease cleavage. Cells initiate DNA repair after induced double strand DNA breaks. However, repair mechanisms including non-homologous end joining (NHEJ) are imprecise and often result in insertions and/or deletions at the breaking point with the potential of generating loss-of-function-mutations.

A 20 bp target sequence at the desired breaking point was selected fulfilling following criteria: The target sequence was followed by a 3 nucleotide PAM sequence NGG and begin with a G to optimize U6 driven transcription.

Complementary sense and antisense oligonucleotides were designed, with overhang sequences 5'–CTTC–3' at the sense oligo and 3'–CAAA–5' at the antisense oligo. Additionally, both oligos were phosphorylated with T4 polynucleotidkinase.

Following reaction was pipetted for phosphorylation:

1 µl sense oligo (100 µM)
1 µl antisense oligo (100 µM)
1 µl 10x T4 ligation buffer (NEB)
1 µl T4 Polynucleotide Kinase (NEB)
6 µl dH₂O

Following thermocycler program was applied to the reaction:

37 °C for 30 min
95 °C for 5 min

The reaction was cooled down to 25 °C at a rate of –0.1 °C/sec.

1 µg *pBFv-U6.2* vector containing ampicillin resistance was cut using BbsI (NEB) according to manufacturer's instructions and purified *via* the NucleoSpin® Extract II Kit (Tab. 5.2). Following ligation reaction was pipetted:

X µl BbsI digested *pBFv U6.2* (50 ng)
1 µl annealed oligo insert

1 µl 10x T4 ligation buffer
1 µl T4 DNA ligase (NEB)
dH₂O to 10 µl

The reaction was incubated at 25 °C for one hour and was used for transformation of chemically competent 10-beta cells (NEB), according to manufacturer's instructions. Inserted gRNA was confirmed by T3 or T7 sequencing. For the generation of plasmids carrying 2 gRNAs, a first gRNA was cloned into *pBFv-U6.2* vector via BbsI restriction sites and a second gRNA was cloned into *pBFv-U6.2B*, a variant of *pBFv-U6.2* carrying a dummy sequence flanked by EcoRI and NotI sites upstream of the U6 promoter. The fragment containing the first gRNA and the U6 promoter was cut from the *pBFv-U6.2* vector using EcoRI and NotI restriction sites and cloned into *pBFv-U6.2B*-gRNA that was previously linearized with EcoRI and NotI (Kondo and Ueda, 2013).

The double gRNA approach was used for homology-directed repair (HDR) when generating *attP* site gene substitution. All injections were conducted by BestGene Inc.

5.9.14 DNA sequencing

The sequencing of DNA was performed by Microsynth. For sequencing of PCR-DNA 18 ng/100 base pairs DNA were dissolved in 12 µl water. For sequencing of plasmid DNA 0.5 µg/kb were dissolved in 12 µl water. The desired sequencing primers (3 µl of 10mM primer per sequencing reaction) were directly pipetted into the sequencing solution or were chosen from a standard primer list at Microsynth. All sequencing was conducted at Microsynth.

5.9.15 DNA and protein sequence analysis

DNA and protein sequences were analyzed with DNASTAR 7.0. The National Center for Biotechnology Information (NCBI; www.ncbi.nlm.gov), including the Basic Local Alignment Search Tool (BLAST), Flybase (www.flybase.org) and UniProt (www.uniprot.org) were used for online database research.

TMHMM2.0 (Transmembrane hidden Markov Model), Center for Biological Sequence Analysis, www.cbs.dtu.dk/services/TMHMM-2.0/, was employed for protein sequence analysis.

5.10 Methods for co-immunoprecipitation

Co-immunoprecipitation (co-IP) experiments were conducted with magnetic Dynabeads[®] (Invitrogen) or GFP-Trap-MA beads (chromotek). The Dynabead[®] surface is covered with protein G, that binds specifically to immunoglobulins. The magnetic properties of the beads allowed the separation of beads from liquids *via* a magnetic field, without the necessity of spinning down.

5.10.1 Homogenization of whole embryos for Co-IP

Embryos of the desired *Drosophila* strain were staged to 18-22 h after egg laying and decorionated as described (sec. 5.3.5). 100 embryos were collected and transferred into a 0.1 ml glass micro tissue grinder (VWR), containing 100 µl co-IP NP40 buffer for embryos (Tab. 5.4). Embryos were homogenized with a glass pistil, until the mixture was smooth. The micro tissue grinder containing the embryo lysate was placed on ice for 2 min. Before adding the embryo lysates to the Dynabeads[®], 300 µl co-IP wash buffer for embryos were added to the lysates.

5.10.2 Preparation of magnetic Dynabeads[®]

Dynabeads[®] were resuspended by vortexing for 10 sec. 50 µl magnetic Dynabeads[®] (Invitrogen) were transferred into a Eppendorf cup, magnetized on a DynaMag magnetic Eppendorf cup holder and the supernatant was discarded. The reaction tubes were removed from the magnetic Eppendorf cup holder and 500 µl PBTw containing 20 µl anti-Mega antibody were added. Dynabeads[®] were incubated on a rotating wheel for 10 min to allow coupling of the antibody to the protein G on the Dynabeads[®] surface. To eliminate unbound antibody, Dynabeads[®] were washed with 1 ml PBTw in 8 washing steps. Embryo lysates were directly added to prepared Dynabeads[®].

5.10.3 Co-IP protocol for embryo lysates

Embryo lysates and Dynabeads[®] were prepared as described (sec. 5.10.1 and sec. 5.10.2). 450 µl embryo lysate were transferred to Dynabeads[®] and incubated on a rotating wheel for 4 h at 4 °C. After incubation, supernatant was transferred into a new reaction tube. Sample buffer was added to the supernatant, the solution was incubated for 10 min at 99 °C in a heating block and stored at -20 °C.

10 washing steps with 1 ml wash buffer for co-IP were performed on the remaining Dynabeads[®]/ protein complex. Uncovered complexes were incubated on ice and mass spectrometry analysis was performed (see sec. 5.11).

For western blot analysis, sample buffer was added to uncovered Dynabeads[®]/ protein complexes, followed by incubation at 99 °C for 10 min and storage at -20 °C. Western blot analysis occurred with distinct calculated amounts of embryo numbers.

5.10.4 Harvesting and homogenization of S2R+ cells for Co-IP

Prior to harvesting and the performance of co-ip, cells were transfected with vectors for expression of desired constructs.

The supernatant was discarded and 1 ml ice cold PBS (Tab. 5.4) was added to the cells in 6-well plates. The cell suspension was transferred into a Eppendorf cup and centrifuged 900 rpm for 5 min at 4 °C. The supernatant was discarded and cells were washed with PBS in three washing steps.

5.10.5 Preparation of GFP-Trap[®] beads

10 µl GFP-Trap[®] beads were equilibrated in 500 µl ice cold wash buffer. The supernatant was discarded magnetically, followed by two additional washing steps with 500 µl ice cold dilution buffer.

5.10.6 Co-IP protocol for cell lysates

Cells were harvested and homogenized as described in section 5.10.4. Cells were resuspended in 200 µl lysis buffer and lysates were incubated on ice for 30 min with pipetting up and down every 10 min. Cell lysates were centrifuged at 15000 rpm for 10 min at 4 °C and supernatants were transferred into a new Eppendorf cup, followed by the addition of 300 µl wash buffer. An input sample was taken by transferring 45 µl cell lysate and 15 µl SDS sample buffer into a new Eppendorf cup and incubated for 10 min at 99 °C in a heating block. This sample is referred to as the input sample.

Diluted lysates were directly added to GFP-Trap[®] beads and incubated at 4 °C for 1 h. 45 µl supernatant and 15 µl SDS sample buffer were transferred into a new Eppendorf cup and incubated for 10 min at 99 °C in a heating block. This sample is referred to as the supernatant sample.

GFP-Trap[®] bead/protein complexes were washed with 500 µl wash buffer and transferred into a new Eppendorf cup. 15 µl SDS sample buffer were added, followed by incubation at 99 °C for 10 min and storage at 4 °C. Western blot analysis was performed with similar calculated protein amounts.

5.10.7 SDS PAGE, Western Blot and Antibody Staining

Co-IP samples were prepared as described in section 5.10.6 and 5.10.3. One dimensional SDS PAGE was performed using a 10 well 4-20% Mini Protean-Gel TGX (BioRad) at 160 V for 55 min. The SDS gel was blotted onto a 0.2 μ m nitrocellulose membrane (GE Healthcare) at 300 mA for 90 min.

The blot was washed with 10 ml PBTw in 4 washing steps for 1 h. Subsequently, the blot was blocked in 10% milk in PBTw (v/v) for 1 h. Primary antibody was added in blocking buffer and incubated over night at 4 °C. On the second day, the blot was washed with 10 ml PBTw in four washing steps for 1 h. Diluted secondary antibody was added in blocking buffer and incubated for 2 h at RT, followed by 4 washing steps with 10 mM PBTw.

The WesternBright Chemiluminescence Substrate Sirius kit was used for the signal detection reaction according to the manufacturer's instructions. Western blots were imaged with a FUJIFILM Intelligent Dark Box II.

DNA fragments of fusion proteins depicted on western blots may differ from the *in silico* calculated molecular weights.

5.11 Mass spectrometry

For mass spectrometric analysis, proteins were enriched by immunoprecipitation (co-IP). Sample preparation took place in two ways:

1. A one dimensional PAGE was conducted and the gel was stained with GelCode Blue. Entire lanes were cut into 23 pieces, followed by in gel digestion with trypsin.
2. Protein complexes were directly digested with Trypsin on beads.

Tryptic peptides were analyzed by liquid chromatography coupled mass spectrometry (LC-coupled-MS) on an QExactive HF-X mass spectrometer (Thermo Fisher Scientific) in a data dependent acquisition mode. Obtained fragment ion spectra were searched against the Uniprot protein database (Uniprot20171117) with MaxQuant version 1.5.6.0 as the search engine. Search parameters were adjusted apart from default MaxQuant settings: carbamidomethyl cysteine and oxidation of methionine as variable modifications, 2 miss cleavages allowed, protein false positive rate was set to maximum 1%. Samples and control samples were defined as separate experiments. Identified proteins were quantified using label-free quantification (LFQ). Statistical analysis and Student's T-test were performed with Perseus version 1.5.6.0.

All mass spectrometry analyses were performed by Iwan Parfentev, Max-Planck-Institute

for Biophysical Chemistry, Research Group Mass Spectrometry.

5.12 Electron microscopy

Embryos of the desired stage were dechorionated (sec. 5.3.5) and placed on a 150 μm flat embedding specimen holder (Engineering Office M. Wohlwend) and frozen in a Leica HBM100 high pressure freezer (Leica). Embedding of the vitrified samples occurred using an Automatic Freeze Substitution Unit (Leica). Substitution was conducted at $-90\text{ }^{\circ}\text{C}$ for 72 h in a solution containing anhydrous acetone, 0.1% tannic acid and 0.5% glutaraldehyde, followed by another substitution step with anhydrous acetone, 2% OsO_4 and 0.5% glutaraldehyde for 8 h.

After incubation at $-20\text{ }^{\circ}\text{C}$ for 18 h, the samples were warmed up to $4\text{ }^{\circ}\text{C}$, washed with anhydrous acetone and embedded in Agar100 (Agar Scientific). The samples were documented on a Philips CM120 electron microscope (Philips Inc.) with a TemCam F416 CMOS camera (TVIPS).

The embedding, high pressure freezing and documentation was kindly performed by Dietmar Riedel, who also provided help in the data analysis.

5.13 Image documentation and microscopy

Agarose gels were imaged with a digital-video-system (FujiFilm) and printed on Thermopaper (Mitsubishi). Larvae and embryo analysis was performed on an Axiophot (Zeiss) with an integrated limelight source. Flies were analyzed with following dissecting scopes: Stemi SV11 (Zeiss) or Stemi 2000 Stereomicroscope (Zeiss) connected to an internal or external limelight source KL1500 LCD (Schott). Homozygous embryo sorting was performed on an Axiovert 200M Epifluorescence microscope (Zeiss). Immunofluorescence microscopy was conducted on a LSM780 confocal microscope (Zeiss). Images of whole embryos were taken with 25x magnification and oil immersion (objective LD LCI Plan-Apochromat 25x/0.8 Imm Corr DIC M27) and images of cell and organ details were taken with a 40x magnification and oil immersion (objective Plan-Apochromat 40x/1.4 Oil DIC M27). Obtained images were edited with ImageJ/Fiji, Adobe Photoshop and Illustrator. All Z-projection images are Maximum-Intensity-Projections generated in ImageJ.

References

- Affolter, M. and Shilo, B. Z. (2000). Genetic control of branching morphogenesis during *Drosophila* tracheal development. *Curr. Opin. Cell Biol.* 12, 731–735.
- Arabzadeh, A., Troy, T.-c., and Turksen, K. (2006). Role of the Cldn6 Cytoplasmic Tail Domain in Membrane Targeting and Epidermal Differentiation In Vivo. *Mol. Cell. Biol.* 26, 5876–5887.
- Arau, S. J., Aslam, H., Tear, G., and Casanova, J. (2005). mummy / cystic encodes an enzyme required for chitin and glycan synthesis , involved in trachea , embryonic cuticle and CNS development — Analysis of its role in *Drosophila* tracheal morphogenesis. *Dev. Biol.* 288, 179–193.
- Bateman, J. R., Lee, A. M., and Wu, C. T. (2006). Site-specific transformation of *Drosophila* via phiC31 integrase-mediated cassette exchange. *Genetics* 173, 769–777.
- Batz, T., Forster, D., and Luschnig, S. (2014). The transmembrane protein Macroglobulin complement-related is essential for septate junction formation and epithelial barrier function in *Drosophila*. *Development* 141, 899–908.
- Baudin-Baillieu, A., Legendre, R., Kuchly, C., Hatin, I., Demais, S., Mestdagh, C., Gautheret, D., and Namy, O. (2014). Genome-wide Translational Changes Induced by the Prion [PSI⁺]. *Cell Rep.* 8, 439–448.
- Baumgartner, S., Littleton, J., Broadie, K., Bhat, M. A., Harbecke, R., Lengyel, J. A., Chiquet-Ehrismann, R., Prokop, A., and Bellen, H. J. (1996). A *Drosophila* Neurexin Is Required for Septate Junction and Blood-Nerve Barrier Formation and Function. *Cell* 87, 1059–1068.
- Behr, M., Riedel, D., and Schuh, R. (2003). The Claudin-like Megatrachea Is Essential in Septate Junctions for the Epithelial Barrier Function in *Drosophila*. *Dev. Cell* 5, 611–620.
- Bellmann, S., Carlander, D., Fasano, A., Momcilovic, D., Scimeca, J. A., Waldman, W. J., Gombau, L., Tsytsikova, L., Canady, R., Pereira, D. I., and Lefebvre, D. E. (2015). Mammalian gastrointestinal tract parameters modulating the integrity, surface properties, and absorption of food-relevant nanomaterials. *Wiley Interdiscip. Rev. Nanomed. Nanobiotechnol.* 7, 609–622.
- Blasig, I. E., Winkler, L., Lassowski, B., Mueller, S. L., Zuleger, N., Krause, E., Krause, G., Gast, K., Kolbe, M., and Piontek, J. (2006). On the self-association potential of transmembrane tight junction proteins. *Cell. Mol. Life Sci.* 63, 505–514.
- Byri, S., Misra, T., Syed, Z. A., Bätz, T., Shah, J., Boril, L., Glashauser, J., Aegerter-Wilmsen, T., Matzat, T., Moussian, B., Uv, A., and Luschnig, S. (2015). The Triple-

- Repeat Protein Anakonda Controls Epithelial Tricellular Junction Formation in *Drosophila*. *Dev. Cell* 33, 535–548.
- Campos-Ortega, J. A. and Hartenstein, V. (1985). *The Embryonic Development of Drosophila melanogaster*. 1 st editi. Springer-Verlag Berlin Heidelberg GmbH, 9–84.
- Chalcroft, J. P. and Bullivant, S. (1970). An interpretation of liver cell membrane and junction structure based on observation of freeze-fracture replicas of both sides of the fracture. *J. Cell Biol.* 47, 49–60.
- Claude, P. and Goodenough, D. A. (1973). Fracture faces of zonulae occludentes from "tight" and "leaky" epithelia. *J. Cell Biol.* 58, 390–400.
- Colegio, O. R., Van Itallie, C. M., McCrea, H. J., Rahner, C., and Anderson, J. M. (2002). Claudins create charge-selective channels in the paracellular pathway between epithelial cells. *Am. J. Physiol.-Cell Physiol.* 283, 142–147.
- Cukierman, L., Meertens, L., Bertaux, C., Kajumo, F., and Dragic, T. (2009). Residues in a Highly Conserved Claudin-1 Motif Are Required for Hepatitis C Virus Entry and Mediate the Formation of Cell-Cell Contacts. *J. Virol.* 83, 5477–5484.
- Deligiannaki, M., Casper, A. L., Jung, C., and Gaul, U. (2015). Pasiflora proteins are novel core components of the septate junction. *Development* 142, 3046–3057.
- Dong, B., Miao, G., and Hayashi, S. (2014). A fat body-derived apical extracellular matrix enzyme is transported to the tracheal lumen and is required for tube morphogenesis in *Drosophila*. *Development* 141, 4104–4109.
- Eliuk, S. and Makarov, A. (2015). Evolution of Orbitrap Mass Spectrometry Instrumentation. *Annu. Rev. Anal. Chem.* 8, 61–80.
- Fehon, R. G., Dawson, I. A., and Artavanis-Tsakonas, S. (1994). A *Drosophila* homologue of membrane-skeleton protein 4.1 is associated with septate junctions and is encoded by the coracle gene. *Development* 120, 545–557.
- Fujita, K., Katahira, J., Horiguchi, Y., Sonoda, N., Furuse, M., and Tsukita, S. (2000). Clostridium perfringens enterotoxin binds to the second extracellular loop of claudin-3, a tight junction integral membrane protein. *FEBS Lett.* 476, 258–261.
- Furuse, M., Fujita, K., Hiiragi, T., Fujimoto, K., and Tsukita, S. (1998). Claudin-1 and -2: Novel integral membrane proteins localizing at tight junctions with no sequence similarity to occludin. *J. Cell Biol.* 141, 1539–1550.
- Furuse, M., Sasaki, H., and Tsukita, S. (1999). Manner of interaction of heterogeneous claudin species within and between tight junction strands. *J. Cell Biol.* 147, 891–903.
- Genova, J. L. and Fehon, R. G. (2003). Neuroglian, Gliotactin, and the Na⁺/K⁺ ATPase are essential for septate junction function in *Drosophila*. *J. Cell Biol.* 161, 979–989.

- Gibson, D. G., Young, L., Chuang, R.-Y., Venter, J. C., Hutchison III, C. A., and Smith, H. O. (2009). Enzymatic assembly of DNA molecules up to several hundred kilobases. *Nat. Methods* 6, 343–345.
- Green, C. R. and Bergquist, P. R. (1982). Phylogenetic Relationships within the invertebrata in Relation to the structure of Septate Junctions and the development of 'Occluding' Junctional types. *J. Cell Sci.* 53, 279–305.
- Gumbiner, B. M. (2000). Regulation of cadherin adhesive activity. *J. Cell Biol.* 148, 399–404.
- Günzel, D. and Yu, A. S. L. (2013). Claudins and the modulation of tight junction permeability. *Physiol Rev.* 93, 525–569.
- Halbleib, J. M. and Nelson, W. J. (2006). Cadherins in development: Cell adhesion, sorting, and tissue morphogenesis. *Genes Dev.* 20, 3199–3214.
- Hamazaki, Y., Itoh, M., Sasaki, H., Furuse, M., and Tsukita, S. (2002). Multi-PDZ domain protein 1 (MUPP1) is concentrated at tight junctions through its possible interaction with claudin-1 and junctional adhesion molecule. *J. Biol. Chem.* 277, 455–461.
- Harris, T. J. C. and Tepass, U. (2010). Adherens junctions: From molecules to morphogenesis. *Nat. Rev. Mol. Cell Biol.* 11, 502–514.
- Hervé, J. C. and Derangeon, M. (2013). Gap-junction-mediated cell-to-cell communication. *Cell Tissue Res.* 352, 21–31.
- Hervé, J. C., Derangeon, M., Sarrouilhe, D., Giepmans, B. N., and Bourmeyster, N. (2012). Gap junctional channels are parts of multiprotein complexes. *Biochim. Biophys. Acta - Biomembr.* 1818, 1844–1865.
- Hijazi, A., Haenlin, M., Waltzer, L., and Roch, F. (2011). The Ly6 protein coiled is required for septate junction and blood brain barrier organisation in *Drosophila*. *PLoS One* 6, e17763.
- Hildebrandt, A., Pflanz, R., Behr, M., Tarp, T., Riedel, D., and Schuh, R. (2015). Bark beetle controls epithelial morphogenesis by septate junction maturation in *Drosophila*. *Dev. Biol.* 400, 237–247.
- Ile, K. E., Tripathy, R., Goldfinger, V., and Renault, A. D. (2012). Wunen, a *Drosophila* lipid phosphate phosphatase, is required for septate junction-mediated barrier function. *Development* 139, 2535–2546.
- Itoh, M., Furuse, M., Morita, K., Kubota, K., Saitou, M., and Tsukita, S. (1999). Direct binding of three tight junction-associated MAGUKs, ZO-1, ZO-2, and ZO-3, with the COOH Termini of Claudins. *J. Cell Biol.* 147, 1351–1363.

- Izumi, Y. and Furuse, M. (2014). Molecular organization and function of invertebrate occluding junctions. *Semin. Cell Dev. Biol.* 36, 186–193.
- Jaspers, M. H. J., Nolde, K., Behr, M., Joo, S.-h., Plessmann, U., Nikolov, M., Urlaub, H., and Schuh, R. (2012). The Claudin Megatrachea Protein Complex. *J. Biol. Chem.* 287, 36756–36765.
- Jinek, M., Chylinski, K., Fonfara, I., Hauer, M., Doudna, J. A., and Charpentier, E. (2012). A programmable dual-RNA-guided DNA endonuclease in adaptive bacterial immunity. *Science* 337, 816–821.
- Joseph, D., Puttaswamy, R. K., and Krovvidi, H. (2013). Non-respiratory functions of the lung. *Contin. Educ. Anaesthesia, Crit. Care Pain* 13, 98–102.
- Kelstrup, C. D., Bekker-jensen, D. B., Arrey, T. N., Hogrebe, A., Harder, A., and Olsen, J. V. (2018). Performance Evaluation of the Q Exactive HF-X for Shotgun Proteomics. *J. Proteome Res.* 727–738.
- Keravala, A. and Calos, M. P. (2008). Site-Specific Chromosomal Integration Mediated by phiC31 Integrase. *Methods Mol Biol* 435, 165–173.
- Klagges, B. R. E., Heimbeck, G., Godenschwege, T. A., Hofbauer, A., Pflugfelder, G. O., Reifegerste, R., Reisch, D., Schaupp, M., Buchner, S., and Buchner, E. (1996). Invertebrate Synapsins : A Single Gene Codes for Several Isoforms in Drosophila. *J. Neurosci.* 16, 3154–3165.
- Knust, E. and Bossinger, O. (2002). Composition and formation of intercellular junctions in epithelial cells. *Science* 298, 1955–1959.
- Kondo, S. and Ueda, R. (2013). Highly improved gene targeting by germline-specific Cas9 expression in Drosophila. *Genetics* 195, 715–721.
- Kondo, T. and Hayashi, S. (2013). Mitotic cell rounding accelerates epithelial invagination. *Nature* 494, 125–129.
- Krämer, H. (2000). The ups and downs of life in an epithelium. *J. Cell Biol.* 151, F15–18.
- Krause, G., Winkler, L., Mueller, S. L., Haseloff, R. F., Piontek, J., and Blasig, I. E. (2008). Structure and function of claudins. *Biochim. Biophys. Acta* 1778, 631–645.
- Kwok, J. B. J., Li, Q.-X., Hallupp, M., Whyte, S., Ames, D., Beyreuther, K., Masters, C. L., and Schofield, P. R. (2000). Novel Leu723Pro amyloid precursor protein mutation increases amyloid β 42(43) peptide levels and induces apoptosis. *Ann. Neurol.* 47, 249–253.
- Laird, D. W. (2006). Life cycle of connexins in health and disease. *Biochem. J.* 394, 527–543.

- Lamb, R. S., Ward, R. E., Schweizer, L., and Fehon, R. G. (1998). Drosophila coracle , a Member of the Protein 4 . 1 Superfamily , Has Essential Structural Functions in the Septate Junctions and Developmental Functions in Embryonic and Adult Epithelial Cells. *Mol. Biol. Cell* 9, 3505–3519.
- Laprise, P., Lau, K. M., Harris, K. P., Silva-Gagliardi, N. F., Paul, S. M., Beronja, S., Beitel, G. J., McGlade, C. J., and Tepass, U. (2009). Yurt, Coracle, Neurexin IV and the Na⁺,K⁺-ATPase form a novel group of epithelial polarity proteins. *Nature* 459, 1141–1145.
- Laprise, P., Paul, S. M., Boulanger, J., Robbins, R. M., Beitel, G. J., and Tepass, U. (2010). Epithelial polarity proteins regulate Drosophila tracheal tube size in parallel to the luminal matrix pathway. *Curr. Biol.* 20, 55–61.
- Laval, M., Bel, C., and Faivre-Sarrailh, C. (2008). The lateral mobility of cell adhesion molecules is highly restricted at septate junctions in Drosophila. *BMC Cell Biol.* 9.
- Llimargas, M., Strigini, M., Katidou, M., Karagogeos, D., and Casanova, J. (2004). Lachesin is a component of a septate junction-based mechanism that controls tube size and epithelial integrity in the Drosophila tracheal system. *Development* 131, 181–190.
- Luschnig, S., Bätz, T., Armbruster, K., and Krasnow, M. A. (2006). serpentine and vermillion encode matrix proteins with chitin binding and deacetylation domains that limit tracheal tube length in Drosophila. *Curr. Biol.* 16, 186–194.
- Moussian, B., Schwarz, H., Bartoszewski, S., and Nüsslein-Volhard, C. (2005). Involvement of Chitin in Exoskeleton Morphogenesis in Drosophila melanogaster. *J. Morph* 264, 117–130.
- Moyer, K. E. and Jacobs, J. R. (2008). Varicose: A MAGUK required for the maturation and function of Drosophila septate junctions. *BMC Dev. Biol.* 8.
- Müller, D., Kausalya, P. J., Meij, I. C., and Hunziker, W. (2006). Familial hypomagnesemia with hypercalciuria and nephrocalcinosis : blocking endocytosis restores surface expression of a novel Claudin-16 mutant that lacks the entire C-terminal cytosolic tail. *Hum. Mol. Genet.* 15, 1049–1058.
- Nelson, K., Furuse, M., and Beitel, G. J. (2010). The Drosophila claudin Kune-kune is required for septate junction organization and tracheal tube size control. *Genetics* 185, 831–839.
- Nilton, A., Oshima, K., Zare, F., Byri, S., Nannmark, U., Nyberg, K. G., Fehon, R. G., and Uv, A. E. (2010). Crooked, Coiled and Crimped are three Ly6-like proteins required for proper localization of septate junction components. *Development* 137, 2427–2437.

- Oda, H., Uemura, T., Harada, Y., Iwai, Y., and Takeichi, M. (1994). A drosophila homolog of cadherin associated with Armadillo and essential for embryonic cell-cell adhesion. *Dev. Biol.* 165, 716–726.
- Oda, H., Uemura, T., Shiomi, K., Nagafuchi, A., Tsukita, S., and Takeichi, M. (1993). Identification of a Drosophila homologue of alpha-catenin and its association with the armadillo protein. *Cell* 121, 1133–1140.
- Oshima, A., Matsuzawa, T., Murata, K., Tani, K., and Fujiyoshi, Y. (2016). Hexadecameric structure of an invertebrate gap junction channel. *J. Mol. Biol.* 428, 1227–1236.
- Oshima, K. and Fehon, R. G. (2011). Analysis of protein dynamics within the septate junction reveals a highly stable core protein complex that does not include the basolateral polarity protein Discs large. *J. Cell Sci.* 124, 2861–2871.
- Paul, S. M., Ternet, M., Salvaterra, P. M., and Beitel, G. J. (2003). The Na⁺/K⁺ ATPase is required for septate junction function and epithelial tube-size control in the Drosophila tracheal system. *Development* 130, 4963–4974.
- Peifer, M. (1993). The product of the Drosophila segment polarity gene armadillo is part of a multi-protein complex resembling the vertebrate adherens junction. *J. Cell Sci.* 105, 993–1000.
- Phelan, P. (2005). Innexins: Members of an evolutionarily conserved family of gap-junction proteins. *Biochim. Biophys. Acta - Biomembr.* 1711, 225–245.
- Piehl, C., Piontek, J., Cording, J., Wolburg, H., and Blasig, I. E. (2010). Participation of the second extracellular loop of claudin-5 in paracellular tightening against ions, small and large molecules. *Cell. Mol. Life Sci.* 67, 2131–2140.
- Piontek, J., Fritzsche, S., Cording, J., Richter, S., Hartwig, J., Walter, M., Yu, D., Turner, J. R., Gehring, C., Rahn, H. P., Wolburg, H., and Blasig, I. E. (2011). Elucidating the principles of the molecular organization of heteropolymeric tight junction strands. *Cell. Mol. Life Sci.* 68, 3903–3918.
- Piontek, J., Winkler, L., Wolburg, H., Müller, S. L., Zuleger, N., Piehl, C., Wiesner, B., Krause, G., and Blasig, I. E. (2008). Formation of tight junction: determinants of homophilic interaction between classic claudins. *FASEB J.* 22, 146–158.
- Prusiner, S. B. (1994). Neurodegeneration in Humans Caused by Prions. *West J Med* 161, 264–272.
- Ribeiro, C., Neumann, M., and Affolter, M. (2004). Genetic Control of Cell Intercalation during Tracheal Morphogenesis in Drosophila. *Curr. Biol.* 14, 2197–2207.
- Robinson, D. N. and Cooley, L. (1997). Examination of the function of two kelch proteins generated by stop codon suppression. *Development* 124, 1405–1417.

- Rüffer, C. and Gerke, V. (2004). The C-terminal cytoplasmic tail of claudins 1 and 5 but not its PDZ-binding motif is required for apical localization at epithelial and endothelial tight junctions. *Eur. J. Cell Biol.* 83, 135–144.
- Samakovlis, C., Manning, G., Steneberg, P., Hacoen, N., Cantera, R., and Krasnow, M. A. (1996). Genetic control of epithelial tube fusion during *Drosophila* tracheal development. *Development* 122, 3531–3536.
- Sambrook, J., Fritsch, E. F., and Maniatis, T. (1989). *Molecular cloning: a laboratory manual*. English. Cold Spring Harbor, NY: Cold Spring Harbor Laboratory Press, xxxviii + 1546.
- Schneeberger, E. E. and Lynch, R. D. (2004). The tight junction: a multifunctional complex. *AJP Cell Physiol.* 286, 1213–1228.
- Schulte, J., Tepass, U., and Auld, V. J. (2003). Gliotactin, a novel marker of tricellular junctions, is necessary for septate junction development in *Drosophila*. *J. Cell Biol.* 161, 991–1000.
- Snow, P. M., Bieber, A. J., and Goodman, C. S. (1989). Fasciclin III: A novel homophilic adhesion molecule in *Drosophila*. *Cell* 59, 313–323.
- Tautz, D. and Pfeifle, C. (1989). A non-radioactive in situ hybridization method for the localization of specific RNAs in *Drosophila* embryos reveals translational control of the segmentation gene hunchback. *Chromosoma* 98, 81–85.
- Tiklová, K., Senti, K.-A., Wang, S., Gräslund, A., and Samakovlis, C. (2010). Epithelial septate junction assembly relies on melanotransferrin iron binding and endocytosis in *Drosophila*. *Nat. Cell Biol.* 12, 1071–1077.
- Tonning, A., Hemphälä, J., Tång, E., Nannmark, U., Samakovlis, C., and Uv, A. (2005). A transient luminal chitinous matrix is required to model epithelial tube diameter in the *Drosophila* trachea. *Dev. Cell* 9, 423–430.
- True, H. L. and Lindquist, S. L. (2000). A yeast prion provides a mechanism for genetic variation and phenotypic diversity. *Nature* 407, 477–483.
- Tsarouhas, V., Senti, K.-A., Jayaram, S. A., Tiklová, K., Hemphälä, J., Adler, J., and Samakovlis, C. (2007). Sequential Pulses of Apical Epithelial Secretion and Endocytosis Drive Airway Maturation in *Drosophila*. *Dev. Cell* 13, 214–225.
- Tyler, S. (2003). Epithelium—The Primary Building Block for Metazoan Complexity. *Integr. Comp. Biol.* 43, 55–63.
- Umeda, K., Ikenouchi, J., Katahira-Tayama, S., Furuse, K., Sasaki, H., Nakayama, M., Matsui, T., Tsukita, S., Furuse, M., and Tsukita, S. (2006). ZO-1 and ZO-2 Independen-

- dently Determine Where Claudins Are Polymerized in Tight-Junction Strand Formation. *Cell* 126, 741–754.
- Van Itallie, C. M. and Anderson, J. M. (2006). Claudins and Epithelial Paracellular Transport. *Annu. Rev. Physiol.* 68, 403–429.
- Van Itallie, C. M., Fanning, A. S., and Anderson, J. M. (2003). Reversal of charge selectivity in cation or anion-selective epithelial lines by expression of different claudins. *Am. J. Physiol.-Renal Physiol.* 285, 1078–1084.
- Van Itallie, C. M., Mitic, L. L., and Anderson, J. M. (2011). Claudin-2 forms homodimers and is a component of a high molecular weight protein complex. *J. Biol. Chem.* 286, 3442–3450.
- Wen, H., Watry, D. D., Marcondes, M. C. G., and Fox, H. S. (2004). Selective Decrease in Paracellular Conductance of Tight Junctions : Role of the First Extracellular Domain of Claudin-5. *Mol. Cell. Biol.* 24, 8408–8417.
- Woods, D. F. and Bryant, P. J. (1991). The discs-large tumor suppressor gene of Drosophila encodes a guanylate kinase homolog localized at septate junctions. *Cell* 66, 451–464.
- Wu, V. M., Yu, M. H., Paik, R., Banerjee, S., Liang, Z., Paul, S. M., Bhat, M. A., and Beitel, G. J. (2007). Drosophila Varicose, a member of a new subgroup of basolateral MAGUKs, is required for septate junctions and tracheal morphogenesis. *Development* 134, 999–1009.
- Wu, V., Schulte, J., Hirschi, A., Tepass, U., and Beitel, G. J. (2004). Sinuous is a Drosophila claudin required for septate junction organization and epithelial tube size control. *J. Cell Biol.* 164, 313–323.
- Yamazaki, Y., Tokumasu, R., Kimura, H., and Tsukita, S. (2011). Role of claudin species-specific dynamics in reconstitution and remodeling of the zonula occludens. *Mol. Biol. Cell* 22, 1495–1504.

A Summary of exchanges, domain switches and deletions of Mega domains

ID	Mega alterations	ID	Mega alterations
M0	wild-type Mega	M38	T12Stop
M1	Mega ECL1 switched with Kune ECL1	M37	F187A
M2	Mega ICL switches with Kune ICL	M39	Y177A, Y184A
M3	Mega ECL2 switches with Kune ECL2	M40	Y98A, Y99A, V100A, I101A
M4	Mega C-terminus switched with Kune C-terminus	M41	Y146A, E147A, W148A, L149A
M5	Mega ECL1 switched with Sinu ECL1	M42	Y81A, F83A, L84A
M6	Mega ICL switches with Sinu ICL	M43	Y177A, W181A, Y184, F187A, Addition of YFP to C-terminus
M7	Mega ECL2 switches with Sinu ECL2	M45	I53A, E54A, S55A
M8	Mega C-terminus switched with Sinu C-terminus	M46	F63A, K64A, N65A
M9	Deletion of amino acids 239-252	M47	C72A, F73A
M10	Deletion of amino acids 213-237	M48	C90A, H91A, N92A
M11	Substitution of all Mega TM domains with CD8 TM domains	M49	N188A, V189A
M12	Deletion of amino acids 2-21	M50	C48A
M13	Addition of a TEV clavage site and YFP to the C-terminus	M51	C48A, C72A, C90A
M14	Addition of Turquoise to the C-terminus	M52	G67A
M15	Addition of YFP to the C-terminus	M53	L68A
M16	Addition of YFP to the N-terminus	M54	W69A

A Summary of exchanges, domain switches and deletions of Mega domains

ID	Mega alterations	ID	Mega alterations
M17	C72A and C90A	M55	D75N
M18	Y177A, W181A, Y184, F187A	M56	R102A
M19	W181A		
M20	Y146A, W148A, L149A	M57	F83A
M21	Deletion of amino acids 253-256	M60	F76A, F83A, F87A, F94A
M22	Addition of a TEV cleavage site at 5' C-terminus	M61	Y78F, Y81F
M23	Addition of a TEV cleavage site after first TM domain	M62	Y98F, Y99F
M24	Deletion of amino acids 212-256	M63	Y78A, Y81A
M25	Deletion of amino acids 22-28	M64	Y98A, Y99A
M26	Deletion of amino acids 4-28	M65	R178A, R179A
M28	Substitution of half Kune C-terminus after G238	M66	R178Q, R179Q
M30	G67A, L68A, W69A	M67	Q86D
M31	G67A, L68A, W69A, C69A, C90A	M68	Q86A
M32	Y177A, D180A, W181A, Y184A, K186A, F187A, N188A	M69	R102Q
M33	Q145A, Y146A, W148A, L149A, L150A, V151A	M70	L38F, T53Y, S120N, V124W, L131W, S154Y, S161Y, M165W, A168F, L204W, L211W
M35	Y177A	M71	T36Y, S120N, S154Y, S161Y, M165W
M36	Y184A	M72	M165W

Table A.1 Detailed description of alterations in *mega* synthetic constructs

B Mass spectrometry data

Nr.	S	Student's T-test Difference LFQ intensity Flag-LFQ intensity Mega	Protein IDs	Protein name	Gene name
1	+	-8,14083	Q9VTZ5	Tsf2	<i>tsf2</i>
2	+	-7,44104	E1JJF9; E1JJF8; M9NEZ5; P20241	Neuroglian	<i>nrg</i>
3	+	-7,24648	Q9VLT3	Macroglobulin	<i>mcr</i>
4	+	-7,06565	Q8IN49		<i>CG31195-RA</i>
5	+	-6,78333	Q9VTM6	Crimpled	<i>crim</i>
6	+	-6,58516	Q7KU09		<i>chinmo</i>
7	+	-6,54312	A0A0B4KEY5; P82147	lethal(2)essential for life	<i>l(2)efl</i>
8	+	-6,53053	CON__ ENSEMBL: ENSB- TAP00000024462		
9	+	-5,96627	Q24372	Lachesin	<i>lac</i>
10	+	-5,57324	Q9VN14	Contactin	<i>cont</i>
11	+	-5,22913	CON__ P02769		
12	+	-4,68215	Q8INX7; X2J6N7; X2JAT7; A8DZ14; P15278	Fasciclin3	<i>fas3</i>
13	+	-3,82107	CON__ ENSEMBL: ENSB- TAP00000014147		

Nr.	S	Student's T-test Difference LFQ intensity Flag-LFQ intensity Mega	Protein IDs	Protein name	Gene name
14	+	-3,76718	E1JIZ1; E1JIZ0; E1JIZ2; A0A0B4K6M4; A0A0B4K7W1; Q7KRY7; A0A0B4KHN3; A0A0B4K6I1; A0A0B4KHY2; A0A0B4K784; A0A0B4KI37	Protein lap4	<i>scrib</i>
15	+	-3,74859	Q8IQH0; Q94887	Neurexin-4	<i>nrx-IV</i>
16	+	-3,6051	Q9W3T7	Boudin	<i>bou</i>
17	+	-3,50362	Q95RA9	GILT1	<i>gilt1</i>
18	+	-3,43295	P41093	60S ribosomal protein L18a	RpL18A
19	+	-3,41692	A1Z6H0	Kune	<i>kune</i>
20	+	-3,03069	Q9VJ19		RpL30
21	+	-3,00351	X2JIQ5; Q9W3W8	60S ribosomal protein L17	RpL17
22	+	-2,99099	CON__ P01966		
23		-2,97917	Q9V9X1		<i>mey</i>
24	+	-2,81636	B7Z0L1; B7Z0L0; Q9VES3; Q8INA9; A0A0B4KH94; A8JR25; P10674	Fasciclin-1	<i>fas1</i>

Nr.	S	Student's T-test Difference LFQ intensity Flag-LFQ intensity Mega	Protein IDs	Protein name	Gene name
25	+	-2,71926	M9PB69; M9MRE5; Q9VLS3; M9PF50; E1JHB4; Q8IPG4; M9PCW8; A0A0S0WGQ9; M9MSG8; M9PCC7; Q0E8L0	Piezo-type mechanosensitive ion channel component	Piezo
26	+	-2,69065	A0A0C4DHE8; Q9VH69	40S ribosomal protein S29	RpS29
27	+	-2,63414	Q9VPG1		<i>zyc</i>
28	+	-2,60177	P13607; E1JIR4; A0A0B4KGG8; A8QI34	Sodium/ potassium -transporting ATPase subunit alpha	<i>atpalpha</i>
29	+	-2,48452	Q9VV24		<i>CG13043-RA</i>
30	+	-2,47281	E1JIE5; Q9VS49		<i>CG43780</i>
31	+	-2,39696	Q9VV25		
32	+	-2,37174	Q9VCI4		<i>CG10217-RA</i>
33	+	-2,33535	M9MRF2; Q9VMU4	60S ribosomal protein L37a	RpL37A
34		-2,3178	M9MRC9; P41092	60S ribosomal protein L27a	RpL27A
35	+	-2,28975	Q9VPR7		<i>cold</i>
36	+	-2,28965	CON__ Q1RMK2		
37	+	-2,27913	Q9VNE9; A0A0B4KFM7	60S ribosomal protein L13a	RpL13A
38		-2,25034	CON__ Q1RMN8		
39	+	-2,23462	A0A0B4LHT3; Q9VAS7	Innexin	<i>inx3</i>
40		-2,22254	Q9V9M7		RpL21

Nr.	S	Student's T-test Difference LFQ intensity Flag-LFQ intensity Mega	Protein IDs	Protein name	Gene name
41		-2,1884	Q9VBE1		TwdIP
42		-2,18188	Q9W077		Cpr62Bc
43		-2,17738	Q94901	RNA-binding protein lark	<i>lark</i>
44		-2,14116	Q9VIQ8		COX4
45		-2,12902	CON__Q3SX09; CON__P02070		
46		-2,11642	A0A0B4LG23; Q9V8R9; A0A0B4LFX4	Protein 4.1 homolog	<i>cora</i>
47		-2,06984	X2JDP6; M9MRG2; Q8T079	Putative oxidoreductase GLYR1 homolog	<i>CG4747</i>
48		-2,03739	P15357; R9PY16; Q9W418; A4V1F9; P0CG69	Ubiquitin-40S ribosomal protein S27a	RpS27A
49		-2,03433	Q9VVN1		
50		-1,97117	Q9VNN7		Osi15
51		-1,90383	Q9W1N3		<i>levy</i>
52		-1,889	Q2PDR9; Q7KT16; M9PDB2; Q9VIJ4		<i>vari</i>
53		-1,88801	P06754; Q8IGY1; Q95TA3; Q8IG84	Tropomyosin-1, isoforms 9A/A/B	Tm1
54		-1,85835	Q9VEH0; Q960Y8		<i>alt</i>
55		-1,83626	Q99323	Myosin heavy chain, non-muscle	<i>zip</i>
56		-1,80714	Q9VV29; Q9VV30		
57		-1,79996	Q960J9		<i>CG1733</i>

Nr.	S	Student's T-test Difference LFQ intensity Flag-LFQ intensity Mega	Protein IDs	Protein name	Gene name
58		-1,78579	Q94516	ATP synthase subunit b, mitochondrial	<i>ATPsyn-b</i>
59		-1,77804	M9PBL3; P02828	Heat shock protein 83	<i>hsp83</i>
60		-1,74566	Q7K VX5; Q9W4N8		Vap-33A
61		-1,74469	Q8SZ28; C6SV36		<i>CG3884-RB</i>
62		-1,706	Q9VBN5	60S ribosomal protein L27	RpL27
63		-1,69804	P29327	40S ribosomal protein S6	RpS6
64		-1,68055	Q9V3F8	Pyrroline-5- carboxylate reductase	P5cr
65		-1,67536	Q9VUZ0	Translocon- associated protein subunit beta	SsRbeta
66		-1,65068	Q9VLT7		RpL36A
67		-1,63155	Q9VYM9		
68		-1,62975	P06605; P06603; P06604	Tubulin alpha-3 chain;Tubulin alpha-1 chain;Tubulin alpha-2 chain	alphaTub84D; alphaTub84B; alphaTub85E
69		-1,62494	M9PG47; P13008	40S ribosomal protein S26	RpS26
70		-1,62128	Q0E9B6; A1Z8U9	40S ribosomal protein S11	RpS11
71		-1,60953	Q2PE37; O76899		pck

Nr.	S	Student's T-test Difference LFQ intensity Flag-LFQ intensity Mega	Protein IDs	Protein name	Gene name
72		-1,60438	A0A0B4JD46; Q8T8R1	CCHC-type zinc finger protein <i>CG3800</i>	<i>CG3800</i>
73		-1,58533	Q8MZI3; Q7KU78		
74		-1,58238	M9PFZ1; Q7KTV5; Q9VNX6; M9MSM4		Nopp140
75		-1,55982	Q9VV52		RAF2
76		-1,5572	Q03427; A0A0B4KFY9	Lamin-C	LamC
77		-1,54266	P17704	40S ribosomal protein S17	RpS17
78		-1,46361	Q9VV23		
79		-1,455	Q9W499		RpL35
80		-1,44646	M9PIM0; O61231	60S ribosomal protein L10	RpL10
81		-1,41272	Q95RE4; M9NFR5		<i>yps</i>
82		-1,32978	Q9W475		
83		-1,32885	Q9VDL2; Q86BR8		TFAM
84		-1,32571	Q9VHF5		
85		-1,30069	P36241	60S ribosomal protein L19	RpL19
86		-1,28031	P55841	60S ribosomal protein L14	RpL14
87		-1,2707	P55828	40S ribosomal protein S20	RpS20

Nr.	S	Student's T-test Difference LFQ intensity Flag-LFQ intensity Mega	Protein IDs	Protein name	Gene name
88		-1,26645	Q8IHB0; Q9VEX2; Q8INB6; Q59DW8; Q86BR9; Q86NK8; Q4AB31; A0A0B4K7C4; A0A0B4K697; A0A0B4KHL4		<i>gish</i>
89		-1,26248	A0A0B4LGB7; P22700	Calcium- transporting ATPase; Calcium- transporting ATPase sarcoplas- mic/endoplasmic reticulum type	Ca-P60A
90		-1,25371	A0A0B4KG06; Q6NN28; A0A0B4K6Y8; CON_Q3SX28		Tm1
91		-1,21903	Q9VRM3		<i>sinu</i>
92		-1,2184	P18432	Myosin regulatory light chain 2	Mlc2
93		-1,18723	Q9VM69		<i>nop5</i>
94		-1,18703	M9PFF0; P41126	60S ribosomal protein L13	RpL13
95		-1,18559	Q29QW0		
96		-1,13658	Q7KLX3		Tapdelta

Nr.	S	Student's T-test Difference LFQ intensity Flag-LFQ intensity Mega	Protein IDs	Protein name	Gene name
97		-1,13331	M9PH59; Q9VXX8	Ribosomal protein L37; Probable 60S ribosomal protein L37-A	RpL37a
98		-1,12594	Q0E924; A8DYI7; A8DYI6		Phb2
99		-1,11845	X2J5G6; P32100	60S ribosomal protein L7	RpL7
100		-1,11757	Q9VP55		Cpr78Cb
101		-1,11574	M9MSI3; Q9V3G8		BG:DS00180.2
102		-1,11451	P20240	Otefin	Ote
103		-1,09979	Q9V9W2; Q9V9W3		RpL6
104		-1,08625	Q59DP9; Q59DP8; Q59DQ0; E6EK17; E6EK15; Q9V4C7; E6EK18	Calcium- transporting ATPase	PMCA
105		-1,07951	Q9VK59		
106		-1,07625	C9QP42; Q02748	Eukaryotic initiation factor 4A	eIF-4a
107		-1,07518	Q00174	Laminin subunit alpha	LanA
108		-1,06044	A0A0B4LGF8; P53777; B7YZP9	Muscle LIM protein 1	Mlp60A
109		-1,04807	Q7JYK1; P18101	Ubiquitin-60S ribosomal protein L40; Ubiquitin; 60S ribosomal protein L40	RpL40

Nr.	S	Student's T-test Difference LFQ intensity Flag-LFQ intensity Mega	Protein IDs	Protein name	Gene name
110		-1,04738	M9PDQ0; M9PBI5; M9PGV6; P13395	Spectrin alpha chain	alpha-Spec
111		-1,03471	X2JCS6; P46223	60S ribosomal protein L7a	RpL7A
112		-1,0274	A1Z871; Q966V0; Q7K1M7; D3DMM3; A1Z870; Q86P80; A1Z866; A0A0B4K7W2; A1Z869; Q7JR75; A0A0B4KEJ6; B7YZD9; A1Z867; A0A0B4KEH7; B7YZD8; A0A0B4K6W0; A0A0B4K7L3; Q966U7; A1Z872		CAP
113		-1,00427	Q9VHE5; Q9VBH8		RpL34b; RpL34a
114		-1,00426	Q9VVU2; Q7JRQ1		RpL26
115		-0,980684	Q9VV62		<i>dsx-c73A</i>
116		-0,970053	D2NUK9; Q9U3Z7	NHP2-like protein 1 homolog	<i>hoip</i>
117		-0,954852	M9NE89; P08928	Lamin Dm0	Lam
118		-0,947113	X2J950; Q03334	40S ribosomal protein S13	RpS13
119		-0,943907	Q9VZ45; Q0KHU0; M9PGV5		Myo10A

Nr.	S	Student's T-test Difference LFQ intensity Flag-LFQ intensity Mega	Protein IDs	Protein name	Gene name
120		-0,939285	Q9VZ69; Q0KHU2; Q8IR99; E1JJM0; M9NF14		Imp
121		-0,93638	X2JCL6; Q9VWE9; Q9V668	Protein transport protein Sec61 gamma-2 subunit;Protein transport protein Sec61 gamma-1 subunit	Sec61gamma; SEC61G1
122		-0,931611	Q9VDH8		RpS30
123		-0,912987	Q9VNB9		RpL35A
124		-0,892314	P48588	40S ribosomal protein S25	RpS25
125		-0,869235	Q9V3E7		Ref1
126		-0,858636	Q24154	60S ribosomal protein L29	RpL29
127		-0,857132	P48148	Ras-like GTP-binding protein Rho1	Rho1
128		-0,833472	X2JAW6; P15215	Laminin subunit gamma-1	LanB2
129		-0,82249	Q9V3L8		Ccp84Aa
130		-0,811575	C6SUW3; P55935; Q95RG1	40S ribosomal protein S9	RpS9
131		-0,805509	Q9VBC8		TwlQ
132		-0,797391	P25171	Regulator of chromosome condensation	Rcc1
133		-0,794212	P35220; X2JBG9	Catenin alpha	alpha-Cat

Nr.	S	Student's T-test Difference LFQ intensity Flag-LFQ intensity Mega	Protein IDs	Protein name	Gene name
134		-0,784937	P84051; Q4AB57	Histone H2A	His2A; His2A: <i>CG33859</i>
135		-0,775806	X2JCX8; C0HKA1; C0HKA0	Myosin-2 essential light chain	RpS14b
136		-0,769183	M9NEW1; P54357		Mlc-c
137		-0,762119	Q7KVQ0	Probable H/ACA ribonucleoprotein complex subunit 1	<i>CG4038</i>
138		-0,761574	O61380; A8DZ29		<i>eIF4G</i>
139		-0,754582	M9PQ5; M9NH88; A4V4Q6; P36188; M9NFC0; E4NKJ3	Troponin I	wupA
140		-0,7481	Q9VND5		
141		-0,726904	A4V4I0; P26308	Guanine nucleotide- binding protein subunit beta-1	Gbeta13F
142		-0,713504	Q9VHC7; A0A0B4K6Z1		<i>rump</i>
143		-0,712477	Q9W229	40S ribosomal protein S24	RpS24
144		-0,693888	Q8IQE6; A8JNR2; A8JNR3; X2JCT5		
145		-0,682119	Q8SYJ2		ND-MLRQ
146		-0,676887	Q8IMV6; A0A126GV03; A0A0B4KGV9		Saf-B

Nr.	S	Student's T-test Difference LFQ intensity Flag-LFQ intensity Mega	Protein IDs	Protein name	Gene name
147		-0,653992	P13060	Elongation factor 2	EF2
148		-0,630688	M9PBK5; P08570	60S acidic ribosomal protein P1	RpLP1
149		-0,628393	M9PF16; Q00963; M9PHG4	Spectrin beta chain	beta-Spec
150		-0,606863	Q7KT70		Gli
151		-0,603282	Q8MS37		tyn
152		-0,601629	X2JFR1; Q8IR16; Q04047; Q24113	Protein no-on-transient A	nonA
153		-0,601023	Q7JZZ3		
154		-0,59273	A0A0B4K6N1; Q8MLY8	40S ribosomal protein S8	RpS8
155		-0,591559	O16797	60S ribosomal protein L3	RpL3
156		-0,573657	A4V2J1; Q24400	Muscle LIM protein Mlp84B	Mlp84B
157		-0,56787	M9PJN8; P07487	Glycer- aldehyde- 3-phosphate dehydrogenase; Glyceraldehyde -3- phosphate dehydrogenase 2	Gapdh2
158		-0,543863	X2JE06; Q9VJY6	60S ribosomal protein L24	RpL24
159		-0,542816	P04359	60S ribosomal protein L32	RpL32
160		-0,541224	Q9W0A8		RpL23A
161		-0,536298	Q9VBE2		TwdIM

Nr.	S	Student's T-test Difference LFQ intensity Flag-LFQ intensity Mega	Protein IDs	Protein name	Gene name
162		-0,522387	P21187	Polyadenylate- binding protein	<i>pAbp</i>
163		-0,522041	Q9VV31		
164		-0,489042	M9PC50; Q9VQ25; X2J6N9		<i>haf</i>
165		-0,481125	Q9VT61		
166		-0,478484	E1JHA6		<i>uif</i>
167		-0,473902	O62619	Pyruvate kinase	PyK
168		-0,471207	A0A0C4DHG5; P26686	Serine-arginine protein 55	B52
169		-0,471109	Q9V3Z9		BG:DS00180.3
170		-0,467862	Q7KUB3		ImpE1
171		-0,444258	A8Y560; O17445	Ribosomal protein L15;60S ribosomal protein L15	RpL15
172		-0,421717	Q9VMY3		<i>CG12581-RA</i>
173		-0,415072	A0A0B4KED0; Q9W5N2	60S ribosomal protein L38	RpL38
174		-0,413712	Q9W1V3	rRNA 2-O- methyltransferase fibrillarlin	Fib
175		-0,390671	Q9W1X5; A0A0B4K7Z1		<i>nahoda</i>

Nr.	S	Student's T-test Difference LFQ intensity Flag-LFQ intensity Mega	Protein IDs	Protein name	Gene name
176		-0,387213	X2JIN0; M9MSA5; X2JDY1; A8JV00; M9PGT0; M9PDW8; REV__X2JIN0; REV__M9MSA5; REV__X2JDY1; REV__A8JV00; REV__M9PGT0; REV__M9PDW8		
177		-0,382858	Q59E58; A0A0B4JD57; A0A0B4JD95; Q59E59; A0A0B4K7Q4		<i>zip</i>
178		-0,363078	X2JC35; P49630	60S ribosomal protein L36	RpL36
179		-0,34319	C0HK95		
180		-0,338868	P55830	40S ribosomal protein S3a	RpS3A
181		-0,319901	A0A0B4KFT0; Q94514	Cytochrome c oxidase subunit 5A, mitochondrial	CoVa
182		-0,3081	Q8SXG9		
183		-0,295443	Q7JRA5		
184		-0,289562	Q9VBU9	40S ribosomal protein S27	RpS27
185		-0,279454	Q8IGK1; M9NFI4		

Nr.	S	Student's T-test Difference LFQ intensity Flag-LFQ intensity Mega	Protein IDs	Protein name	Gene name
186		-0,272778	A0A0B4LGZ0; Q9VH91; A0A0B4LI11; A0A0B4LGY1; E1JIH2; E1JIH3; Q8INN5; Q8INN7; Q9VH92; A0A0B4LGY0; Q8INN6; E1JIH1; A0A126GUR5		Unc-115a; Unc-115b
187		-0,268342	A0A0B4KH25; P08985	Histone H2A;Histone H2A.v	His2Av
188		-0,264235	Q9VBE0		TwdlB
189		-0,255554	Q7JWM6		
190		-0,235593	Q8IR10		TwdlY
191		-0,233557	P11046	Laminin subunit beta-1	LanB1
192		-0,219275	E2QD65; P39018	40S ribosomal protein S19a	RpS19a
193		-0,213967	A0A0B4LHV4; H1UUJ8; A0A0B4KGX1; Q01989	Myosin heavy chain 95F	jar;jar-RG
194		-0,213397	M9NH07; B9EQV5		<i>up1857</i>
195		-0,207212	P09180	60S ribosomal protein L4	RpL4
196		-0,204089	Q9VN21		<i>lost</i>
197		-0,200607	P02283	Histone H2B	His2B

Nr.	S	Student's T-test Difference LFQ intensity Flag-LFQ intensity Mega	Protein IDs	Protein name	Gene name
198		-0,199539	M9PJM6; M9PHJ0; M9PHR2; P19351; E1JJP0; X2JBP9	Troponin T, skeletal muscle	<i>up</i>
199		-0,180263	A0A0B4LG52; Q9W237	40S ribosomal protein S16	RpS16
200		-0,17688	Q960D3; Q9VBX3; A0A0S0X2W5; D2A6L8		vig2; FDY
201		-0,165841	P38040	Guanine nucleotide- binding protein subunit gamma-1	Ggamma1
202		-0,165768	A0A0B4LGZ5; P46222	60S ribosomal protein L11	RpL11
203		-0,165019	A0A0B4K7A5; A0A0B4K849; A8DYJ2; Q02645	Protein hu-li tai shao	<i>hts</i>
204		-0,164197	M9NDG5; Q9VZR6		
205		-0,161628	M9PHM6; Q9VS34	60S ribosomal protein L18	RpL18
206		-0,160598	X2JGM9; P41042	40S ribosomal protein S4	RpS4

Nr.	S	Student's T-test Difference LFQ intensity Flag-LFQ intensity Mega	Protein IDs	Protein name	Gene name
207		-0,157644	Q9W4Y4; M9NFS1; E1JJC0; M9NDL5; M9NES6; Q9W4Y3; M9NGL3; Q8IRV9; M9NE61; X2JCE8; M9NGK3; M9NDM1; Q8IRV8; M9NET2; X2JDK9; X2JE09; A0A023GRW4; M9NFR6; M9NE56; Q8MPN3 ;Q8IRV7; X2JAC7		<i>trol</i>
208		-0,156202	E1JGV6; O44081; A0A0B4K8B2	H/ACA ribonucleoprotein complex subunit 4	Nop60B
209		-0,152566	Q9VMZ5; Q8IR08		Twd1F
210		-0,151539	Q4AB54; P02255; Q4ABE3; Q4ABD8; Q4AB94	Histone H1	His1: <i>CG33861</i> ; His1; His1: <i>CG33801</i> ; His1: <i>CG33807</i> ; His1: <i>CG33834</i>
211		-0,147093	A1ZB32; Q8SXJ4		
212		-0,135704	Q9VFE4A0A0B4K683	40S ribosomal protein S5b	RpS5b
213		-0,126387	M9PB84; P31009	40S ribosomal protein S2	RpS2
214		-0,122751	Q6NMX2		

Nr.	S	Student's T-test Difference LFQ intensity Flag-LFQ intensity Mega	Protein IDs	Protein name	Gene name
215		-0,120649	Q9VS14		Cpr65Ec
217		-0,106399	A0A023GQA5; P24156	Protein l(2)37Cc	l(2)37Cc
218		-0,0931784	Q9VB14	40S ribosomal protein S10a	RpS10a
219		-0,0887089	X2JKU5; Q24186	40S ribosomal protein S5a	RpS5a
220		-0,0790545	Q9V3G1	60S ribosomal protein L8	RpL8
221		-0,0774314	A0A0B4KFP1; Q0KI92; Q9VH17; A0A0B4KFK4		
222		-0,0692158	Q9VBD2		TwldID
223		-0,068133	M9PC85; Q9V3V0		x16
224		-0,0618827	X2JFW6; Q9VX35		
225		-0,0607306	Q9VAG2		<i>neo</i>
226		-0,0562121	Q70VI1; Q9VFC7; Q95U15; C1C553; A0A0B4KG65; E1JIK9; E1JIK6; Q8INF1; Q8I062; Q9VFC6; C1C529		Mf
227		-0,0548808	P50887	60S ribosomal protein L22	RpL22
228		-0,0361691	Q8SWS3		
229		-0,0340481	A4V4A5; Q9VZ23	GTP-binding nuclear protein Ran	Ran; <i>ran</i>
230		-0,0260817	Q9VTP4	60S ribosomal protein L10a-2	RpL10Ab

Nr.	S	Student's T-test Difference LFQ intensity Flag-LFQ intensity Mega	Protein IDs	Protein name	Gene name
231		-0,0251223	C6TP87; P08736; A4V3Q6; P05303	Elongation factor 1-alpha; Elongation factor 1-alpha 1	Ef1alpha48D- RA; Ef1alpha48D
232		-0,0225372	M9ND95		Mhc
233		-0,0180181	C0MJA0; Q05783	High mobility group protein D	HmgD
234		-0,0117811	E1JJF3; Q9V427	Innexin;Innexin inx2	Inx2
235		-0,010423	Q8IH13		TwdIW
236		- 0,00469462	A0A0B4LHL1; Q9VC50; Q8IMV7		CG13627-RB
237		- 0,00191943	Q24560; A1ZBL0; P61857; A0A0B4LGH1; P08841; Q9VAX7; Q8MST5; CON_ ENSEMBL: ENSB- TAP00000025008	Tubulin beta-1 chain	betaTub56D
238		-4,45E-06	M9PBI9; M9PDZ9; M9PDS3; M9PBJ0; M9PGY4; M9PDZ6; M9PEA0; Q9I7U4; M9NDX0; M9PDS8; M9PEA5; M9PEA9; M9PGZ0	Titin	<i>sls</i>
239		0,00203896	A4V1N8; P35415; A4V1N9; P35416	Paramyosin, long form	Prm
240		0,00322851	Q9VY31		
241		0,0075887	A0A0B4LFD9; Q8T3U2	40S ribosomal protein S23	RpS23

Nr.	S	Student's T-test Difference LFQ intensity Flag-LFQ intensity Mega	Protein IDs	Protein name	Gene name
242		0,0223096	M9PD75; Q94920	Voltage- dependent anion-selective channel	porin
243		0,0343812	Q9V9X0		<i>nyo</i>
244		0,0350393	P02299	Histone H3	His3
245		0,0469786	Q9V3W7		SF2
246		0,0497405	X2JCP8; P10987; P02572	Actin-5C;Actin- 42A	Act5C;Act42A
247		0,055165	Q0E980		
248		0,0632369	P41073; M9NG39	Zinc finger protein on ecdysone puffs	Pep
249		0,0638618	A1ZBD8		
250		0,0658487	A0A0B4K7G4; P13469	DNA-binding protein modulo	mod
251		0,0660413	Q9VD35		
252		0,0742054	M9PCC1; O18640; M9PB67	Guanine nucleotide- binding protein subunit beta-like protein	Rack1
253		0,0758375	Q9VDJ8		Cpr92F
254		0,0778777	X2JCI6; P47949; A0A0B4LF64; P47948	Troponin C, isoform 3;Troponin C, isoform 2	TpnC73F; TpnC47D
255		0,078228	Q9W2X6		ATPsyndelta
256		0,0881246	Q7K5M0		<i>scaf</i>

Nr.	S	Student's T-test Difference LFQ intensity Flag-LFQ intensity Mega	Protein IDs	Protein name	Gene name
257		0,088569	M9PG76; P19889	60S acidic ribosomal protein P0	RpLP0
258		0,0972576	X2JD55; P02843	Vitellogenin-1	Yp1
259		0,0978661	O97061		Ccp84Ad
260		0,0987854	E1JHJ3; M9NF46; M9NCU7; A0A0S0WIH4; Q8IPH6; Q8IPH7; Q7JQV2; Q9VLZ3; Q8IPH8		Mhc
261		0,0990734	F3YDH0; P29844	Heat shock 70 kDa protein cognate 3	Hsc70-3
262		0,109804	G3M3A2; Q06559	40S ribosomal protein S3	RpS3
263		0,109952	E1JJM9; P48149; Q7KR04	40S ribosomal protein S15Aa;40S ribosomal protein S15Ab	RpS15Aa; RpS15Ab
264		0,118727	Q9W141	Putative ATP synthase subunit f, mitochondrial	CG4692
265		0,136975	O97062		Ccp84Ae
266		0,143378	Q9W1B9		RpL12
267		0,14602	E1JJ68; C7LAE4; P19109; A0A0B4K624; A0A0B4K6A3; A0A0B4K6K1; A0A0B4K6T7	ATP-dependent RNA helicase p62	Rm62; Rm62-RE

Nr.	S	Student's T-test Difference LFQ intensity Flag-LFQ intensity Mega	Protein IDs	Protein name	Gene name
268		0,162744	P49455	Tropomyosin-1, isoforms 33/34	Tm1
269		0,166129	Q9W2X5		
270		0,168595	Q8SZM2		
271		0,170347	Q8IRH6; Q9W0H1		
272		0,171792	A0A0B4LG88; Q9W255; A0A0B4LGB9		<i>qkr58E-1</i>
273		0,180338	Q9VIX7; Q8INW9; M9PDP3		<i>fon</i>
274		0,193905	M9PER0; Q8IGP1; M9PC24; Q7KUD8; Q867T3; M9PER6; Q86BH9; M9PF57; Q86LF6; M9PC30; Q8IGH4; Q9VT55; M9PHY1; M9PF03		<i>CG8154</i>
275		0,200916	P48159	60S ribosomal protein L23	RpL23
276		0,206437	Q9VBD5		TwdlN
277		0,208467	A0A0B4KFE9; A1Z8P9	Nucleoprotein TPR	Mtor
278		0,209039	X2JDU0; P50882	60S ribosomal protein L9	RpL9
279		0,209839	O17452		Peritrophin-A
280		0,218279	Q8IR01		
281		0,222221	Q8T3W3		
282		0,226639	Q8IMI7; Q9VA91	40S ribosomal protein S7	RpS7
283		0,227026	A4V2K7; P22058	Chromosomal protein D1	D1

Nr.	S	Student's T-test Difference LFQ intensity Flag-LFQ intensity Mega	Protein IDs	Protein name	Gene name
284		0,231603	M9NCR4; M9NER8; M9PCJ6; M9PB32; M9PEH5; M9PEI1; M9PC45; M9PC41; M9PBZ0; M9PB30; M9PCJ8; M9PEI7; M9PBZ4; M9PC48; M9NE82; M9PB31	Dumpy	<i>dp</i>
285		0,241858	Q9VV75		UQCR-C2
286		0,243691	Q8I0N3; Q9VBD9; Q9VBD8		TwdIL
287		0,249891	Q9VMZ6		TwdIG
288		0,253807	M9PFB2; M9PCB7; M9PFF9; M9PFG3; Q9VTZ0; M9PI44; M9PF14; M9PF20	Trailer hitch	<i>tral</i>
289		0,25493	A0A0B4LHS1; P06742	Myosin light chain alkali	Mlc1
290		0,283652	D1Z3A1; Q9VZS5; REV__ Q9VGU6	60S ribosomal protein L28	RpL28
291		0,286709	Q9VPW1	Protein asteroid	<i>ast</i>
292		0,288345	Q9VBD0	Tubby	<i>tb</i>
293		0,291419	Q9VYM5		Cpr11A
294		0,309315	P35381	ATP synthase subunit alpha, mitochondrial	<i>blw</i>
295		0,311062	X2JC80; P38979	40S ribosomal protein SA	<i>sta</i>
296		0,311794	C7LA75; P11147; Q8I0E9	Heat shock 70 kDa protein cognate 4	Hsc70-4-RA; Hsc70-4

Nr.	S	Student's T-test Difference LFQ intensity Flag-LFQ intensity Mega	Protein IDs	Protein name	Gene name
297		0,325042	X2JB48; Q26365; O62526	ADP,ATP carrier protein	<i>sesB</i>
298		0,32888	P54397	39 kDa FK506-binding nuclear protein	FK506-bp1
299		0,329579	A0A0B4KHJ9; P09491	Tropomyosin-2	Tm2
300		0,34614	C0HK92; A0A0B4LGZ7; C0HK94		
301		0,35747	Q9VS12		Cpr65Ea
302		0,365132	Q9VYT7		
303		0,366821	Q9VMV5		<i>vkg</i>
304		0,389867	Q7JZW2; A1ZAH8		RpS15
305		0,394564	P41094	40S ribosomal protein S18	RpS18
306		0,408918	X2JH42; L0MQ04; Q05825	ATP synthase subunit beta; ATP synthase subunit beta, mitochondrial	ATPsynbeta; ATPsyn-beta
307		0,42031	Q9V597	60S ribosomal protein L31	RpL31
308		0,421535	E1JIK0; P48810	Heterogeneous nuclear ribonucleoprotein 87F	Hrb87F
309		0,422093	Q9VP16		
310		0,432062	E1JGK7; Q7KRI2	Longitudinals lacking protein-like	lolal
311		0,433064	Q868Z9	Papilin	Ppn

Nr.	S	Student's T-test Difference LFQ intensity Flag-LFQ intensity Mega	Protein IDs	Protein name	Gene name
312		0,445721	Q9W4Z2		mRpL14
313		0,457887	X2JGG6; P02517	Heat shock protein 26	Hsp26
314		0,45892	A0A0B4KI71; Q8IMF5; P23226	205 kDa microtubule- associated protein	Map205
315		0,459042	E1JHA4; P48809	Heterogeneous nuclear ribonucleoprotein 27C	Hrb27C
316		0,473082	R9Q794; Q9W5R8	60S ribosomal protein L5	RpL5
317		0,496387	M9NCS8; P33438	Glutactin	Glt
318		0,497269	Q9VTC6; Q9VTC7		Cpr67Fa1; Cpr67Fa2
319		0,502525	Q8SZK9		Clect27
320		0,508156	O46084; X2JC94	Serine/threonine- protein phosphatase Pgam5, mitochondrial	Pgam5
321		0,511649	M9NEQ9; Q9VWG3	40S ribosomal protein S10b	RpS10b
322		0,528282	Q8IR11		TwdlX
323		0,544675	Q8SWU6		
324		0,555794	X2JEM4; Q9W334	40S ribosomal protein S28	RpS28b
325		0,556313	A0A0B4KFZ9; P84040	Histone H4	His4r; His4
326		0,559428	X2JB25; P02844	Vitellogenin-2	Yp2
327		0,565859	Q9VJ80		

Nr.	S	Student's T-test Difference LFQ intensity Flag-LFQ intensity Mega	Protein IDs	Protein name	Gene name
328		0,595446	E1JHJ4; E1JHJ5		Mhc
329		0,598927	Q9VVZ4		
330		0,613061	B7Z0B9; Q86NR7; Q9VRM2; B7Z0B7; B7Z0B8; A8JNL3; Q8T018		
331		0,661711	X2JDD7; Q9VMD9	Tiggrin	Tig
332		0,664701	X2JEX8; P06607; Q4V566; Q9VPH3; M9NFL7; Q9VX69	Vitellogenin-3	Yp3
333		0,755306	O97064		Ccp84Ag
334		0,762398	Q9V5P6	H/ACA ribonucleoprotein complex subunit 3	<i>CG7637</i>
335		0,774731	P92201	Larval cuticle protein 8	Lcp65Ag1
336		0,79321	P53501	Actin-57B	Act57B
337		0,831885	Q9VVZ6; Q9VVZ7		<i>CG18294</i>
338		0,864498	Q9VFT4		<i>rin</i>
339		0,878657	CON_ P00761		
340		0,880879	A1Z9J3		<i>shot</i>
341		0,960996	Q8IQU7; Q8IQU6; Q8IQU8		825-Oak
342		0,966909	A0A0B4LFD2; P29845	Heat shock 70 kDa protein cognate 5	Hsc70-5
343		0,969003	Q9VZF9		Cpr64Ad
344		1,03509	Q9W2U8		Neb-cGP
345		1,18913	Q9VVG2		

Nr.	S	Student's T-test Difference LFQ intensity Flag-LFQ intensity Mega	Protein IDs	Protein name	Gene name
346		1,70473	Q9I7Q6		Lcp65Ag3
347		1,88616	Q8IR57		
348		1,88984	Q9VV18		
349	+	4,19639	Q7PLL1; Q8SYL3; L7EEF1; Q7PLL3		<i>eIF-4B</i>
350	+	4,36111	R9PY46; A8JV12; A8JV11; A0A023GPJ3		
351	+	4,86844	Q9V4B8		<i>CG10323</i>

Table B.1 Putative interaction partners of Mega.

Abbreviations: S: Student's T-test Significance, $p < 0.05$; LFQ: label-free-quantification. Student's T-test calculated Difference LFQ intensity Flag - LFQ intensity Mega. Negative Student's T-test numbers indicate enriched interactors of Mega, whereas positive Student's T-test numbers indicate enriched interactors of Flag. 31 proteins were identified as significant for Mega binding, whereas 3 proteins were identified significant for Flag binding. 17 known SJ components (highlighted in cyan) were identified in the Mega co-immunoprecipitate. *CG43780/wrm* is highlighted in pink. 9 contaminations were identified.

C FRAP intensities

Rel. Fluor. recovery of Nr _x -GFP in wt embryos							Rel. Fluor. recovery of Nr _x -GFP in <i>vari</i> embryos						
Time (min)	E1	E2	E3	E4	E5	mean	Time (min)	E1	E2	E3	E4	E5	mean
-1	1	1	1	1	1	1	-1	1	1	1	1	1	1
bleach	0	0	0	0	0	0	bleach	0	0	0	0	0	0
1	0,0155	0,0188	0,0288	0,0178	0,0111	0,0184	1	0,0594	0,0861	0,0776	0,0791	0,1660	0,0936
2	0,0196	0,0316	0,0185	0,0166	0,0286	0,0230	2	0,1218	0,1398	0,1340	0,1895	0,2365	0,1643
3	0,0263	0,0430	0,0447	0,0337	0,0421	0,0380	3	0,2383	0,1936	0,1606	0,2447	0,2081	0,2090
4	0,0343	0,0563	0,0613	0,0375	0,0505	0,0480	4	0,2307	0,2312	0,2300	0,2659	0,1391	0,2194
5	0,0371	0,0610	0,0655	0,0367	0,0474	0,0495	5	0,2644	0,2891	0,2097	0,2925	0,1307	0,2373
6	0,0414	0,0584	0,0809	0,0428	0,0597	0,0566	6	0,2332	0,2834	0,2437	0,3901	0,1582	0,2617
7	0,0511	0,0611	0,0796	0,0442	0,0532	0,0578	7	0,2927	0,2212	0,2352	0,3810	0,2103	0,2681
8	0,0537	0,0707	0,0921	0,0398	0,0605	0,0634	8	0,2752	0,2303	0,2648	0,3963	0,1544	0,2642
9	0,0492	0,0518	0,0942	0,0372	0,0697	0,0604	9	0,3563	0,2604	0,1970	0,4512	0,1979	0,2926
10	0,0474	0,0659	0,1195	0,0536	0,0540	0,0681	10	0,3647	0,2176	0,2277	0,4398	0,1715	0,2843
11	0,0504	0,0612	0,1410	0,0387	0,0514	0,0685	11	0,3798	0,2395	0,2810	0,4316	0,1670	0,2998
12	0,0437	0,1114	0,1474	0,0484	0,0461	0,0794	12	0,3312	0,2581	0,2947	0,4806	0,2340	0,3197
13	0,0463	0,0733	0,1308	0,0456	0,0586	0,0709	13	0,3687	0,2599	0,3487	0,3906	0,2400	0,3216

Rel. Fluor. recovery of Nr _x -GFP in <i>wrm^{IE/IE}</i> embryos								Rel. Fluor. recovery of ATP _α -GFP in wt embryos						
Time (min)	E1	E2	E3	E4	E5	E6	mean	Time (min)	E1	E2	E3	E4	E5	mean
-1	1	1	1	1	1	1	1	-1	1	1	1	1	1	1
bleach	0	0	0	0	0	0	0	bleach	0	0	0	0	0	0
1	0,0351	0,0600	0,1341	0,1102	0,1392	0,0484	0,1080	1	0,0103	0,0070	0,0079	-0,0313	0,0137	0,0015
2	0,1368	0,1196	0,2007	0,2292	0,2495	0,1146	0,1985	2	0,0287	0,0170	0,0103	-0,0187	0,0321	0,0139
3	0,0964	0,1553	0,3032	0,3001	0,3408	0,1633	0,2769	3	0,0366	0,0362	0,0226	-0,0041	0,0710	0,0324
4	0,1042	0,1893	0,2986	0,2846	0,4199	0,1582	0,2903	4	0,0636	0,0283	0,0174	0,0018	0,0577	0,0338
5	0,1201	0,1764	0,2764	0,3435	0,3904	0,1686	0,2947	5	0,0699	0,0290	0,0264	0,0099	0,0482	0,0367
6	0,1319	0,1990	0,3186	0,3414	0,3953	0,1611	0,3041	6	0,0776	0,0309	0,0248	0,0295	0,0863	0,0498
7	0,1264	0,1524	0,3035	0,4324	0,4416	0,1987	0,3440	7	0,0885	0,0358	0,0398	0,0232	0,0637	0,0502
8	0,1552	0,1746	0,3855	0,4718	0,4640	0,1871	0,3771	8	0,0950	0,0374	0,0410	0,0279	0,0723	0,0547
9	0,1278	0,1985	0,4597	0,4679	0,4578	0,1958	0,3953	9	0,0997	0,0380	0,0525	0,0323	0,0619	0,0569
10	0,1232	0,2421	0,4854	0,4363	0,5340	0,1987	0,4136	10	0,1092	0,0399	0,0448	0,0403	0,0634	0,0595
11	0,2906	0,3525	0,5719	0,4793	0,5283	0,2223	0,4504	11	0,1230	0,0349	0,0447	0,0553	0,0769	0,0670
12	0,2240	0,2202	0,5965	0,4666	0,5593	0,2423	0,4662	12	0,1302	0,0388	0,0558	0,0528	0,0755	0,0706
13	0,2001	0,2522	0,5691	0,4634	0,5838	0,2257	0,4605	13	0,1311	0,0417	0,0460	0,0333	0,0618	0,0628

Rel. Fluor. recov. of ATP α -GFP in <i>mega</i> ⁻ embryos						Rel. Fluor. recovery of ATP α -GFP in <i>wrm</i> ^{IA/IA} embryos									
Time (min)	E1	E2	E3	E4	mean	Time (min)	E1	E2	E3	E4	E5	E6	E7	E8	mean
-1	1	1	1	1	1	-1	1	1	1	1	1	1	1	1	1
bleach	0	0	0	0	0	bleach	0	0	0	0	0	0	0	0	0
1	0,0575	0,0288	0,0419	0,0382	0,0416	1	0,0419	0,0572	0,0844	0,0467	0,0682	0,0647	0,0545	0,0701	0,0610
2	0,1421	0,0630	0,0454	0,0619	0,0624	2	0,0795	0,1070	0,1847	0,1054	0,1394	0,1390	0,0897	0,1576	0,1253
3	0,1661	0,0956	0,0564	0,1844	0,1400	3	0,0893	0,1493	0,2106	0,1286	0,1816	0,1931	0,1266	0,1993	0,1598
4	0,1886	0,0944	0,0636	0,1643	0,1294	4	0,1144	0,1447	0,2783	0,1573	0,2432	0,2092	0,1320	0,2666	0,1932
5	0,1517	0,1451	0,0660	0,2818	0,2135	5	0,1410	0,1821	0,2834	0,2285	0,2672	0,2415	0,1472	0,3024	0,2242
6	0,1935	0,1172	0,1464	0,2019	0,1596	6	0,1522	0,1903	0,3142	0,2468	0,2679	0,2969	0,1794	0,2635	0,2389
7	0,2040	0,1194	0,2370	0,3333	0,2264	7	0,1956	0,1954	0,3625	0,2634	0,3021	0,3300	0,1645	0,2758	0,2611
8	0,2433	0,1419	0,1916	0,2307	0,1863	8	0,2115	0,2185	0,3493	0,2428	0,3153	0,3241	0,1928	0,3007	0,2694
9	0,2740	0,1557	0,1957	0,3154	0,2355	9	0,1947	0,2228	0,3404	0,2411	0,2646	0,3602	0,2125	0,2844	0,2651
10	0,2624	0,1647	0,2183	0,2492	0,2070	10	0,1846	0,2416	0,3251	0,2965	0,3088	0,3910	0,2261	0,2799	0,2817
11	0,2640	0,1551	0,2343	0,4211	0,2881	11	0,2491	0,2561	0,3321	0,2931	0,2878	0,4313	0,2272	0,3023	0,2974
12	0,3393	0,1745	0,2127	0,3874	0,2810	12	0,2305	0,2673	0,3477	0,3893	0,2957	0,3830	0,2417	0,3150	0,3088
13	0,2516	0,2003	0,2664	0,3515	0,2759	13	0,2119	0,2683	0,3436	0,3624	0,3614	0,3999	0,2422	0,2905	0,3100

Table C.3 Fluorescent recovery after photobleaching profiles

D Synthesized double stranded DNA fragment

Fragment of the *wrm* genomic region with an in-frame insertion of a TwinStrep encoding sequence 3' of the *wrm* ORF encoding Wrm1:

```
TATGTTTATAAACATTGTTTAATATATTTAAATTCTAACAAATAACTTAATGTCTAA
ATGTATGCAGTAAAAAATTTACACAACCTGCACTTGCATCGATGAATGGTTATCGATC
GCTTGCAACCATGCGGCGAGTCCACAAAGTGCCATCACTAGCACACTGAGCCTGGCTTT
TGGGCGTTGTTTTTCGTAGCAGCAAAGTGGCTGAAATTAATAACATTTAAGAGCAGAAGT
GTGTAACACACCTGAATGGGACTTGTGCCAATCTCAGTGACCACCAATCGCGCGCAAAT
GGTAAGTGCAATCCGCATATAAGCTGCTAAGTGGGGAGCTGCTGGTGCTGCTAGTTAGT
TTACTTTGGTGACGCCACGCCCAATGTGACAAATTGGAATCGGTGGCAATTGGTTTCGG
GGTGCAAGTGGCATGCAGCGTGGTGGTTGAACCGCTTTCTCACTCTTCTTCCCCTGCCC
TCCAGACCATTGAGCATTGTGCAGCAGGCTATTGAGGCTCTTGCAAGTGACCACACCCC
TATAAGACTATGTCCACAATCGAAGAGGAACGCAAGGCGTACGAAAAGAATCCCTACTT
CACCGGCCACATCTACGGCAACTTCTCGCCGTTTTATGTGACCATTGCCATCTGCACGG
TTGTCCTGGGCACGATCATAATACTGAACATTATCTTGGGCTGCTGCTCCAAGCATCGC
AAGTACTGGCAGGACAGGCACACGGGCAATCGCTGGTTGGTTTCCATTTGGTCTGCCAC
GCCCCACAATCAGCCGCCATTGGATTTCACTGAGCTGAAGGACGCCTCATACTTTCAGC
GCTTCCATGTGAGTATTCGGTTTTTTGGCCAGAGCCCGAAAAATCGTGGCTTATTGTTT
GGAAACTATTACTTTTTCTAGCCCACAACCCATCAGCAAGTGTTCCCCGACGACGTTGT
CATCGGCGTTGACGACTTGGAGCCCGTGCACCTCGGCGCACCATCATCATCACCAGCAGC
AGCACCAGCGTCCACCACGTCCAGAGGGTTCGCACTTTGCACCAGCAGCGCCAGCGCGAG
GAATACGTGGAGTTGCAGAAGCGCGAGAGCGACATCggcAGTGCATGGAGTCATCCGCA
GTTTGAAAAGGGTGGCGGATCAGGAGGTGGCAGCGGTGGAAGTGCATGGAGCCATCCCC
AATTCGAGAAGTAAGTAGCAATGGCTCTTTACTTCCCTTTATCCCGCCGTGGCCGCCGTC
GCCCTGTTTCATCGTGGGCGTTATCATTGTTCATGCTGCGCTACGGACCGCGTTTGTGCGG
TTTGCGCCACCATGCGCTTCCCGATGACGAGGATCTGCGGGGAAAGACGTATGAGCATG
AGATTAGCTATGCCTAATATTGGGGTGTTCAGGGGTGTCCATTAATCCCATCAACCA
ATGGGTATTGTTGGTGATTTCTTGACAGCCCTGCCTTTAATTTACATACTTATACATG
CCGGCAATGCTACGAATTGCTTCTTATATATCTCTCTCCCCCAAATAATCCTAGCT
```


D Synthesized double stranded DNA fragment

ACTGTAAGAGCCCCTAACCCGTCTGCACCCACCAACCATATCAGTTTTGCATGCAGTA
CAAATAGTTTCATTAGCAACCAGTTTTGTTTCGAGCCGATTCCATTCCATTAATCGCAAT
CTGACAATGTGCCTTTCACGTAGAGACTCGTAAGAAATTTATACCGTCCAAGTGTCTTT
TCTAGCGCCGTAAGATCGAATTGTATTTTTACATTTAATACCCATTTAGGGTAGTCTGT
CTACAGATGCTGCATTTAATGTTGTCCAATATTCTACTCGTATGAAAATATCAGTGTCT
TGTATCTACTACAACTCTATACATTTGTATTCGTCCATTAGTTTTGTAATATTGTATT
TTGAAGTTGCATCAAATAAATCTACGGCCCCCAAATAATATTGTGTTTTTTAATC

This fragment was cloned into the *pGE-attB* vector via *XhoI* and *EcoRI* restriction sites, generating the *pGE-attB-WrmI::Strep3'* vector.

Abbreviations

(v/v)	volume to volume
°C	degree Celsius
A	alanine
aa	amino acid
ATP α	Sodium/potassium-transporting ATPase subunit alpha
Bark	bark beetle
BBS	borate buffered saline
BCIP	5-Bromo-4-chloro-3-indolyl phosphate
<i>btl</i>	<i>breathless</i>
BSA	bovine serum albumine
C	cysteine
CBP	chitin binding probe
CNS	central nervous system
Co-IP	co-immunoprecipitation
Crim	Crimpled
CRISPR	Clustered Regularly Interspaced Short Palindromic Repeats
D	aspartic acid
Da	Dalton
Dlg	Discs large
DMSO	dimethyl sulfoxide
DNA	deoxyribonucleic acid
dNTP	deoxyribonucleotide triphosphate
dH ₂ O	demineralized water
DTT	Dithiothreitol
E	glutamic acid
ECL1	extracellular loop 1
ECL2	extracellular loop 2
<i>E. coli</i>	<i>Escherichia coli</i>
EDTA	ethylenediaminetetraacetate
ER	endoplasmatic reticulum
EtOH	ethanol
F	phenylalanine

FasIII	Fasciclin3
FITC	Fluoresceinisothiocyanate
Fig.	Figure
FRAP	fluorescent recovery after photobleaching
G	glycine
GFP	green fluorescent protein
gRNA	guide ribonucleic acid
H	histidine
HCl	hydrochloric acid
HRP	horse radish peroxidase
ICL	intracellular loop
k	kilo
K	lysine
kb	kilo base
Kune	Kune-kune
L	leucine
l	liter
LC	liquid clearance
LFQ	label-free quantification
M	methionine
mA	milliampere
Mega	Megatrachea
<i>mega</i>	<i>megatrachea</i>
ml	milliliter
mM	millimole
min	minute
MX	Mega construct X
N	asparagine
ng	nano gram
MgCl ₂	magnesium dichloride
NaAc	sodium acetate
NaCl	sodium chloride
Na ₃ PO ₄	trisodium phosphate
NBT	4-Nitro-Blue-Tetrazolium-Chloride
NrxIV	NeurexinIV

ORF	open reading frame
PCR	polymerase chain reaction
PBS	phosphate buffer saline
Q	glutamine
R	arginine
RNA	ribonucleic acid
RNAi	RNA interference
RT	room temperature
rpm	rounds per minute
S	serine
SDS	sodium dodecyl sulfate
sec	second
sec.	section
Serp	Serpentine
Sinu	Sinuuous
SJ	septate junction
ss DNA	salmon sperm DNA
SSC	saline sodium citrate
st	stage
T	threonine
TAE	Tris Acetate EDTA
TJ	tight junction
Tris	Tris-aminomethane
Tw	Tween
UAS	upstream activator sequence
V	volt
W	tryptophan
<i>w</i>	<i>white</i>
wt	wild-type
<i>wrm</i>	<i>würmchen</i>
Wrm1	Würmchen 1
Wrm2	Würmchen2
Y	tyrosine
µm	microliter
µm	micrometer

List of figures

1.1	Schematic representation of cell-cell contacts of invertebrates and vertebrates.	4
1.2	Timeline and key components of SJ maturation.	5
1.3	Claudin structure of vertebrates and invertebrates.	7
3.1	Generation of the <i>mega^{attP}</i> allele	12
3.2	Localization of Mega in the hindgut epithelium of representative <i>mega</i> mutant lines.	18
3.3	Localization of Dlg in different <i>mega</i> mutant embryos.	19
3.4	Localization of Kune in M18 mutant embryos.	20
3.5	Tracheal localization of Mega and Kune in M18 mutant embryos.	21
3.6	Epithelial barrier function is defective in M18 mutant embryos.	22
3.7	SJ mediated exocytosis is affected in tested Mega constructs.	23
3.8	LC and tracheal branch morphology are affected in <i>CG43780</i> tracheal knockdown.	26
3.9	Genomic organization of <i>wrm</i> and protein sequences encoded by <i>wrm</i>	27
3.10	Expression pattern of <i>wrm</i> transcript during embryogenesis.	28
3.11	Generation of the <i>wrm^{ΔattP}</i> allele.	30
3.12	Genomic alterations in the <i>wrm</i> mutant alleles and schemes of affected Wrm1 proteins.	31
3.13	Genomic alterations of the <i>wrm</i> mutant alleles and schemes of affected Wrm2 protein.	32
3.14	<i>wrm</i> mutant embryos affecting Wrm2 are lethal during 2nd instar larvae.	33
3.15	Expression pattern of Wrm1.	34
3.16	Tracheal phenotypes of <i>wrm</i> mutant alleles.	36
3.17	LC is impaired in <i>wrm</i> alleles affecting Wrm1.	37
3.18	Tracheal barrier function is defective in <i>wrm</i> mutant embryos affecting Wrm1.	38
3.19	CNS barrier function is defective in <i>wrm</i> mutations affecting Wrm1.	39
3.20	Wrm1 is essential for the normal localization of Mega.	40
3.21	Wrm1 is essential for the normal localization of Kune.	41
3.22	Wrm1 and Wrm2 are not essential for the localization of Crumbs.	42

3.23	Exocytosis is impaired in <i>wrm</i> mutant embryos affecting Wrm1. . . .	43
3.24	<i>wrm</i> mutant embryos affecting Wrm1 display SJ and taenidial folds defects.	45
3.25	Würmchen1 is essential for SJ core complex stability.	47
3.26	Tracheal specific overexpression of Wrm1 leads to elongated tracheal branches and impaired LC.	48
3.27	Wrm1 binds to claudins as well as itself <i>in vitro</i>.	49
3.28	Wrm1 and Wrm2 bind to Mega <i>in vitro</i>.	51
3.29	Wrm1 binds to Wrm2 <i>in vitro</i>.	52
3.30	Mega, Wrm1 and Wrm2 show no cell adhesion capability in S2R+ cells.	54
4.1	Scheme of viable mutations in Mega.	59
4.2	Scheme of lethal mutations in Mega.	59
4.3	Scheme of an ectodermally derived epithelium in <i>Drosophila</i>.	61

List of tables

3.1	Summary of generated synthetic <i>mega</i> mutant fly lines	17
3.2	Tracheal gene knockdown of potential Mega interactors.	26
5.1	List of suppliers	64
5.2	List of commercially available kits	66
5.3	List of reagents	66
5.4	List of solutions and buffers	67
5.5	List of nutrient media for cell culture	70
5.6	List of nutrient media for cloning	70
5.7	List of nutrient media for fly work	71
5.8	<i>Drosophila melanogaster</i> strains	71
5.9	List of cell lines	73
5.10	List of <i>Escherichia coli</i> strains	73
5.11	List of plasmids	74
5.12	List of oligonucleotides	75
5.13	List of primary antibodies	78
5.14	List of secondary antibodies	79
5.15	List of analysis and imaging software	79
A.1	Detailed description of alterations in <i>mega</i> synthetic constructs	107
B.1	Putative interaction partners of Mega.	134
C.3	Fluorescent recovery after photobleaching profiles	137

Acknowledgements

First of all, I would like to thank Prof. Dr. Reinhard Schuh for giving me the opportunity to write my PhD thesis in his research group. I also thank him for the kind and warm working environment as well as the weekly cake seminars. Many thanks also go to my second reviewer Prof. Dr. Ernst Wimmer, who supported me throughout my studies, and Prof. Dr. Jörg Großhans for guiding comments and scientific discussions during Thesis Committee meetings. Furthermore, I would like to express gratitude to Prof. Dr. Ahmed Mansouri, PD Gerd Vorbrüggen and Dr. Nico Posnien for accepting membership in my extended examination board.

Additionally, I would like to thank our wonderful technical assistant Dajana Burghardt for her help in the lab and also for the vivid discussions on private matters. Special thank go to Leo Drees for the introduction to *Drosophila* work, critical comments and discussions. Also, I am grateful to Dominik Becker, Annika Müller-Eigner and Fred Manz for their supporting work, friendship and the many laughs in the lab.

Moreover, I give thanks to Prof. Dr. Herbert Jäckle and all members of the former Jäckle Department who provide a supportive environment and fantastic infrastructure.

Many thanks go to my family and friends for believing in me and their support during difficult times. I show most gratitude towards my daughter and my husband for keeping me sane and on track during the PhD process.